A novel approach towards a lubricant-free deep drawing process via macro-structured tools

Von Der Fakultät Maschinenwesen

der

Technische Universität Dresden

zur

Erlangung des akademischen Grades

Doktoringenieur (Dr.-Ing.)

angenommene Dissertation

Ali Mousavi, M.Sc.

Geboren am 18.09.1985 in Iran

Tag der Einreichung: 24.05.2019

Tag der Verteidigung: 17.10.2019

Gutachter: Prof. Dr.-Ing. Alexander Brosius

Prof. Dr.-Ing. habil. Marion Merklein

Vorsitzender der Promotionskommission: Prof. Dr.-Ing. habil. Thorsten Schmidt

„If you are not part of the solution, you are part of the problem“

ELDRIDGE CLEAVER

Acknowledgement

This thesis is written during my times as a research assistant at the chair of Forming and Machining Processes at TU Dresden.

Firstly, I would like to express my sincere gratitude to my advisor Prof. ALEXANDER BROSIUS for the continuous support of my Ph.D study and related research, for his patience, motivation, and immense knowledge. His guidance helped me in all the time of research and writing of this thesis. I have been extremely lucky to have a supervisor who cared so much about my work, and who responded to my questions and queries so promptly.

Besides my advisor, I would like to thank the rest of my thesis committee: Prof. MARION MERKLEIN, Prof. ANDRÉS LASAGNI, Prof. MICHAEL SCHOMÄCKER and Prof. UWE FÜSSEL for their insightful comments and encouragement.

I would also like to thank all staff members at chair of Forming and Machining Processes especially my closest colleagues CHRISTINA GUILLEAUME, NIKLAS KÜSTERS, RÉMI LAFARGE, CHRISTIAN STEINFELDER, MARC TULKE and ALEXANDER WOLF for the stimulating discussions, for the sleepless nights we were working together before deadlines, and for all the fun we have had in the last years.

I would also like to extend my thanks to the technicians of the laboratory of the department for their help in preparation of equipment for the experiments.

I am most grateful to my family members. My parents have always loved me and supported my every choice. As I know, they are the happiest and the most proud when seeing their son gets this degree, I dedicate this thesis to them.

Dresden, October 2019 ALI MOUSAVI

Abstract

In today's industry, the sustainable use of raw materials and the development of new green technology in mass production, with the aim of saving resources, energy and production costs, is a significant challenge. Deep drawing as a widely used industrial sheet metal forming process for the production of automotive parts belongs to one of the most energy-efficient production techniques. However, one disadvantage of deep drawing regarding the realisation of green technology is the use of lubricants in this process. Therefore, a novel approach for modifying the conventional deep drawing process to achieve a lubricant-free deep drawing process is introduced within this thesis.

In order to decrease the amount of frictional force for a given friction coefficient, the integral of the contact pressure over the contact area has to be reduced. To achieve that, the flange area of the tool is macro-structured, which has only line contacts. To avoid the wrinkling, the geometrical moment of inertia of the sheet should be increased by the alternating bending mechanism of the material in the flange area through immersing the blankholder slightly into the drawing die.

Therefore, the developed process can, besides the reduction of the contact area and the blankholder force, also increase the resistance of the sheet metal against wrinkling. Furthermore, through adjusting the immersion depth, it is possible to control the material flow and enlarge the process window. The induced alternating bending to stabilise the sheet metal against wrinkling during deep drawing with macro-structured tools generates an additional force in the drawing direction. The created non-frictional restraining force can be used positively to compensate the springback behaviour of the workpiece.

Table of contents

I. Symbols and abbreviations iv

1. Introduction 1

2. State of the art 3

2.1 Fundamentals of deep drawing process 3

2.1.1 Total forming force of a rotationally symmetric deep drawn cup 5

2.1.2 Process window in deep drawing 6

2.2 Tribology in metal forming 7

2.2.1 Lubrication mechanisms in metal forming 7

2.2.2 Friction models in metal forming 9

2.2.3 Diversity of lubricants in metal forming 12

2.3 Economic and ecological disadvantages of lubrication 13

2.4 Effects of lubricants on the quality of the deep drawing process 14

2.5 Possibilities for friction reduction in the deep drawing process 15

2.5.1 Surface coating 16

2.5.2 Surface micro-structuring 19

2.6 Tribological testing methods 22

2.6.1 Tribometer 22

2.6.2 Strip-drawing and the draw-bend test 23

2.7 Summary of Chapter 2 24

3. Objectives 26

4. Methodology and approach 28

4.1 Macro-structuring: Tip to Tip 30

4.2 Macro-structuring: Tip to Hutch 30

4.3 Summary of Chapter 4 34
5. Experimental setup 35
5.1 Press machines 35
5.1.1 Hydraulic press BUP 600 35
5.1.2 Hydraulic press Röcher RZP 250 36
5.2 Tooling material 37
5.3 Workpiece materials 37
5.4 Conventional and macro-structured tools 40
5.4.1 Tools for draw bending of U-Channels 40
5.4.2 Tools for deep drawing of axial symmetric parts 41
6. Process modeling and determination of process criteria 43
6.1 Process modelling: buckling stability 44
6.1.1 Identification of the most unstable part of the flange area 44
6.1.2 Buckling analysis of the free end part of the sheet 45
6.2 Process modelling: forming energy 46
6.3 Extension of the model for deep drawing of non-rotationally symmetric parts 50
6.4 Development of a criterion for the prediction of wrinkling 51
6.5 Development of a criterion for prediction of bottom cracks 54
6.6 Developement of a criterion for prediction of dimensional accuracy of the parts 56
6.7 Summary of Chapter 6 59
7. Results 61
7.1 Investigation about the effects of macro-structuring on process characteristics 61
7.1.1 Investigation about friction reduction through macro-structuring 61
7.1.2 Investigation about process stabilisation through macro-structuring 63

7.1.3 Investigation about springback reduction through macro-structuring 66
7.2 Verification of the developed analytical methods 69
7.2.1 Verification of the developed process model: forming energy 69
7.2.2 Verification of the developed criterion: prediction of wrinkling 71
7.2.3 Verification of the developed criterion: prediction of bottom cracks 72
7.2.4 Verification of the developed criterion: prediction of dimensional accuracy 73
7.3 Summary of Chapter 7 76
8. Transfer of the methodology into the complex geometries 77
8.1 Construction of a deep drawing tool to form a T-Cup 77
8.2 Determination and evaluation of optimum initial blank geometry 79
8.3 Test Procedure and interpretation of results 81
8.4 Summary of Chapter 8 85
9. Possibilities for process improvement 87
9.1 Use of rotary elements as macro-structured elements 87
9.2 Macro-structured tools with variable wavelengths 88
9.3 Summary of Chapter 9 91
10. Summary and conclusions 92
II. Zusammenfassung 95
III. List of Figures 98
IV. List of Tables 103
V. References 104

I. SYMBOLS AND ABBREVIATIONS

Symbol	Unit	Meaning
a	mm	Length of rectangular element in buckling analysis
a	-	Material constant
A_0	mm^2	Cross sectional area of the drawn part
A_0	mm^2	Original area of the sheet metal before forming
A_{80}	%	Elongation at fracture
A_1	mm^2	Increased area after stretch drawing
A_a	mm^2	Apparent contact area
A_i	mm^2	Partial contact area in macro-structured tool
A_r	mm^2	Real contact area
b	mm	Width of rectangular element in buckling analysis
b	mm	Flange width
C_R	-	Crack factor
E	GPa	YOUNG modulus
E_0	GPa	Plastic buckling modulus
E_B	Nm	Bending energy into a half sine wave segment in the wrinkled flange
E_b	Nm	Bending energy
E_f	Nm	Frictional energy
E_id	Nm	Ideal forming energy
E_L	Nm	Energy due to the lateral loading of the surface in the wrinkled flange
E_t	Nm	Energy due to the tangential compressive forces in the wrinkled flange
f	-	Modified friction factor
F_1	kN	Pulling force
F_2	kN	Back tension force
F_b	kN	Bending force
F_bc	kN	Bottom crack force
F_BH	kN	Blankholder force
F_f	kN	Friction force
F_fd	kN	Friction force in die edge radius
F_ff	kN	Friction force in flange area
F_id	kN	Ideal forming force
F_N	kN	Normal force
F_tot	kN	Total punch force
h	mm	Punch displacement / drawing depth
I	kg m^2	Moment of inertia
k	MPa	Shear yield stress

l	mm	Length of a half sine wave segment
m	-	Friction factor
m	-	Characteristic strain constant
m	-	Number of half sine waves in tangential direction in the buckled mode
M_{b}	Nm	Bending moment due to tangential stresses over the sheet thickness
$M_{\mathrm{b}}^{\mathrm{eb}}$	Nm	Required elastic bending moment to close the split ring
$M_{\mathrm{b}}^{\mathrm{res}}$	Nm	Bending moment because of residual stress in the intact ring
n	-	Flattering factor for the intermediate transition from the COULOMB to the shear friction model
n	-	Number of half sine waves in radial direction in the buckled mode
n	-	Strain hardening coefficient
P	MPa	Surface pressure
P	-	Slope of the stress–strain curve at a given value of strain
P_{i}	MPa	Partial surface pressure in macro-structured tool
P_{Total}	MPa	Total surface pressure in macro-structured tool
q	mm^2	Flange surface
r	mm	Radius of an arbitrary point in flange area
$\bar{r}$	-	Mean vertical anisotropy
r_0	mm	Blank initial radius
r_1	mm	Mean radius of cut out ring
r_2	mm	Mean radius of cut out and split ring
r_{a}	mm	Blank current outer radius
R_{a}	µm	Arithmetical mean deviation of surface roughness
r_{b}	mm	Bending radius
r_{i}	mm	Inner radius of the die
r_{i}^*	mm	Inner radius of the flange
R_{C}	mm	Corner radius
R_{M}	mm	Die edge radius
R_{m}	MPa	Ultimate tensile strength
r_{m}	mm	Mean flange radius
R_{max}	µm	Maximum depth of the assessed profile of surface roughness
r_{p}	mm	Punch edge radius
r_{s}	mm	Radius of macro-structures
r_{θ}	mm	Radius of the die edge from the centre
R_{z}	µm	Average distance between the highest peak and lowest valley of surface roughness
s_0	mm	Sheet thickness
t	s	Time
v	$mm.s^{-1}$	Sliding velocity between two friction bodies

V	mm^3	Volume
w	mm	Deflection of plate in z-direction in buckled mode
α	-	Contact area ratio
α	Rad	Coordinate of the local intersection coordinate system
α	Rad	Deflection angle of punch edge radius
β	-	Drawing ratio
β_1	Rad	Springback angle regarding the sidewall of the U-Channel
β_2	Rad	Springback angle regarding the flange of the U-Channel
δ	mm	Immersion depth
Δ	mm	Opening gap of split ring
φ_t	-	Tangential compression factor at the outlet of punch edge radius
δh	mm	Virtual punch displacement
δr_θ	mm	Virtual displacement at outlet of the die edge radius
δu	mm	Virtual displacement at the flange inner edge
δV	mm^3	Virtual volume change
δW_{ext}	Nm	Virtual external work
δW_{int}	Nm	Virtual internal work
$\delta\varepsilon_{ij}$	-	Virtual strain
ε_{pl}	-	Plastic strain
$\varepsilon^{eb}_{max,out}$	-	Maximum of tangential elastic bending strain due to the springback at the outer surface of the intact ring
$\varepsilon^{eb}_{max,inn}$	-	Maximum of tangential elastic bending strain due to the springback at the inner surface of the intact ring
η	-	Triaxiality
η	Pa.s	Lubricant viscosity
η_F	-	Forming efficiency
θ	Rad	Bending angle
Λ	µm	Period of micro-structures
λ	mm	Wavelength of macro-structures
μ	-	Friction coefficient
ν	-	Poisson's ratio
ρ	mm^{-1}	Curvature in the sidewall of the U-Channel
Σ	MPa	External stress
σ_∞	MPa	Asymptotic value for saturation strength
σ_{eq}	MPa	Equivalent stress
σ_I	MPa	First principle stress
σ_{II}	MPa	Second principle stress
σ_{ij}	MPa	Internal stress

σ_{Iso}	MPa	Pure isotropic stress
σ_{Kin}	MPa	Pure kinematic stress
σ_{m}	MPa	Mean stress
σ_{n}	MPa	Normal stress
σ_{r}	MPa	Radial stress
σ_{t}	MPa	Tangential stress
$\sigma_{\mathrm{t,cr}}$	MPa	Critical tangential stress
σ_{y}	MPa	Yield stress
$\sigma_{\mathrm{y,1}}$	MPa	Yield stress before bending over the die edge radius
$\sigma_{\mathrm{y,2}}$	MPa	Yield stress after bending over the die edge radius
σ_{y0}	MPa	Initial yield stress
σ_{ym}	MPa	Mean yield stress
$\sigma_{\mathrm{ym,1}}$	MPa	Average yield stress over the flange area
$\sigma_{\mathrm{ym,2}}$	MPa	Average yield stress over the die edge radius
$\sigma_{\mathrm{max}}^{\mathrm{eb}}$	MPa	Maximum of tangential elastic bending stress over the sheet thickness
$\sigma_{\mathrm{max,inn}}^{\mathrm{el}}$	MPa	Maximum of tangential elastic bending stress at the inner surface of the cup
$\sigma_{\mathrm{max,out}}^{\mathrm{el}}$	MPa	Maximum of tangential elastic bending stress at the outer surface of the cup
τ_{a}	MPa	Average shear stress at contacting asperity peaks of surface roughness
τ_{b}	MPa	Average shear stress in the valleys of surface roughness
τ_{f}	MPa	Frictional shear stress

BUP	Blech Universal Prüfmaschine (English: sheet metal universal testing machine)
CVD	Chemical Vapour Deposition
DLC	Diamond Like Carbon
DLIP	Direct Laser Interference Pattering
EDM	Electrical Discharge Machining
FEM	Finite Element Method
o/w	Oil in Water
PVD	Physical Vapour Deposition
ta-C	Tetrahedral amorphous carbon

1. INTRODUCTION

Metal forming belongs to one of the oldest technologies. During the first industrial revolution (18^{th} -19^{th} century), a mostly experience-based industrial metal forming technology developed for the first time after centuries or even millennia of traditional craftsmanship. It matured during two subsequent phases of development from approximately 1920 to 1960 with the establishment of the first scientific background of plasticity theory, materials technology, and experimental process analysis. Since 1960, the third phase of metal forming technology development was characterised by the introduction of the computer that revolutionised nearly all aspects of metal forming: process analysis and optimised design, materials technology and science, process-oriented tool technology, metrology and process control, etc. Consequently, product quality, productivity, flexibility, and economy were substantially improved [1]. Among the metal forming techniques, sheet metal forming is one of the most frequently used primary methods to produce different variety of components. Figure 1-1 shows for example the majority of the formed sheet metal parts in a car body.

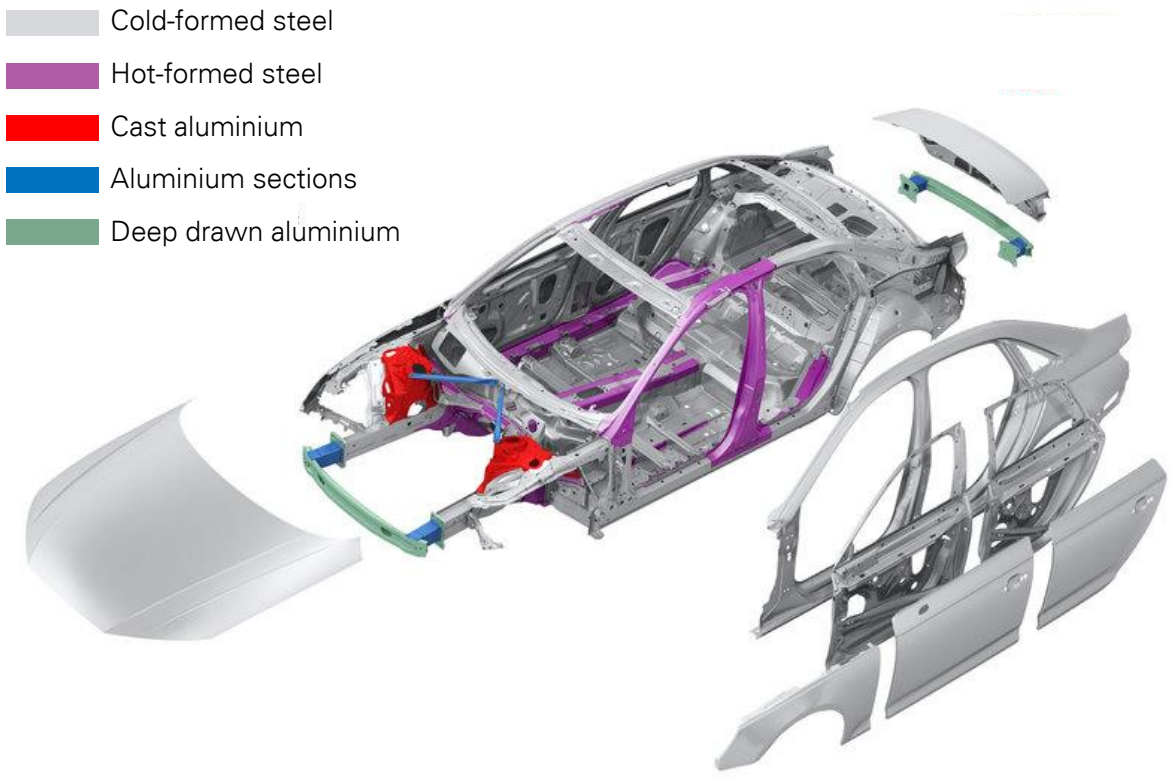

Figure 1-1: Structure of Audi A4 limousine with hang on parts [2]

Deep drawing as a widely used industrial sheet metal forming process for the production of automotive parts, households, etc. belongs to one of the most energy-efficient production techniques, based on its high material utilisation. In today's industry, the sustainable use of raw materials and the development of new green technology in mass production, with the

aim of saving resources, energy and production costs, is a significant challenge. But one disadvantage of deep drawing regarding the realisation of green technology is the use of lubricants in this process. Therefore, a novel approach for modifying the conventional deep drawing process to achieve a lubricant-free deep drawing process is introduced within this thesis.

Generally, in deep drawing the process window is limited by the occurrence of wrinkles and bottom cracks. Increasing the friction in the deep drawing process leads to an increase of the total punch force and as a result the risk of bottom cracks and a decrease of the process window become more probable. Moreover, in most cases, increasing the friction between the tool and the workpiece reduces the lifetime of the tool. That is why lubricants are mostly inevitable in the metal forming, especially in deep drawing for successful operation and reduction in energy consumption. However, the huge amount of lubricant used has economic and ecological disadvantages in today's industry. Regarding economic aspects, using mineral-oil-based lubricants leads to an increase of production steps, because an additional post-treatment process is required for cleaning the workpiece by means of degreasing agents which are usually solvent-based [3]. Moreover, more than 15% of the total cost of sheet metal forming is spent on lubricating liquids, including buying the lubricants, machines for their application and cleaning lubricated parts [4]. Besides that, lubricants are often either harmful to health or harmful to the environment. Therefore, it is of great interest to develop a process which permits a significant reduction of the amount of lubricating agents or even lubricant-free metal forming. However, this poses a great difficulty in application for sheet metal forming in general. In recent years, numerous studies on the application of dry lubricants, as well as environmentally friendly lubricants during the forming process, have been performed [5]. Various tool materials and coatings have superior tribo-properties and have been investigated widely for general purposes in tribology. Nevertheless, all of these studies and proposed methods are based on laboratory conditions and none of them can realise a total lubricant-free forming process [6]. Therefore, a process without any lubrication with the capability to transfer into industrial application is of major interest. Within the scope of this thesis, a new, lubricant-free, deep drawing process is developed, which ensures the process window despite the absence of lubricants. Since the largest contribution of frictional force in the deep drawing process is on the die edge radius and flange area, these parts of the tool should be adapted for a stable lubricant-free deep drawing process. Reduction of friction on the die edge radius through tool coating and micro-structuring is already state of the art. However, a new tool design should be developed to reduce the amount of friction in the flange area of the drawing tool. Therefore, in order to decrease the present friction forces for a given friction coefficient, the integral of contact pressure over the whole contact area should be reduced. Thus, as one of the most promising methods, macro-structured deep drawing tools have been developed within the scope of this thesis to reduce the contact area with contact lines or points. For a time efficient process design and also to analyse the influence of process parameters on the process stability in advance, the newly developed process was modelled analytically. The results of the model were verified through experimental tests as well as FEM.

2. STATE OF THE ART

In this chapter, the fundamentals of the deep drawing process are introduced. Furthermore, the advantages and disadvantages of using lubricants for a stable and efficient process are determined. Moreover, the already existing approaches for the reduction of friction in the deep drawing process are studied, with the aim of avoiding lubricants and to reach the vision of a lubricant-free deep drawing process.

2.1 FUNDAMENTALS OF DEEP DRAWING PROCESS

Nowadays, the classification of the forming processes can take place with regard to the temperature (cold forming, warm forming, or hot forming), process technology (sheet and bulk metal forming), and stress state [7]. According to DIN 8582 [8], depending on the main direction of the applied stress, they can be subdivided into five groups:

- Forming under compressive conditions,
- Forming under combined tensile and compressive conditions,
- Forming under tensile conditions,
- Forming by bending,
- Forming under shear conditions.

In order to assess the relative economic importance of sheet metal forming compared with other procedures, Table 2-1 gives an overview.

Table 2-1: Comparison between different forming processes regarding their economic importance [9]

Process	Sheet metal forming	Hot forming	Cold forming	Warm forming
Relative ratio of production	100	10	1	0.2 – 0.3

DIN8584-3 defines the deep drawing process as follows: "Deep drawing is the forming of a flat sheet blank (or foil/plate, section/blank, depending on the material) into a hollow shape or of a hollow shape to a hollow shape with smaller perimeter by pressing it through a die without intended change of the blank thickness" [10]. Its main fields of application are now in the automotive industry (structural and body components), in the branch of components made by sheet metal for household applications (dishwashers, washing machines, catering containers, etc.), as well as in the aerospace sectors [11].

Deep drawing of sheet metal is performed with a punch, blankholder, and drawing die. Generally, a basic deep drawing operation can be the forming of a sheet blank into a rotationally symmetric cup as illustrated in Figure 2-1. Understanding the material flow during the process is essential for understanding the present stresses on the workpiece. Considering

a rotationally symmetric deep drawing process, the material under the punch is forced into the cavity, pulling material in the flange area into the hole. Because of the applied tensile stress in the radial direction, the outer radii in the flange area decrease continuously, and this leads to induce a compressive stress in the tangential direction. It can cause an uneven distribution of thickness in the flange area, with the minimum at the inner and maximum at the outer part. Unless holding down pressure is applied from the blankholder, the induced compressive stress will cause the blank to buckle. In order to prevent the buckling of the blank and be able to control the material flow, the blankholder with predefined blankholder force F_{BH} press the blank in the normal direction. When the blank passes the flange area, it is subjected to bend and slide over the die edge radius. After bending, the blank unbends to flow downward along the part wall. However, as the complexity goes up, the manufacturing difficulties increase. Deep drawing for complex geometries and large height-diameter ratio components is generally done in multiple steps due to limitations regarding the properties of the sheet material, especially its formability [12]. The most commonly used sheet materials for deep drawing applications are steel and aluminium alloys because of their mechanical properties, natural availability, and cost-effectiveness. Among them, cold-rolled steels because of their good ductility [13] and aluminium-magnesium alloys due to their excellent balance between formability and strength [14] are usually used for deep drawing. The tool is subjected to repeated contacts with the blank material during forming processes.

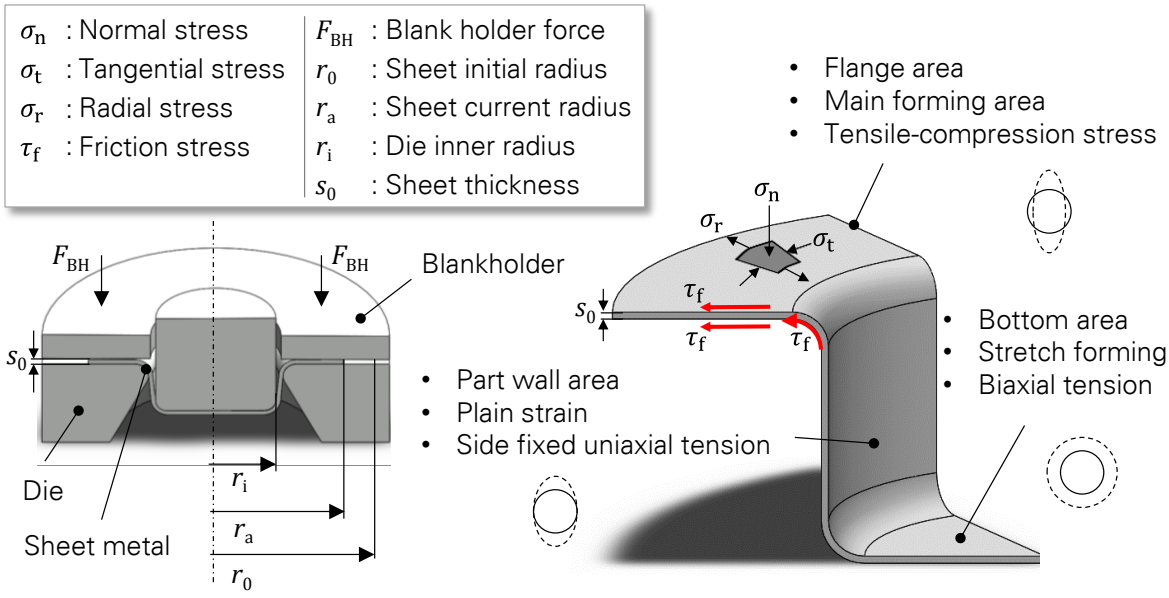

Figure 2-1: Deep drawing mechanism, geometrical variables, and acting stresses [10]

For better understanding the process mechanism and also to find out the interrelationship between the process-relevant parameters, it is required to analyse the total punch force regarding its constituent parts. In the following, the parameters affecting the punch force are introduced.

2.1.1 Total forming force of a rotationally symmetric deep drawn cup

Considering the rotationally symmetric deep drawing process, the total forming force F_{tot} consists of the superposition of four individual forces as follows:

$$F_{\mathrm{tot}} = F_{\mathrm{id}} + F_{\mathrm{b}} + F_{\mathrm{ff}} + F_{\mathrm{fd}} \qquad 2\text{-}1$$

Here, F_{id} is the ideal forming force in the flange area, F_{b} is the bending force on the die edge radius, F_{ff} are the friction forces between the workpiece and the tool in the flange area, and F_{fd} is the frictional force between the workpiece and the die edge radius. These forces can be calculated individually based on SIEBEL`s calculations [15] as follows:

$$F_{\mathrm{id}} = 2 \cdot \pi \cdot r_{\mathrm{i}} \cdot s_0 \cdot 1.1 \cdot \sigma_{\mathrm{ym},1} \cdot \ln\frac{r_0}{r_{\mathrm{i}}} \qquad 2\text{-}2$$

$$F_{\mathrm{b}} = 2 \cdot \pi \cdot r_{\mathrm{i}} \cdot s_0^2 \cdot \frac{\sigma_{\mathrm{ym},2}}{4 \cdot R_{\mathrm{M}}} \qquad 2\text{-}3$$

$$F_{\mathrm{ff}} = 2 \cdot \mu \cdot F_{\mathrm{BH}} \qquad 2\text{-}4$$

$$F_{\mathrm{fd}} = (e^{\mu \cdot \alpha} - 1) \cdot (F_{\mathrm{id}} + F_{\mathrm{ff}}) \qquad 2\text{-}5$$

In these equations, r_0 and r_{i} designate the initial radius of the sheet and the cup radius respectively, $\sigma_{\mathrm{ym},1}$ is the average yield stress over the flange area, R_{M} denotes the bending radius at the die edge radius, $\sigma_{\mathrm{ym},2}$ is the average yield stress over the die edge radius, F_{BH} is the blankholder force, μ is the COULOMB friction coefficient and α is the deflection angle at the die edge. Figure 2-2 represents a schematic overview of these force components.

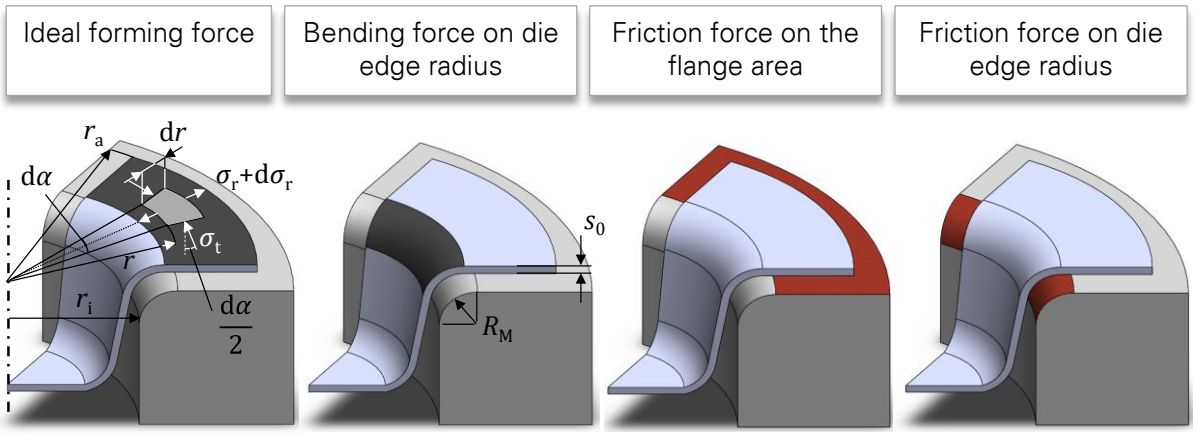

Figure 2-2: Individual components of the total forming force in deep drawing of the rotationally symmetric cup

The total deep drawing punch force is the sum of all individual force components:

$$F_{\mathrm{tot}} = 2 \cdot \pi \cdot r_{\mathrm{i}} \cdot s_0 \cdot \left[e^{\mu \cdot \alpha} \left(1.1 \cdot \sigma_{\mathrm{ym},1} \cdot \ln\left(\frac{r_0}{r_{\mathrm{i}}}\right) + \frac{\mu \cdot F_{\mathrm{BH}}}{\pi \cdot r_0} \right) + \sigma_{\mathrm{ym},2} \cdot \frac{s_0}{2 \cdot R_{\mathrm{M}}} \right] \quad \text{2-6}$$

As the Equation 2-6 implies, there are many parameters, which influence the punch force, like the geometry of the workpiece, sheet thickness, material properties, friction coefficient and blankholder force. For a stable process, a good balance is required between the process parameters. In general, the working area for a stable deep drawing can be described through the process window.

2.1.2 Process window in deep drawing

In the deep drawing process, wrinkling, bottom cracking and earing are the most common process defects. Control of material flow is one of the most important issues in the deep drawing process for preventing defects in the deep drawn part [16]. Earing is one of the characteristic defects observed during the deep drawing process due to the anisotropic nature of sheet metal, which is defined as the formation of waviness on the uppermost portion of the deep drawn cup and can be reduced by modifying the initial blank geometry [17]. Plastic buckling in the flange area of the deep drawing process occurs because of high compressive stress and inadequate blankholder force leading to wrinkling. In order to ensure a stable process regarding the wrinkling, a high amount of blankholder force is required [18]. However, it increases the normal surface pressure and results in an increase of frictional forces in the flange area. Increasing the friction in deep drawing due to the relative motion between tools and the workpiece in the flange area, as well as the die edge radius under a high surface pressure, leads to an increase of total punch force which consequently results in exceeding the formability limits of the material. As a consequence, the risk of bottom cracking becomes more probable. Bottom cracks indicate material instability caused by strain localisation, when the plastic deformation carried out by the punch force exceeds the formability limit of the material [19]. Wrinkling and bottom cracking can lead to an immediate loss of part properties and functionality. Therefore, in deep drawing, the process window, which can be characterised as the working area for the production of faultless parts by means of a stable process, is limited by the occurrence of wrinkles and bottom cracks (see Figure 2-3).

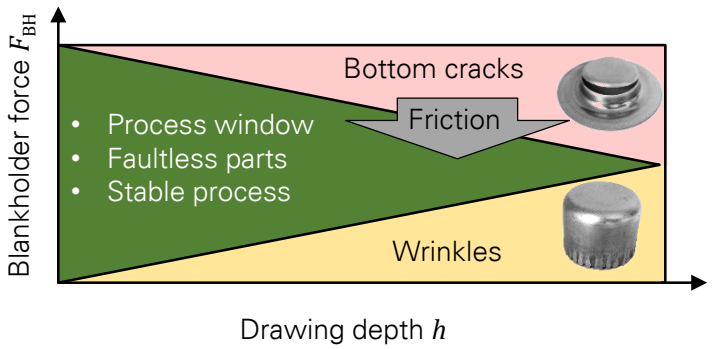

Figure 2-3: Process window in deep drawing

Generally, achieving the maximum process window and increasing the product quality are the indisputable targets in industrial production. That is why the control of material flow in deep drawing for enlargement of the process window is of importance. However, there are some methods to control the material flow in order to reach the greatest possible process window. For example, the geometry of the sheet metal plays an important role in material flow. Therefore, for deep drawing of complex geometries, the sheet metal geometry should be optimised to reach the greatest process window [20]. Furthermore, drawbeads can also be used to control the material flow during the process. Drawbeads restrain the material flow, causing a change of the strain distribution, which consequently hinders the material flow [21]. Above all, the reduction of friction can postpone the occurrence of bottom cracks and consequently the enlargement of the process window [22]. Hence, besides an optimum tool design, an excellent tribological system in the deep drawing process is essential for increasing the process quality and the enlargement of the process window through prevention of process failures.

2.2 TRIBOLOGY IN METAL FORMING

In the previous section, the mechanism of the deep drawing process was introduced and it was pointed out that the tribological behaviour of the deep drawing process is of importance to ensure a stable process with a large process window. The word tribology was first used in England in the 1960's, and is defined as the science and technology of interacting surfaces in relative motion. It comes from the Greek word "tribos" meaning to rub [23]. The term was coined as a conscious attempt to combine the historically independent fields of friction, lubrication and wear in an interdisciplinary manner [24]. Based on the lubricant viscosity, entrainment velocity and the surface pressure, different lubrication mechanisms can take place in the forming process. These mechanisms are discussed in the following section.

2.2.1 Lubrication mechanisms in metal forming

In sheet metal forming processes, the lubricant acts under a high normal pressure, and therefore the mechanism of lubrication depends on the lubricant viscosity η and the process properties (sliding velocity v and normal pressure P). The influence of these parameters can be described by the Stribeck curve [25], in which the friction coefficient is controlled by a single parameter produced by all three decisive factors. In a Stribeck curve (see Figure 2-4), these parameters are plotted in a logarithmic diagram and present four primary lubrication mechanisms (i.e. dry / boundary / mixed film / hydrodynamic) [26]. A dry (lubricant-free) condition means no lubrication is supplied at the mating surfaces; therefore, the friction is high and all the force is guided through from one body to another by contact at the asperities. Moreover, this can lead to pure intermetallic contact and cold welding (see section 2.4). Boundary lubrication is defined as a condition where the solid surfaces are so close together that the surface interaction between single or multi-molecular films of lubricants and the solid asperities dominates the contact, and force can be partially transmitted through this molecular

layer [27]. In the ideal situation, when such boundary layers are formed, and the underlying surfaces subsequently start to slide along each other, molecules of the lubricant are sheared off or pulled off the surfaces, and are then replaced by a new lubricant molecule. Boundary lubrication is the most widely encountered lubrication condition in the deep drawing process because of the high normal pressure and the minimum distance between the blank and tools [28]. With increasing load, the lubricant film becomes thinner and thinner, but as long as there is only one monolayer of lubricant present, friction remains relatively low. Besides boundary lubrication, mixed-layer lubrication is also frequently encountered in the deep drawing process [28].

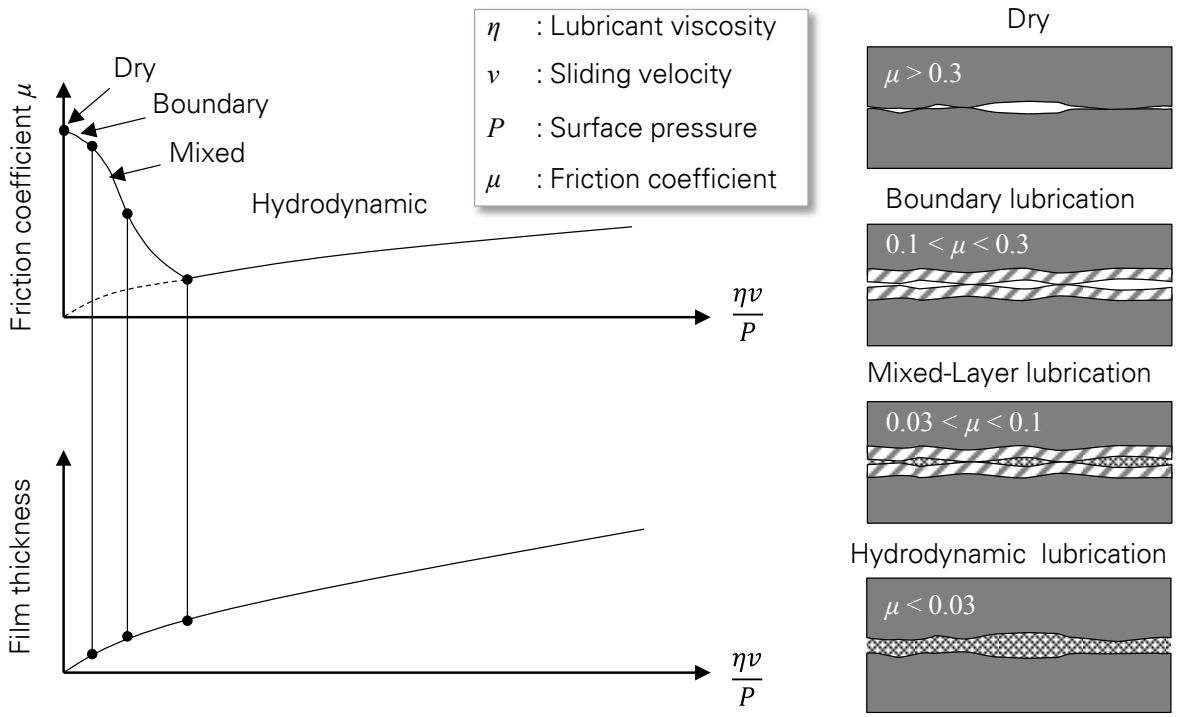

Figure 2-4: The Stribeck curve showing the onset of various lubrication mechanisms [29]

In this case, the micro-peaks of the metal surface experience boundary lubrication conditions and the micro-valleys of the metal surface become filled with the lubricant [30]. At some parts of the surfaces, the load is carried by the boundary layer, while at other parts a full lubricant film is built up [31]. The hydrodynamic lubrication mechanism occurs when the two surfaces are fully separated by a lubricant film. In this case, the relative tangential displacements lead to shear in the lubricant film only. The resisting force is now caused by this shear in the lubricant. In actual hydrodynamic lubrication, the lubricant is dragged into a lubricant film by the relative velocity of the surfaces and the shape of these surfaces [32]. This mechanism can be rarely seen in metal forming [28].

Understanding the physical background of the frictional condition in metal forming processes is important for process design. Furthermore, for simulation procedures, depending on the process, it is important to apply the proper friction model. In the following section, the most

relevant friction models in metal forming are introduced and their fields of application are discussed in detail.

2.2.2 Friction models in metal forming

A quantitative description of friction in different conditions comes from the first investigation of THERMISTIUS in 350 BC [33]. He found that the friction for sliding is greater than that for rolling. This conclusion led to the investigation in modern terms that the static friction coefficient is greater than the kinetic. It was observed in the 1500's by DA VINCI [34], retrieved by AMONTONS in 1699 [35], verified by EULER in 1750 and COULOMB in 1781 that friction is proportional to the load and independent of the sliding contact area [36]. Thus, the friction coefficient is independent of velocity in the case of dry sliding [37]. In the theory of plasticity, this is usually known as the COULOMB friction model in the form:

$$\tau_{\mathrm{f}} = \mu \cdot P \qquad 2\text{-}7$$

Where τ_{f} denotes the frictionally-induced shear stress, μ is the COULOMB's friction coefficient and P is the normal surface pressure. In many forming processes, the normal surface pressure P can reach a multiple of the yield stress of the material. At this point, the workpiece can start to deform plastically by shearing at the tool interface. Thus, the linear relationship between τ_{f} and P, as described by Equation 2-7, may not be valid at high surface pressure levels because the frictional shear stress τ_{f} cannot exceed the shear yield stress k of the deformed workpiece material. Therefore, the friction coefficient is no longer meaningful when $\mu{\cdot}P$ exceeds τ_{f}. Thus, to avoid this limitation of COULOMB's model, the shear friction model can alternatively be used [38]. This model assumes that the frictional shear stress τ_{f} must be linked with the shear yield stress k of the softer material with the following relation:

$$\tau_{\mathrm{f}} = m \cdot k \qquad 2\text{-}8$$

Whereby the proportionality factor m is the friction factor ($0 \leq m \leq 1$) and k is the shear yield stress. In this model, m equals to zero for no friction, and m equals to unity for a sticking friction condition, which is the case where sliding at the interface is purely by shearing of the base material (adhesion). The shear yield stress k depends on the yield stress of material σ_{y}, and yield criterion. When the Tresca yield criterion is considered, the shear friction model can be written as follows:

$$\tau_{\mathrm{f}} = m \cdot \frac{\sigma_{\mathrm{y}}}{2} \qquad 2\text{-}9$$

Moreover, by using the V. MISES yield criterion, it can be formulated as follows:

$$\tau_{\mathrm{f}} = m \cdot \frac{\sigma_{\mathrm{y}}}{\sqrt{3}} \qquad 2\text{-}10$$

The maximum of friction force in the shear friction model is independent of the normal pressure, but depends on the size of the contact area. This leads to an overestimation of friction in the case of low surface pressure. By summarising these two friction models, it can be concluded that the COULOMB's friction model is well suited for friction modelling with low surface pressures, but it overestimates the friction stress under high contact pressure. On the other hand, the shear friction model is suitable for high surface pressure, but it overestimates the friction stress under low contact pressure. Beyond that, the real surface pressure is dependent on the part of the contact area, which is participating in the friction. Since the tool is rigid, it cannot be deformed. The workpiece surface can also be plastically deformed, which leads to the enlargement of the surface topography and as a result affects the real surface pressure. These loading parameters, i.e. surface pressure and surface enlargement, can be used in metal forming to describe the process and thus to select the tribological system and the tool design. It is more relevant in bulk metal forming because of the relative high surface pressure (locally even up to 3000 MPa) and the surface enlargement (in special cases up to 20) [39]. Figure 2-5 compares the range of surface pressure and the resulting surface enlargement between the bulk and sheet metal forming process.

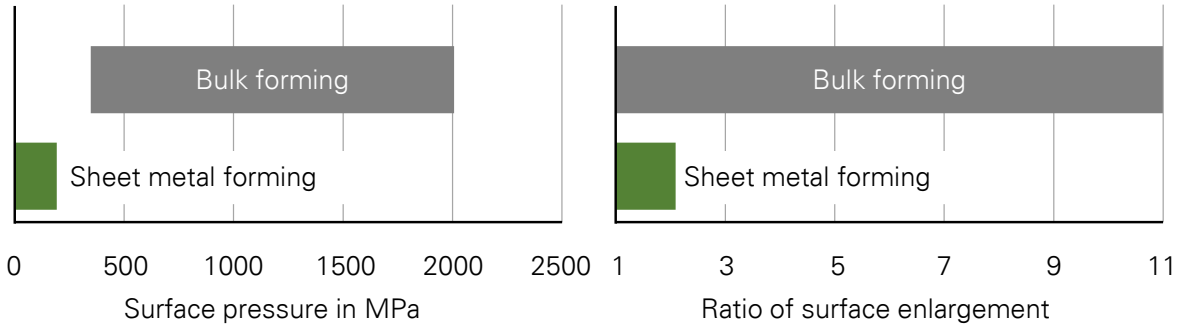

Figure 2-5: Comparison between bulk and sheet metal forming regarding the surface pressure and the resulting surface enlargement according to [40]

To take the effect of surface pressure in the friction calculation into account, OROWAN combined in Equation 2-11 both the friction models mentioned above (Equations 2-7 and 2-8), together with the goal of using the advantages of COULOMB's model for low surface pressure and adequacy of the shear friction model for high surface pressure [41].

$$\tau_f = \begin{cases} \mu \cdot P \ , & P \leq \dfrac{m \cdot k}{\mu} \\ m \cdot k \ , & P > \dfrac{m \cdot k}{\mu} \end{cases} \qquad 2\text{-}11$$

However, a disadvantage of the Orowan friction law is the sudden transition from the COULOMB to the shear friction model. Since the first slipping of the surfaces begins locally in small regions, this is not justified physically with the OROWAN model. In addition, the sudden change of the friction model has a negative effect on the stability of a numerical implementation. SHAW et al. solve this problem in [42] by a continuous transition from the

COULOMB model in the area of small surface pressures to the shear friction model in the area of large surface pressures. The frictional shear stress in the Shaw friction law can be represented by means of a hyperbolic tangent as follows:

$$\tau_f = k \sqrt[n]{tanh\left(\frac{\mu \cdot p}{k}\right)^n} \qquad 2\text{-}12$$

The parameter n determines the behaviour of the friction law in the transition region. Figure 2-6 shows an overview of all the models mentioned above and compares their estimation about the progress of frictional shear stress as a function of surface pressure.

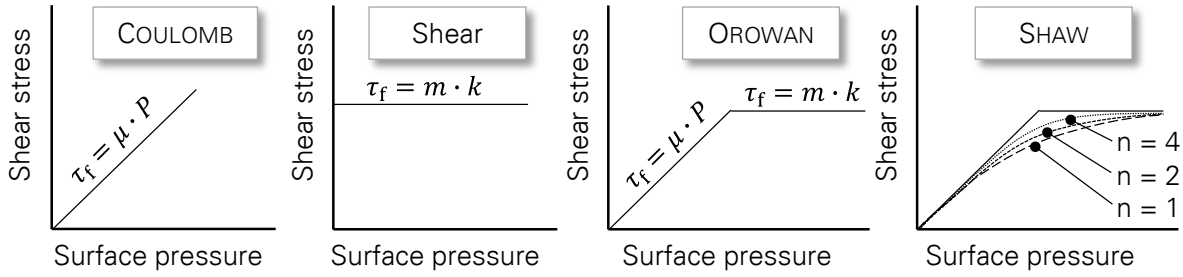

Figure 2-6: An overview of COULOMB [37], shear friction [38], OROWAN [41], and SHAW [42] friction models

However, none of these models considers the surface roughness of the bodies. Actually, when two nominally flat surfaces are placed in contact, surface roughness causes discrete contact spots. The total area of all these discrete contact spots constitutes the real contact area A_r, and in most cases, this will be only a fraction of the apparent contact area A_a. The ratio of the real contact area to the apparent contact area is known as the real contact area ratio α:

$$\alpha = \frac{A_r}{A_a} \qquad 2\text{-}13$$

To consider the effect of the real contact area ratio α on the frictional behaviour of bodies, WANHEIM and BAY proposed in [43] a general friction model:

$$\tau_f = f \cdot \alpha \cdot k \qquad 2\text{-}14$$

Where f is the modified friction factor. In this model, the friction shear stress τ_f is a function of the real contact area ratio α. Although this is a relatively precise model, it cannot consider the effects of the lubricant during the process. For this purpose, a complex model for friction is proposed by BOWDEN and TABOR in [44]. In this model, the frictional shear stress τ_f is given by:

$$\tau_f = \alpha\tau_a + (1 - \alpha)\tau_b \qquad 2\text{-}15$$

Here τ_a is the average shear stress at contacting asperity peaks, which is related to the real contact area ratio α, and τ_b is the average shear stress in the valleys (lubricants pockets), which can be estimated from the Newtonian viscous behaviour of the lubricant. It is also influenced by viscosity, pressure, film thickness of the lubricant, and the sliding speed of bodies. If the friction partners are in a lubricant-free condition, τ_b will be zero, and the friction shear stress τ_f will be only a function of the real contact area ratio. In order to indicate the relevant surface pressure for different manufacturing processes, KALPAKJIAN and SCHMID showed in [45] the nonlinear relation between frictional shear stress and surface pressure as a function of the real and apparent contact areas. Figure 2-7 classified the application range of each process based on these relations.

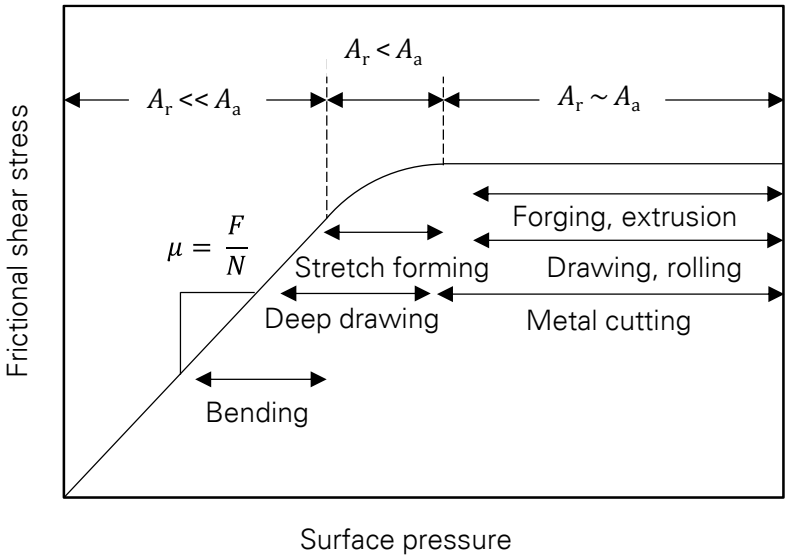

Figure 2-7: Friction force as a function of normal force and the range of applications for various manufacturing processes (the ranges shown are for unlubricated cases) according to [45]

Apart from process parameters, the types of lubricants and their physical properties have major influences on the lubrication mechanism. In the following, different types of lubricants used in metal forming are introduced.

2.2.3 Diversity of lubricants in metal forming

There are very many different types of lubricants in use for metal forming operations. Depending on many parameters, such as the tool and workpiece material, surface roughness and reactivity, temperature, contact pressure and sliding velocity, these may be classified as non-emulsifiable oils, oily emulsions, water-soluble synthetics, as well as consistent lubricants including pastes, greases, soaps, waxes, and solid lubricants [46]. Petroleum-based oil lubricants incorporate the most common technology. This product category has been used successfully in metal forming for many decades [47] and is classified into two types: non-emulsifiable oils and oily emulsions. Non-emulsifiable oils (straight oils) differ in viscosity, and

the presence and concentration of lubricity additives and polar and nonpolar additives [48]. There is a vast variety of oil-soluble additives, which may be used to achieve the desired property of the lubricating oil, such as sulphurs or phosphorous carriers, esters, alcohols, and sulfonates. The product selection strongly depends on the application of interest. Solvent diluted oils, including vanishing oils, may be used in aluminium forming or shear cutting. Medium-viscosity straight oils are used for drawing, extrusion, or fine cutting, while high-viscosity oils are usually used in heavy-duty forming operations. Emulsifiable oil concentrates represent an alternative to low viscosity or even solvent diluted oils. They can be diluted with water to achieve the desired viscosity and performance [49]. At low to medium concentrations, oil-in-water (o/w) emulsions are formed. Apart from ingredients that are susceptible to hydrolysis, most additives found in straight oils can also be used in emulsifiable concentrates. To that extent, there are few delimitations in the choice of additives [50]. While petroleum lubricants incorporate a very diverse set of products for the metal forming industry, the category of water-soluble synthetic lubricants may have come to incorporate an even larger group of products. It has come to represent most water-soluble lubricants that do not contain mineral oil. This definition includes products composed of vegetable oils, palm derivatives, and other natural ingredients [51].

When necessary to improve lubricant performance or film stability, thixotropic oils, greases, waxes, pastes, and even solid lubricants such as graphite and molybdenum disulphide (MoS_2) may be used [52]. Recent studies have shown that dry film lubricants provide better lubrication in deep drawing when compared with oil-based liquid lubrication [53]. This factor, as well as the savings for the lubricant used, has helped promote the use of dry film lubricants in the automotive industry for deep drawing of aluminium and high-strength steel parts [54]. Apart from the technical and process-based advantages of lubrication, they have many environmental and economic disadvantages that are described in the next section.

2.3 ECONOMIC AND ECOLOGICAL DISADVANTAGES OF LUBRICATION

From both the economic as well as the ecological points of view, all types of lubricants have several disadvantages in the sheet metal forming process. For the upcoming process steps after forming, such as joining, coating, and painting processes, which are required to have a perfectly clean surface, it is essential to remove the lubricant from the workpiece [55]. Removing the lubricant from the semi-finished parts can be done after some post-treatment process using many degreasing agents, which are costly and time consuming. Therefore, using the lubricant in the process leads to an increase in the number of process steps and as a result, an increase of the cycle time [56]. Focused on the economic point of view, the cost-saving potential reached by lubricant-free processing can amount to about 2–17 % of the workpiece-specific production costs, depending on the selected production process [3]. Besides the economic problems, lubricants in the metal forming process have environmental and health burden disadvantages. Generally, two important manufacturing challenges in the 21st century can be identified as environmental shifts and the deficiency of energy and

resources. This is not only due to increased production, which is already too high and leads to an oversupply in many industries, but also is mostly related to how the raw materials and energy are provided for the production and operation [57]. Based on [58] about 1% of the total mineral oil consumption is used to produce lubricants. World lubricant demand has remained flat at around 35 million tonnes per year since 1991, e.g. 37.4 million tonnes of lubricants were consumed worldwide in 2004: 53% automotive lubricants, 32% industrial lubricants (primary hydraulic oils) , 10% process oils (metal working fluid), and 5% marine oils [59]. The same holds true for the EU where the total lubricant demand of about 5.3 million tonnes annually has stayed unchanged since 1982. Germany is the largest national market for lubricants in Europe and ranks fifth in global terms with a total lubricant consumption (2.5 million tonnes yearly), while industrial lubricants account for 1.7 million tonnes and process oils for 0.6 million tonnes per year, respectively [60]. An estimation from MANG and DRESEL shows that approximately 50% of the total mineral oil consumption of European countries can be recovered by recycling and / or further utilisation of waste oil, while the other half is lost to the environment [59]. MADANHIRE and MBOHWA have characterised in [61] the potential human health and environmental hazards of widely used classes of lubricating oils because of their toxic additives. However, lubricants are mostly expected in sheet metal forming for a successful operation. In the next section, it shall be shown how the lubricants affect the process stability and the quality of the product through the reduction of tool wear and the frictional forces between the tool and the workpiece.

2.4 EFFECTS OF LUBRICANTS ON THE QUALITY OF THE DEEP DRAWING PROCESS

Generally, many parameters have an influence on the deep drawing process and the quality of the final product. Material properties, tool geometry, blankholder force and friction can be considered as the main factors affecting the process. Most notably, friction can directly affect the lifetime of a tool and the efficiency of the process. In the following, some beneficial effects of lubricants regarding the prevention of wear and galling are pointed out.

One of the most important parameters for the efficiency of a deep drawing operation, i.e. the production rate, is the operational limits of the forming tools. The lifetime of the tool and the production speed, have to be carefully balanced to optimise the process efficiency [62]. Increasing the efficiency of the deep drawing operation often goes together with a higher mechanical load on the forming tools, resulting in higher wear and a shorter lifetime [63]. Wear, defined as the progressive loss of substance from the operating surface of a body, occurring as the result of relative motion at the surface [64], is one of the most important sources of process disturbance in sheet metal forming [65]. Tool wear influences the stability of the equipment, the production speed, and the quality of the products and the product's surface [66]. Volume loss of the forming tool and volume loss of the sheet material are two types of wear in sheet metal forming, resulting from a combination of adhesive wear, abrasive wear, surface fatigue wear, and tribochemical wear [67]. Among these mechanisms, adhesion

and abrasion are known as the principal wear mechanisms in sheet metal forming [62]. Adhesive wear in sliding contact is a process where the contact surfaces adhere to each other so strongly that the atomic bonding forces occurring between the materials on the interface are stronger than the strength of the surrounding area in both materials [68]. A consequence of this shear may be the generation of wear particles or a transfer of material from one surface to the other. Patches of adhered hard material increase the surface roughness of the tool and when subsequent workpieces are to be formed, the adhered material may indent or scratch the surface and thereby worsen the surface finish of the product. In sheet metal forming, this problem is usually referred to galling [69]. The abrasive wear is the removal of material by a ploughing effect of the hard object into a softer surface [70]. The ploughing can be caused by a hard asperity on one of the contacting surfaces (two-body wear) or by wear particles in the contact (three-body wear) [71]. Both the adhesive and abrasive wear behaviour of contact bodies depend on different influencing parameters. Besides the material properties (chemical composition, microstructure, surface finish, and hardness), the geometry of the contact area, surface pressure, and the lubrication system have a major influence on the wear behaviour of the contact bodies [72]. Increasing the tool wear during the process prevents the control of strain distribution and as a result the loss of quality and the dimensional accuracy of the workpiece. Generally, there are three concepts to control the wear in sheet metal forming: improving the surface roughness of contact bodies to prevent the abrasive wear, changing the chemistry of either one or both surfaces to lower the adhesion between the sheet and tool surface, and using the lubricant to separate the sliding surface. Here, the lubricant can work as a layer of material with lower shear strength than the surfaces themselves [73]. However, the lubricant may not completely prevent the direct contact, although it will reduce it and may reduce the strength of the junctions formed [72].

2.5 POSSIBILITIES FOR FRICTION REDUCTION IN THE DEEP DRAWING PROCESS

As the Equation 2-6 implies, there are many parameters, which influence the punch force, like geometry of the workpiece, sheet thickness, material properties, friction coefficient and blankholder force. But, the friction coefficient and the blankholder force have a direct influence on the friction force in the deep drawing process. Reduction of the blankholder as mentioned in previous sections leads to process instability in the form of wrinkling. As a result of this, improving the tribological behaviour of the tool through surface treatment can be considered as the first step towards realisation of a lubricant-free (or minimal quantity lubrication) deep drawing process. Studies on metal forming without lubricants have shown that results highly depend on the material combinations to decrease the friction coefficient and wear in critical parts of the tools [3]. Generally, the different approaches to achieve a lubricant-free or minimal quantity lubrication forming process can be divided into three categories: ceramic tools [74], self-lubricating coating systems [75], and hard material coatings [76]. KATAOKA et al. investigate in [77] the prosperity of ceramic materials like SiC, Si_3N_4, and Al_2O_3 (oxide ceramics) as tool materials for a drawing die within a lubricant-free deep drawing process. However, this

was by providing a smaller limiting drawing ratio, compared to lubricated processes. Moreover, a high lubricant-free deep draw ability could be attained with these ceramic materials for mild steel, whereas no or little improvement could be seen for titanium and aluminium sheets. TAMAOKI et al. examined in [74] the electro-conductive ceramic tooling like ZrO_2-WC and Al_2O_3-TiC for lubricant-free deep drawing applications. This type of ceramic tooling has a higher limiting drawing ratio compared with monolithic ceramic tools in a lubricant-free condition, but it remains below the lubricated case. Using environmental friendly self-lubricating materials such as graphite or colloidal suspension can reduce the friction coefficient significantly; however, they do not attribute further economic benefits to the lubricant-free deep drawing process [75].

There are many types of surface treatments available to improve the tribological behaviour of the forming process for lubricant-free applications, which can be categorised in surface coating and surface functionalisation [78]. The different surface coatings vary in composition, thickness, and mechanical properties [79]. The two main groups of coating types are deposited coatings and reactive coatings [80]. Deposited coatings can be obtained by deposition of extra material on the surface, while the reactive coatings can be obtained, in which a thin layer of the base surface or the surface of deposited coating is modified through thermal, thermomechanical or radiation methods [81]. Here, either an alloying element enters to the base material by diffusion or beam techniques, or the topology of the deposited coating changes via laser techniques. Some examples are nitriding, carburising, and ion implantation for direct fabrication of periodic structures on the surfaces.

2.5.1 Surface coating

Since the 1980s, there have been studies on the use of hard material coatings in forming tools for lubricant-free processes in the context of metal forming [3]. Nowadays, PVD and CVD coating processes are attractive for industrial applications because the deposition of these coatings, besides the improvement of the tribological behaviour of the tool, leads to increasing its lifetime to a large extent [82]. In deep drawing applications, in particular, Titanium Carbide (TiC), Titanium Nitride (TiN) and TiC/TiN coatings have been used to assure a long lifetime of the tool because of their high resistance to abrasive and adhesive wear [83]. They provide a powerful means in those cases where the use of lubricants cannot be completely avoided and a minimal quantity of lubrication may provide technological and ecological advantages [84].

In recent years, the introduction of the diamond like carbon coatings (DLC) has represented an attractive solution for the development of lubricant-free forming or processes with minimal quantity of lubrication due to their excellent tribological behaviour [85]. DLC possesses an array of valuable properties: an extremely low friction coefficient, abrasion and wear resistance, exceptional hardness, and high dielectric strength [86]. DLC is considered as an amorphous material, containing a mixture of sp^2 - and sp^3 -bonded carbon. Based on the percentage of sp^3 carbon and the hydrogen content, four different types of DLC coatings have

been identified: tetrahedral carbon (ta-C), hydrogenated amorphous carbon (a-C:H hard and soft), and hydrogenated tetrahedral carbon (ta-C:H) [87]. JIANG et al. showed in [88] that the hydrogen content in amorphous carbon films affects their hardness and tribological properties significantly. Tetrahedral amorphous carbon (ta-C), with a high fraction of sp^3-bonded carbons (up to 80%) and less than 1% hydrogen content, has shown promising tribological and mechanical properties, such as a low friction coefficient, high hardness (slightly less than that of diamond) [89], low roughness [90], high inertness, and low mass diffusivity [91]. Figure 2-8 compares the different amorphous carbons, regarding the hydrogen content, their bonding states and also summarises the properties of ta-C coating. Through evaporation of graphite as a source of carbon, in the PVD process with arc discharge (vacuum arc PVD) under ultrahigh vacuum conditions, a pure carbon layer can be reached [92]. Through setting the deposition parameters like pressure, it is possible to adjust the fraction of sp^2 and sp^3-bounded carbons [93]. Because of the vacuum arc process, small graphitic particles (micro-particles), which are emitted from the carbon source, are incorporated in the coating. This leads to a disturbance of the layer growth and thus increases the surface roughness [94]. Due to their poor bonding to the layer composite, these particles reduce the corrosion resistance.

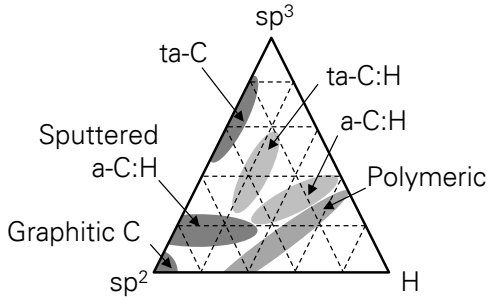

Properties of ta-C:
- Atomic arrangement: amorphous carbon
- Bonding state: up to 80% sp^3
- Hydrogen content: less than 1%
- Hardness: 55-65 GPa
- Friction coefficient: 0.12 – 0.19 (without lubrication)
- Ideal for structuring / pattering

Figure 2-8: Threefold diagrams of amorphous carbon types and the properties of ta-C coating [95]

Pores or pinholes, because of the growth defects are positions with an increasing corrosion potential. This leads to a local delamination of the coating [96]. Particularly in the case of hard coatings, such as ta-C, increased roughness decreases the running behaviour of the friction system. This can result in an increased friction and wear of the counter body [97]. Hence, a process like brushing is required for roughness reduction of the coated surface.

KUNZE et al. brushed the ta-C coated tools for 5 min using a wire brush (low alloy steel, wire diameter of 0.2 mm) with a brush force of 50 N. The rotating speed of the wire brush was 6,000 rpm and that of the tool (rotating contrarily) was 150 rpm. They showed in in [98] that the surface roughness of the coated tools in terms of R_a, R_z, and R_{max} can be reduced down to the roughness of the substrate through a brushing process (see Figure 2-9), while no changes in coating thickness were observed, as concluded from calotte grinding prior and after brushing. Furthermore, they showed that an additional brushing does not lead to a further reduction in surface roughness.

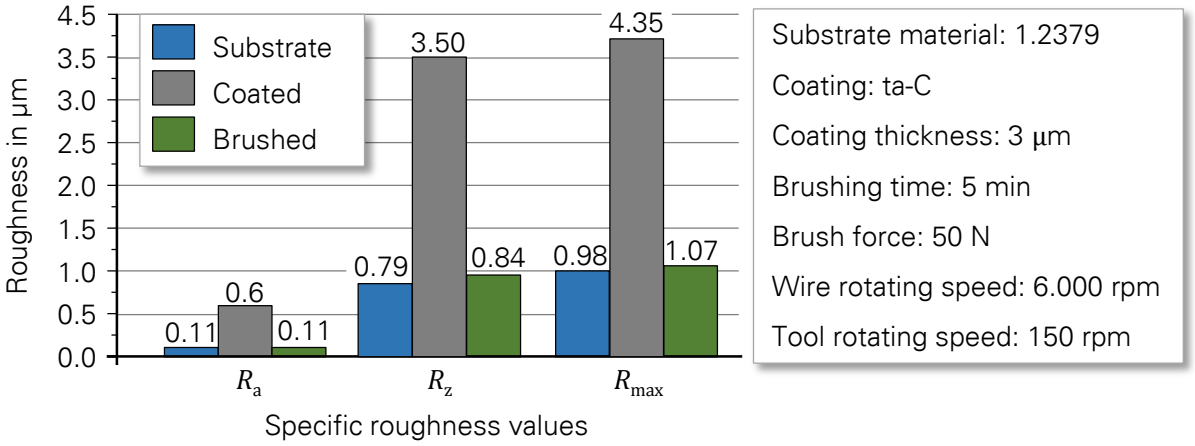

Figure 2-9: Average of specific roughness valuesfor the substrate, coated and brushed surfaces [98]

KUNZE et al. examine in [99] the tribological characteristics of the ta-C coated cylindrical specimens with a layer thickness of 3 - 5 µm via the draw-bend test (see section 2.6) at room temperature, with a constant drawing velocity of 100 mm/s and a contact surface pressure of 50 MPa. They tested the ta-C coated specimens under lubricant-free conditions and the uncoated tools under lubricant-free as well as lubricated conditions (lubricating oil "WISURA ZO 3368") against workpiece strips from commercially sourced DC04 steel (1.0338) with 1 mm thickness, 20 mm width, and 1000 mm length. Each tool was subjected to 100 draw-bend tests corresponding to an effective testing distance of 40,000 mm. To assure total lubricant-free conditions, each strip was cleaned using a citrus-based cleaner, and finally treated with acetone to remove all traces of pre-lubricants. The resulting average friction coefficient for the uncoated tool (lubricant-free and lubricated) and the ta-C coated tool (lubricant-free) are shown in Figure 2-10.

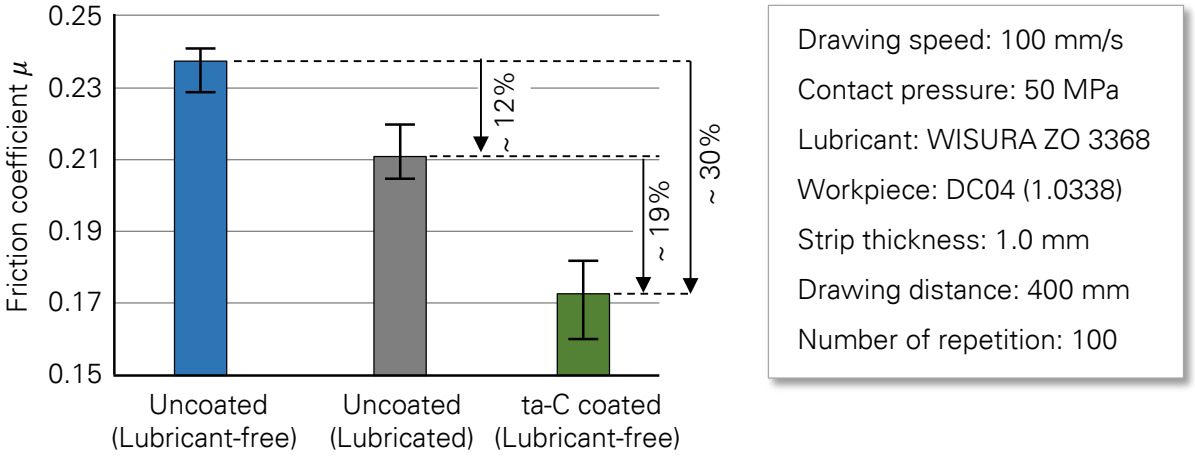

Figure 2-10: Comparison between the friction coefficient of the ta-C coated tool in lubricant-free conditions and uncoated tools in lubricant-free and lubricated conditions resulting from draw-bend tests with a range of results

As this diagram indicates, the friction coefficient can be reduced from 0.24 to 0.21 (~12%) through lubrication. However, coating the tool with ta-C reduces the friction coefficient to ~0.17 (lubricant-free conditions) which is about 30% and 19% less than in the uncoated case under lubricant-free and lubricated conditions, respectively. These results show that the ta-C tool coating employed introduces a well-defined boundary layer, which is capable of taking over the tribological functions of the lubricant. More particularly, because of its disordered network of carbon atoms [100], changing the fraction of sp^2 and sp^3-bounded carbons is feasible with the aim of wear resistance improvement.

2.5.2 Surface micro-structuring

Surface structuring to control frictional forces has been intensively used since ancient times [101]. For example, during the Tong Dynasty in China, ridged patterns or dimples were placed on the soles of shoes for labourers to help them work on muddy, slippery ground. For approximately fifty years, surface micro-structuring has been studied as a means of controlling friction and wear in sliding contacts [102], because of its relative simplicity for implementation and as it may be used in conjunction with other lubrication approaches for industrial applications [103]. FRANZEN et al. showed in [104] the influence of surface micro-structuring on the friction between the forming tool and the workpiece in comprehensive strip drawing and deep drawing experiments, for different product shapes considering steel and aluminium sheets. Generally, from the tribological point of view, the surface should fulfil three main requirements. The surface has to store and transport lubricant and additionally has to pick up wear particles. The micro-spaces on the conventionally very smooth tool surface can store and reserve the lubricant during the process (lubricant pockets), and consequently improve the tribological properties of the surface. Also in lubricant-free conditions, the wear particles can be collected between the micro-holes and improve the lifetime of the tools by preventing the wear and galling [105]. There are different techniques or manufacturing processes of surface texturing. LASAGNI et al. compared in [106] the different micro-structuring methods regarding the fabrication speed and structure size (see Figure 2-11). The conventional micro-milling processes can achieve a relatively high surface structuring speed (~10^{-2} m²/min), but with a limited resolution, generally between 15 and 100 µm. Electron and Ion-Beam lithographic methods have been also used to fabricate high-resolution surface patterns with feature sizes even smaller than 100 nm, but with a very slow fabrication speed [107]. In addition, almost all lithographic methods are limited to planar surfaces. A very advantageous method for micro-structuring is provided by laser processing techniques. Laser-based fabrication methods offer several advantages due to their remote and thus contactless operation, their flexibility during materials processing, as well as their precise energy deposition. *Direct Laser Writing* (DLW) has been, for example, utilised to structure several materials with features generally between 1 and 100 µm [108]. However, achieving resolutions lower than 5 µm is normally associated with an increased technical complexity and long processing times [106].

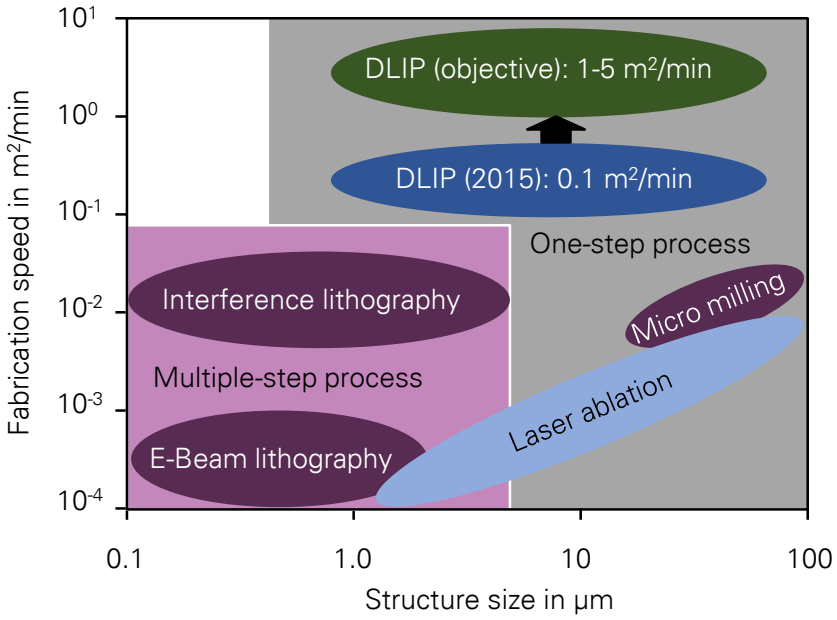

Figure 2-11: Different micro-structuring technologies differing from the surface fabrication speed and structure size [106]

An innovative solution for high-speed surface patterning of periodic structures in a one-step process is *Direct Laser Interference Patterning* (DLIP). Here, periodic structures can be produced in different materials including metals, ceramics, polymers, and coatings in a single step process [109]. A significant advantage of this technique compared with other surface structuring methods is that large areas can be processed within a short period. This method is particularly suited to fabricate periodic patterns on planar, as well as non-planar surfaces. Moreover, DLIP enables the fabrication of complex structures by systematically varying the dimensions of the gratings superimposed upon each other [110]. The DLIP process employs the interference generated by coherently overlapping two or more laser beams and thereby, producing a periodic modulation of the laser intensity (see Figure 2-12-A).

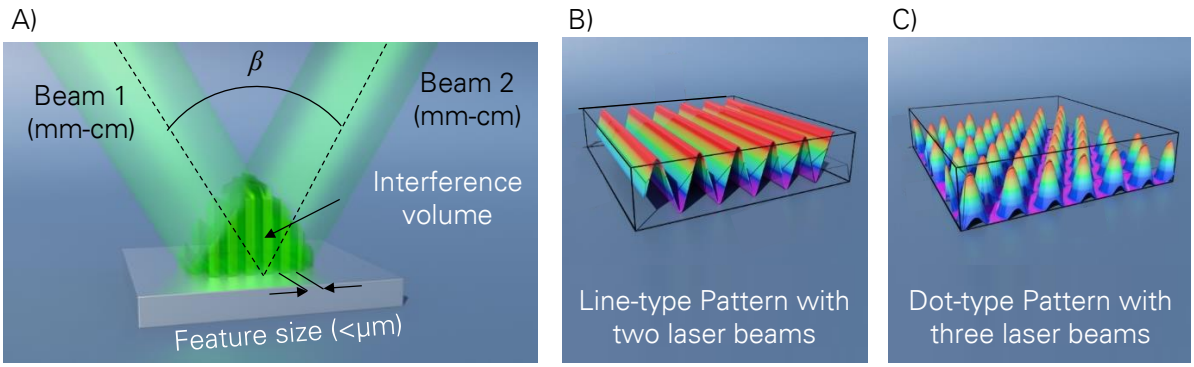

Figure 2-12: Direct Laser Interface Pattering; A) schematic of the interference principle, B) line-type pattern with corresponding two laser beams and C) dot-type pattern with corresponding three laser beams [111]

The shape of the interference pattern is directly transferred to the material surfaces and depending on the number of beams used, different geometries are possible [112]. In order to fabricate one and two-dimensional periodic microstructures on the surface, a two and three beam interference setup can be utilized (Figure 2-12-B and Figure 2-12-C) [111]. Recent studies show that the tribological performance of ta-C coatings can be further improved by a texturing of the surface [113].

In [114], the effect of local transformation of the ta-C coating by means of the DLIP method from sp^3-hybridised carbon into sp^2-rich material is investigated. In this study, the ta-C coated samples of the draw-bend test are structured with the DLIP process using a 532 nm ns-pulsed laser system. Three different patterns (dot-like, line-like and, cross-like patterns) with a structure period of Λ = 10 μm are compared with an unstructured ta-C coated tool (reference) to investigate the impact of local graphitisation of the ta-C film on its wear behaviour, and the results are shown in Figure 2-13-A. As the diagram indicates, all three types of DLIP structured samples exhibit much more resistance against wear. The light microscopic images of the sample shown in Figure 2-13-B reveal that the height of structures after 40000 mm drawing is not decreased dramatically.

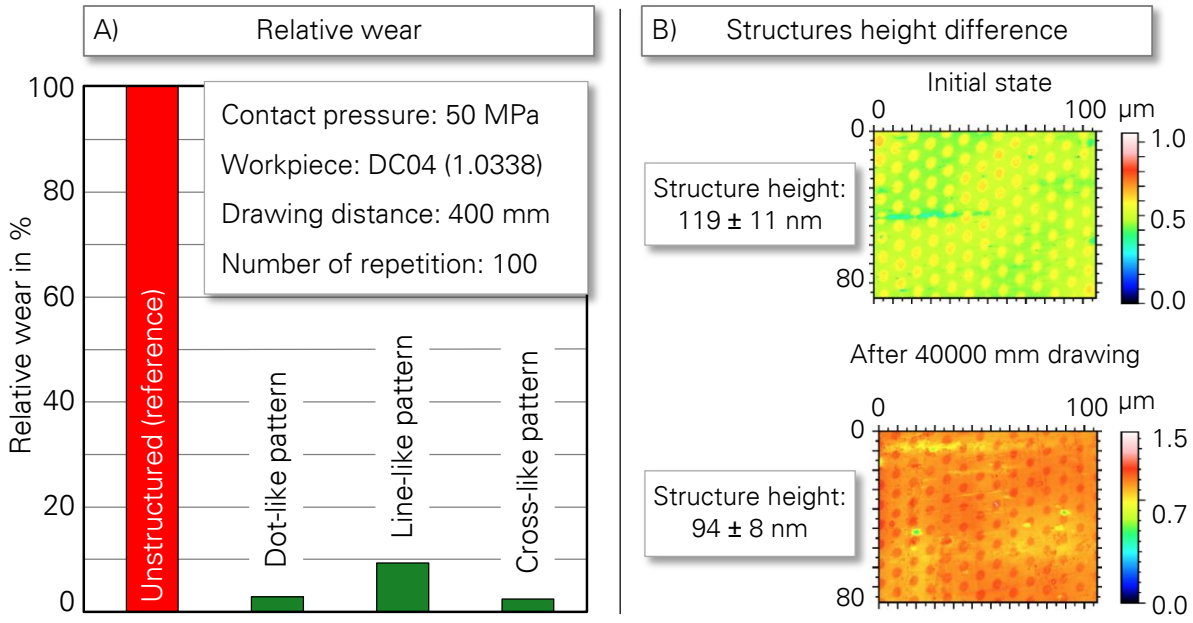

Figure 2-13: Comparison between unstructured and DLIP structured ta-C coating regarding wear reduction by the draw-bend test; A) relative wear and B) structure height differences before and after testing [114]

This fact can be explained by the interaction of wear particles in the contact zone and the role of sp^2-bonded carbons on the adhesion strength of the coated layer. For the unstructured samples, wear particles strongly interact in the contact zone, as they tend to continuously agglomerate and collapse, resulting in an increase of shear stress in the interface between the substrate and the coated layer, and as a consequence leads to further delamination of the

layer. On the other hand, the patterned surfaces offer the possibility to store wear particles in the topographic valleys [115]. Therefore, the topology of microstructures can affect the storage manner of wear particles and then the wear behaviour of the tool. The second reason for wear reduction through micro-structuring is due to the physical properties of sp^2-bonded carbons in the ta-C layer. Here, the localised sp^2-bonded carbons become more intense towards the substrate-film interface to provide better roughness and adhesion, while the remaining sp^3- bonds have the beneficial effect of friction reduction as shown by MERKLEIN in [116].

Apart from surface treatment technologies, the reduction of the frictional contact area, as well as the integral of the contact pressure over the contact area, can also reduce the amount of frictional forces. This is discussed in Chapter 4 in detail.

2.6 TRIBOLOGICAL TESTING METHODS

Large amounts of test methods for the measurement of the friction coefficient, often referred to as tribometers, have been developed over the years for a variety of purposes. In this section, only a small number of tests are presented. These tests are considered either because of being frequently used, or for representing interesting recent developments in the field of tribotesting [117].

2.6.1 Tribometer

A tribometer is the general name given to a machine or device used to perform tests and simulations of friction, wear and lubrication, which are the subject of the study of tribology. Pin-on-disk and ball-on-disk are two common types of tribometers. According to DIN 50324 [118], in the pin-on-disk (or ball on disk) a pin with a rounded tip is positioned perpendicular to the other, usually a flat circular disk. A ball, rigidly held, is often used as the pin specimen. The testing machine causes either the disk specimen or the pin specimen to rotate about the disk centre. In either case, the sliding path is a circle on the disk surface. The pin specimen is pressed against the disk at a specified load. In this way, by knowing the pressing force, based on the COULOMB friction model, the friction coefficient can be measured [119]. However, this testing method does not consider the surface enlargement during the process in metal forming. Furthermore, due to the high level of uniform pressure (HERTZIAN pressure) in this testing method, the friction coefficient cannot be measured under conditions similar to those encountered in the real forming process. Therefore, in the sheet metal forming process, the friction coefficient will be evaluated through other testing methods like strip-drawing or the draw-bend test.

2.6.2 Strip-drawing and the draw-bend test

For the forming processes with high normal pressure, the dependency of the friction coefficient on the parameters like pressure, velocity, and sliding direction has to be measured through a proper friction test method [120]. Strip-drawing and draw-bend friction tests are regarded as the best candidates for this purpose because of their known capability to change the contact pressure and sliding velocity [121]. In the strip-drawing test, a strip of metal is drawn through two friction pads that are pressed together with a defined normal force. The resultant friction force on the metal strip can be recorded with a metrological device, with which the COULOMB friction model is determined [7]. However, the non-uniform pressure distribution at the die edge radius with an arbitrary bending angle can be mapped in the draw-bend test [122]. The draw-bend test will be performed in a two-step process. First, a strip will be drawn over a freely turning roller and due to bending and unbending forces, F_b can be determined as the difference between the pulling and the back tension forces F_1 and F_2, respectively. A second strip will then be drawn over a fixed roller, and the corresponding pulling and back tension forces F_1 and F_2 can be measured. Figure 2-14 shows the mechanism of a draw-bend test under deflection angle of θ.

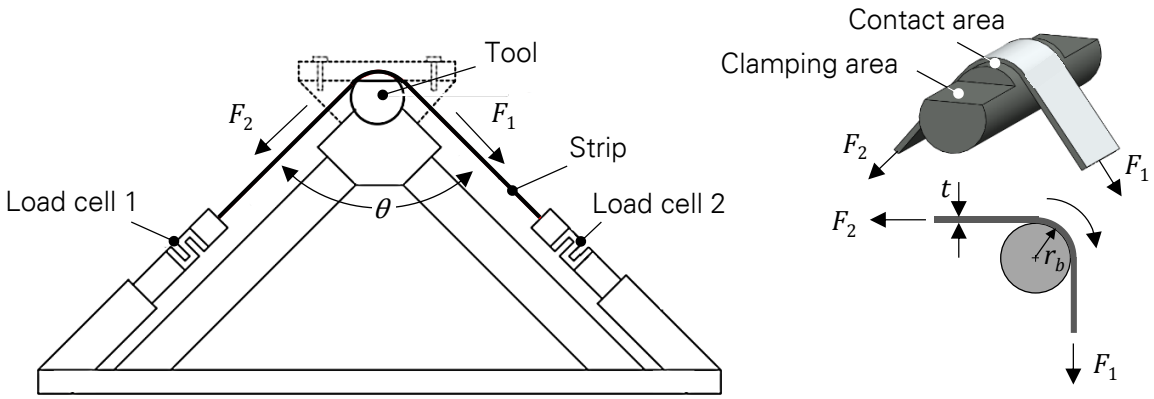

Figure 2-14: Schematic overview of a draw-bend test for the calculation of the friction coefficient under high non-uniform pressure

Several considerations, each derived based on different sets of assumptions, have been developed to determine the friction coefficient from the measured forces during a draw-bend test [123]. FOX et al. developed a model in [124] to express the friction coefficient for a general deflection angle θ based on an integrated force balance solution (Equation 2-16). In order to consider the effects of the bending radius r_b and the sheet thickness s_0, FOX et al. modified this model in [124] and developed a more detailed expression of the friction coefficient in a draw-bend test (Equation 2-17). This equation, which was originally obtained from a force balance, is equivalent with the model of SULONEN et al. [125], which was developed with an incremental energy balance integrated over a 90° arc (Equation 2-18). A fourth solution developed by WILSON et al. [126] is based on a macroscopic force balance that assumes the external forces should be balanced by a roller force due to the effects of the contact pressure

and an average frictional force (Equation 2-19). Their result ignores both the effects of bending and sheet thickness. It should be noticed that the friction coefficient from Equation 2-19 is derived from a system force equilibrium and gives the averaged value of the pressure distribution at the pin / strip contact [127]. Table 2-2 summarises the Equations 2-16 to 2-19.

Table 2-2: Common equations used to calculate the friction coefficient for the draw-bend test

Summary of approaches	Equation	
Incremental force balance; ignore sheet thickness; variable bending angle	$\mu = \frac{1}{\theta} \ln \frac{F_1 - F_b}{F_2}$	2-16
Incremental force balance; include sheet thickness; variable bending angle	$\mu = \frac{1}{\theta} \left(\frac{r_\mathrm{b} + 0.5 s_0}{r_\mathrm{b}} \right) \ln \left(\frac{F_1 - F_b}{F_2} \right)$	2-17
Incremental force balance; include sheet thickness; 90° bending angle	$\mu = \frac{1}{\pi} \left(\frac{r_\mathrm{b} + 0.5 s_0}{r_\mathrm{b}} \right) \ln \left(\frac{F_1 - F_b}{F_2} \right)$	2-18
System force balance; ignore sheet thickness; variable bending angle	$\mu = \frac{2}{\theta} \left(\frac{F_1 - F_2}{F_1 + F_2} \right)$	2-19

2.7 SUMMARY OF CHAPTER 2

The majority of automotive parts are manufactured by means of the sheet metal forming technology. The process window in sheet metal forming is highly dependent on the material flow and restricting parameters. For a given blank shape and final part geometry, it is necessary to optimise the retention forces applied to the blank in order to control the material flow and as a result, enlargement of the process window. Friction is one of the most restricting parameters in sheet metal forming operations. In most cases, it is beneficial to reduce the friction between the tool and the workpiece to increase the process window, the extension of the tool life, the prevention of galling and seizure, and the improvement in the surface finish of the products. There are a number of ways to reduce the friction, like lubricating, improving the surface roughness, reducing the forces acting on the surfaces, surface texturing and reducing the contact area.

In the sheet metal forming process, using lubrication reduces the total punch force. However, from both an economic as well as an ecological point of view, there exists a strong demand to avoid lubricants within metal forming processes. For the upcoming process steps after

forming, which are required to have a perfectly clean surface, it is essential to remove the lubricant from the workpiece. Removing the lubricant from the semi-finished parts can be done after some post-treatment process, which are costly and time consuming. Therefore, using the lubricant in the process leads to an increase in the number of process steps. Besides the increase of process steps, lubricants in the metal forming process have environmental and health burden disadvantages. Therefore, various green manufacturing strategies under laboratory conditions have been developed by manufacturers to reduce the friction forces, and as result reduce the amount of lubrication.

3. OBJECTIVES

The conservation of required energy, lubricants and other resources for forming processes is a major engineering challenge from the economic and ecological points of view. Therefore, developing economically beneficial green technologies - from process and tooling to the entire enterprise - is one way to insure that future manufacturing systems are sustainable. To achieve this, innovation in advanced manufacturing is needed.

In sheet metal forming, especially the deep drawing process, lubricants are of importance to reduce the frictional forces in order to enlarge the process window and increase the lifetime of tools. So far, the elementary requirements for a nearly lubricant-free deep drawing process are usually discussed along with tools materials and tool coating to decrease the frictional force and increase their lifetime. However, a totally lubricant-free deep drawing process has economic as well as ecological advantages. Figure 3-1 shows the schematic benefits of a lubricant-free deep drawing process for industrial applications.

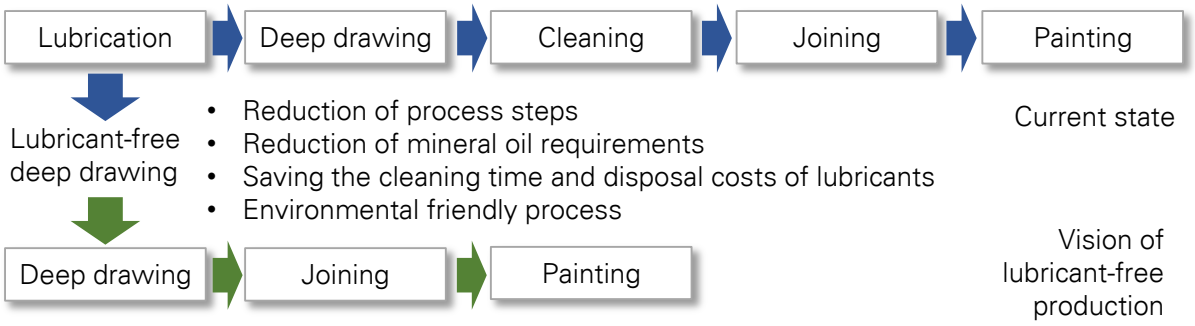

Figure 3-1: Advantages of a lubricant-free deep drawing process according to [128]

In order to realise an economically applicable lubricant-free deep drawing process, an adapted tool design is required to minimise the frictional force during the process. The overall goal of this thesis is to design a lubricant-free deep drawing process by means of adapted tools, which ensures the process window despite the absence of lubricants by minimisation of frictional forces between the sheet and tools, and also the control of material flow during the process.

Since in the absence of lubricants, relevant shear stresses arise because of relative movement between the sheet and tools, the new tool design must be able to reduce the frictional forces to the smallest possible extent. In order to decrease the amount of frictional force for a given friction coefficient, the integral of the contact pressure over the contact area has to be reduced by means of macro-structured tools. In this way, the contact area between the workpiece and tools will be reduced to some lines or even some points. As a result of this, the risk of wrinkling in the unsupported part of the sheet metal increases, because the usually utilised blankholder force is not applicable. By increasing the geometrical moment of inertia of the sheet, this effect can be avoided. This can be achieved by immersing the peaks of the blankholder's

structure slightly into the valleys of the drawing die and generating a wave structure in the sheet metal perpendicular to the tangential stress. This method can increase the buckling stiffness of the sheet metal. Therefore, the macro-structured tool can ensure the process stability regarding the process limits, i.e. avoiding wrinkling and bottom cracking during the lubricant-free deep drawing to ensure a process-reliable production.

Generally, the method developed for the lubricant-free deep drawing process should fulfil the function of usual lubricants by means of the process and tool design. Moreover, an increase in sustainability should be achieved against conventional process chains.

For understanding the process and its influencing parameters, as well as a time efficient process design in advance, the process limits should be modelled analytically. Therefore, the sub-goal of the thesis is to develop an analytical model for the deep drawing of rotationally symmetric parts based on plasto-mechanical approaches, which can predict the stability of the process as a function of the tool and workpiece input parameters. In the further development step, the model should be extended to allow the prediction of process stability for complex 3D geometries. The feasibility of the process, the results of the analytical models and the shape accuracy of the deep drawn parts should be verified by means of numerical simulations as well as experimental tests.

4. METHODOLOGY AND APPROACH

As already discussed in previous chapters, there exists a strong demand to realise a lubricant-free deep drawing process without any negative effects on the process window. For this purpose, the amount of frictional forces has to be reduced. In section 2.1.1, the Equations 2-4 and 2-5 showed that the flange area and the die edge radius of the deep drawing die are the most critical area regarding the friction. In section 2.5, it was shown that there are several investigations and examinations which focus on reducing the friction on the die edge radius of deep drawing tools by means of various surface treatments in order to realise a lubricant-free process. However, in order to realise a total lubricant-free deep drawing process, the friction in the flange area should also be minimised. In order to study the importance of friction on the flange area of a deep drawing process, a number of calculations based on Equation 2-2 to 2-6 are performed. The results show that the share of friction on the flange area F_{ff} from the total punch force in deep drawing of rotationally symmetric cups may be about 20%, depending on the dimension of the parts. In this context, the friction coefficient and the blankholder force play an important role. In order to clarify the importance of these process parameters on friction reduction in the flange area, Figure 4-1 gives an overview.

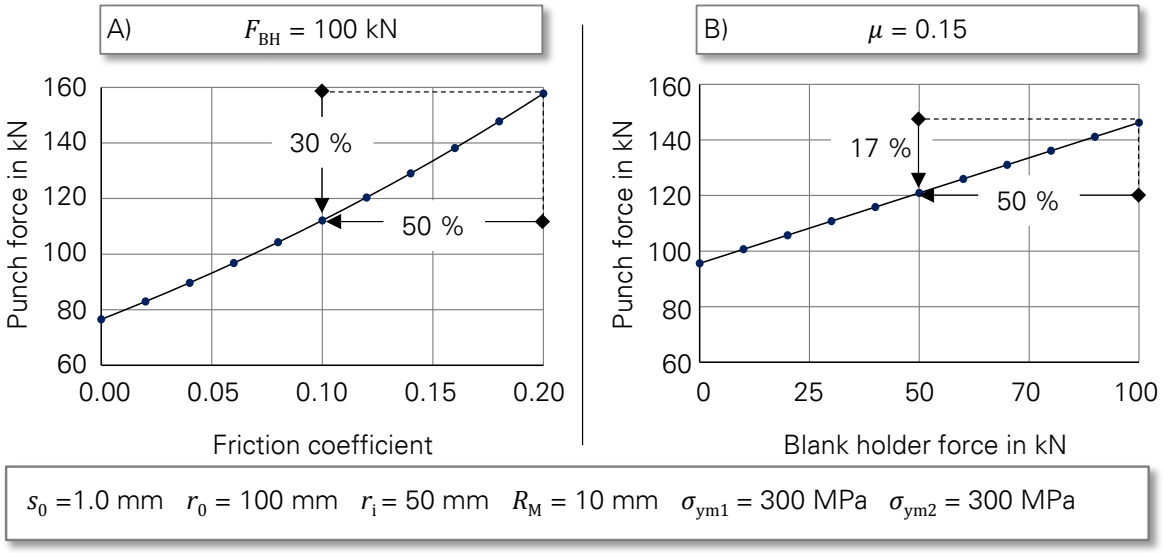

Figure 4-1: Reduction of punch force in deep drawing process through 50% reduction of A) friction coefficient and B) blankholder force

The diagram in Figure 4-1-A shows that for a constant blankholder force (F_{BH} = 100 kN), 50% reduction of the friction coefficient leads to almost 30% reduction of the total punch force, while the diagram in Figure 4-1-B indicates that for a constant friction coefficient (μ = 0.15), 50% reduction of the blankholder force can reduce the total punch force by up to 17%. Therefore, improving the tribological behaviour of the tool through surface treatment as the current state of the art, and reduction of the total surface pressure, are two methods to decrease the frictional force. Consequently, a combination of these approaches can lead to

realising a total lubricant-free deep drawing process. Since reducing the integral of the contact pressure over the contact area can reduce the amount of frictional force, a novel approach should be taken towards reduction of the contact area in the flange area. Therefore, the proposed strategy in this thesis is to minimise the whole contact surface in the forming tool through macro-structuring. In the following, this is described in detail.

Generally, the frictional force is the product of frictional shear stress and the contact area as follows:

$$F_\mathrm{f} = \int \tau_f \cdot \mathrm{d}A_\mathrm{r} \qquad 4\text{-}1$$

Here F_f is the frictional force, τ_f the frictional shear stress (see section 2.2.2) and A_r the real contact area. This equation can be developed based on the COULOMB friction model:

$$F_\mathrm{f} = \int \tau_f \cdot \mathrm{d}A_\mathrm{r} = \int \sigma_\mathrm{n} \cdot \mu \cdot \mathrm{d}A_\mathrm{r} \qquad 4\text{-}2$$

Here, σ_n is normal stress and μ the friction coefficient. As the Equation 4-2 shows, the normal stress, friction coefficient and real contact area have a contributing role in friction force during the process. Based on this equation, a way to reduce the total friction force is reduction of the contact area. However, this leads to increase of contact pressure locally, because of the HERTZIAN contact mechanism [129]. But, since the relative high normal contact pressure acts on only very small zone, the resulting friction force in the integral sum will be minimised. Based on this consideration, to reduce the contact area between the tools and the workpiece, macroscopic-structuring of the tools is proposed in this thesis. In this way, the contact area between the workpiece and the tools will be reduced to a small number of lines, and as a result the integral of the total contact pressure over the contact area will be reduced compared with conventional tools. This is depicted schematically in Figure 4-2.

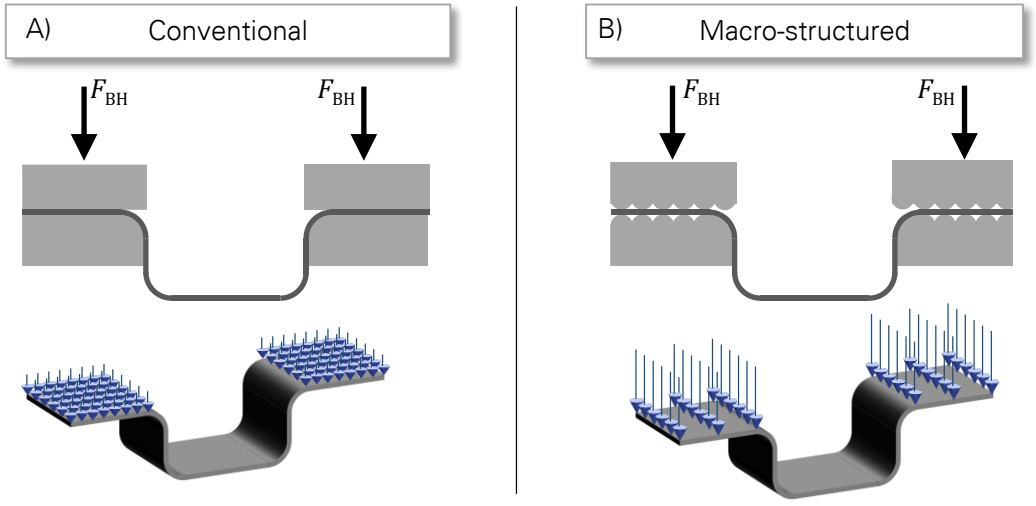

Figure 4-2: Surface pressure in A) conventional and B) macro-structured deep drawing tool

In addition, macro-structuring can be used as an analogy to the drawing bead, in order to control the material flow in the flange area. This aspect is contrary to the reduction of friction, but is essential for the successful design of a deep drawing process. Thus, the macro-structuring is provided to reduce the frictional force, as well as for control of the material flow. For this purpose, two different tooling arrangements can be considered with the capability to improve the frictional behaviour, as well as to influence the material flow in the flange area of the deep drawing tool. These differ in the radial offset between the structures of the blankholder and the drawing die as shown in Figure 4-3. In the next sections, the functions and application types of each tooling arrangement are discussed regarding the process stability.

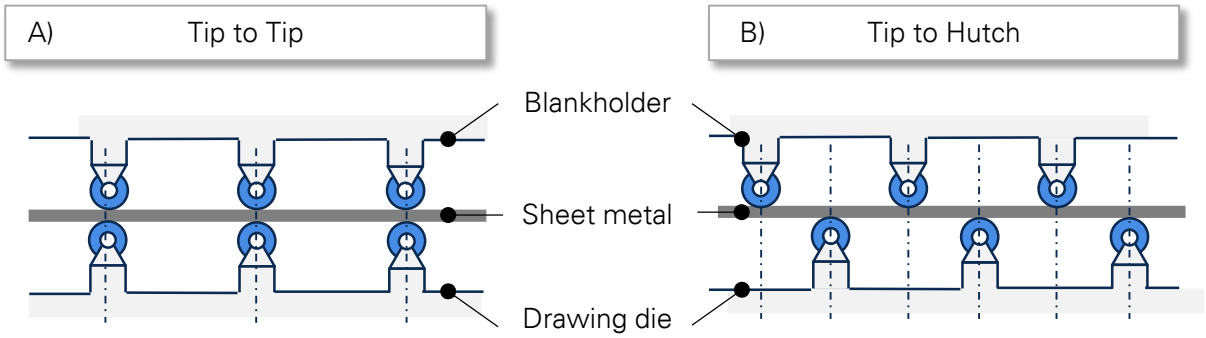

Figure 4-3: Tooling arrangement for macro-structured deep drawing; A) Tip to Tip and B) Tip to Hutch

4.1 MACRO-STRUCTURING: TIP TO TIP

In the deep drawing of parts with relatively complicated geometries and the existence of tangential compressive stress in the flange area, the risk of wrinkling in the unsupported sheet metal area will be increased, because the usually utilised blankholder force is not applicable. To avoid this, the geometrical moment of inertia of the sheet metal should be increased. But, this is not applicable with the tooling arrangement of Tip to Tip, due to a two-sided contact between the sheet metal and the tool. Therefore, it can be concluded that this tooling arrangement can enlarge the process window regarding bottom cracking and cannot prevent the risk of wrinkling. Nevertheless, this tooling arrangement can be applied only for simple geometries, where there is no tangential compressive stress in the flange area like the draw bending of U-Channels.

4.2 MACRO-STRUCTURING: TIP TO HUTCH

As mentioned above, in order to avoid the risk of wrinkling and enlarge the process window in the deep drawing process with macro-structured tools, the geometrical moment of inertia of the sheet metal against tangential compressive stresses should be increased. This can be achieved in the tooling arrangement Tip to Hutch by immersing the blankholder slightly into the drawing and die inducing an alternating bending mechanism. This creates a wave structure

in the flange with the desired increased geometrical moment of inertia. Contrary to draw beads, which are primarily used to control the material flow, macro-structured deep drawing tools with the Tip to Hutch arrangement can be used to reduce the frictional force due to a minimal contact area and to increase the resistance against wrinkling. Consequently, based on fundamental studies regarding the macro-structured deep drawing tool with induced alternating bending, following positive and stabilising effects can be achieved [130]:

- reduction of the contact area up to 80%,
- increasing the resistance of the sheet against wrinkling and
- possible material flow control.

Figure 4-4 compares schematically the conventional and macro-structured tool regarding the amount of friction, and also shows how the generated alternating bending can increase the geometrical moment of inertia of the sheet metal to prevent the wrinkling.

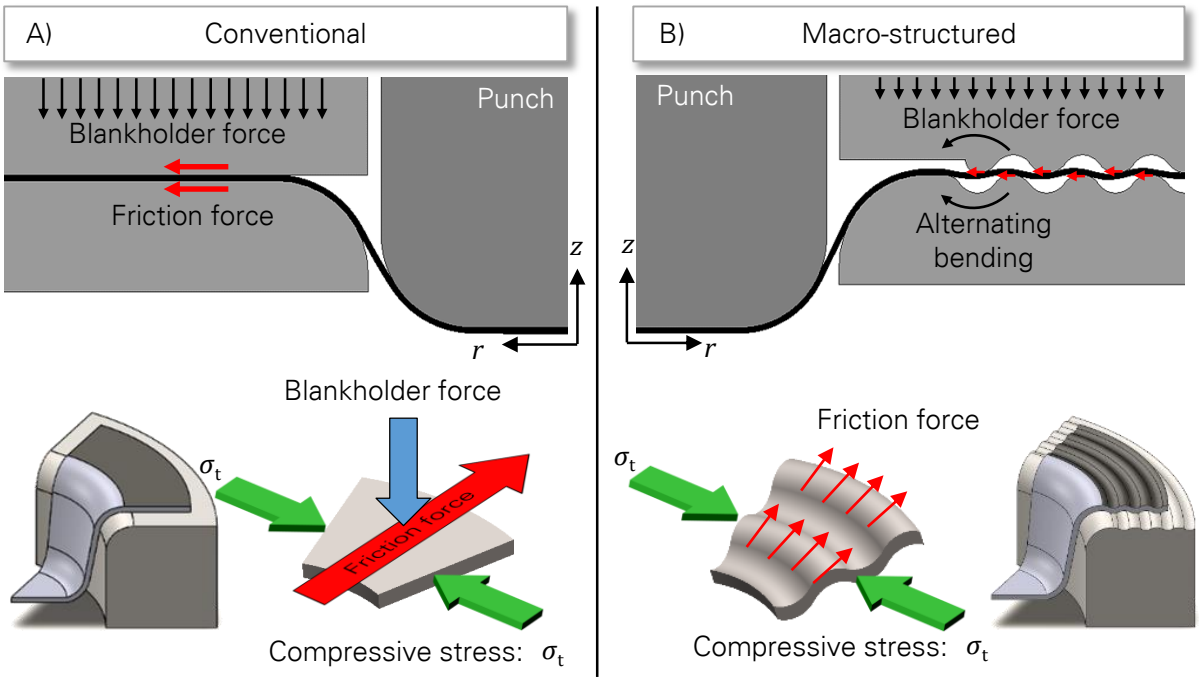

Figure 4-4: Comparison between the A) conventional and B) macro-structured deep drawing process

Since the alternating bending increases the stiffness of sheet metal, it can be expected that the process window will be enlarged in contrast to the Tip to Tip tooling arrangement regarding the reduction of bottom cracks as well as wrinkling. Figure 4-5 compares the process window in the conventional and macro-structured deep drawing process.

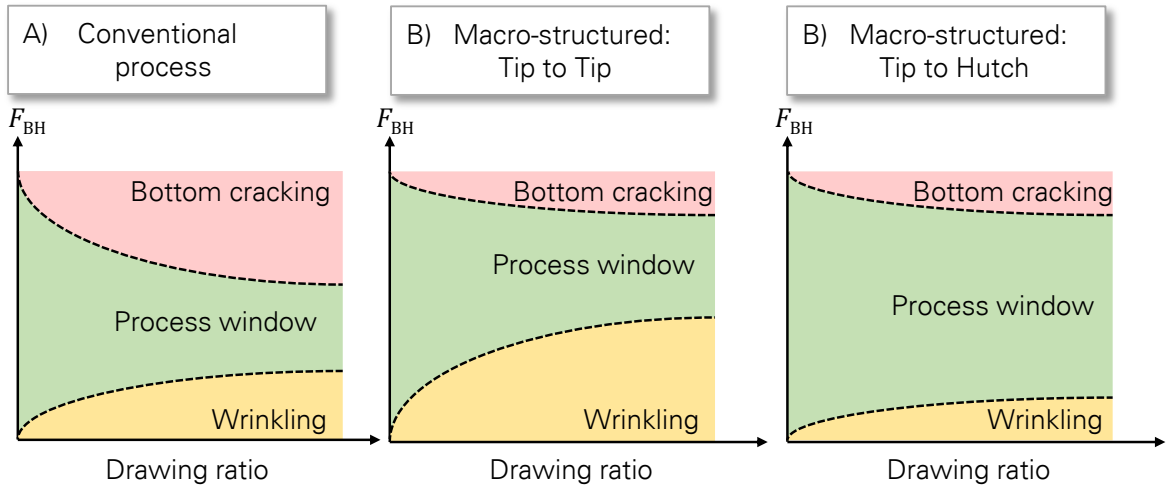

Figure 4-5: Process window in A) a conventional deep drawing process, B) macro-structuring the tools with Tip to Tip tooling arrangement, and C) macro-structuring with Tip to Hutch tooling arrangement

However, the geometry of induced alternating bending plays an important role in process stability. Wavelength and immersion depth are two parameters which determine the geometry of alternating bending. Wavelength λ is the distance between two supporting points and immersion depth δ is the height difference between the peak of the die and the blankholder's structures as shown in Figure 4-6.

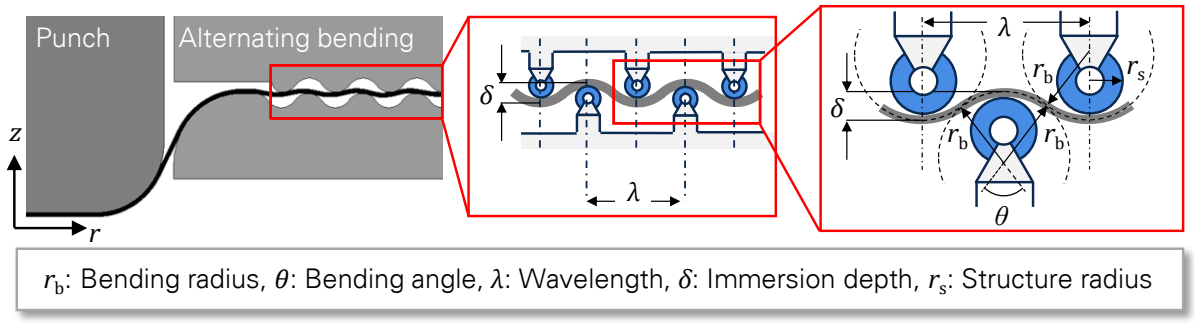

Figure 4-6: Geometrical parameters of induced alternating bending during the process

These two parameters can be used as setting parameters in order to ensure a stable process for the deep drawing with macro-structured tools. Even by a very low immersion, a plastic bending mechanism and consequently a further strain hardening in the sheet metal can occur. That is why besides the geometry part, material properties and the sheet metal thickness, the radius of alternating bending is an important influencing factor in the stability conditions of products. Assuming that there are constant mean radius in the sheet metal over the flange area, the alternating bending radius can be calculated as a function of the wavelength and immersion depth as follows:

$$r_b = \frac{\lambda^2}{16\delta} + \frac{\delta}{4} \qquad 4\text{-}3$$

Figure 4-7 shows how the bending radius from Equation 4-3 will be reduced by increasing the immersion depth for different wavelengths. Assuming that the plastic strain begins from ε_{pl} = 0.002, for a sheet metal from steel with a thickness of s_0 = 0.6 and 0.8 mm, the critical bending radius to start a plastic bending mechanism will be 150 and 200 mm, respectively. This value corresponds to an immersion depth of δ > 0.05 mm. Based on this assessment, even by small immersion depths and large wavelengths, a plastic bending mechanism will occur which leads to a further strain hardening in the flange area. However, inducing plastic alternating bending requires further forming energy, which will be delivered from the punch force.

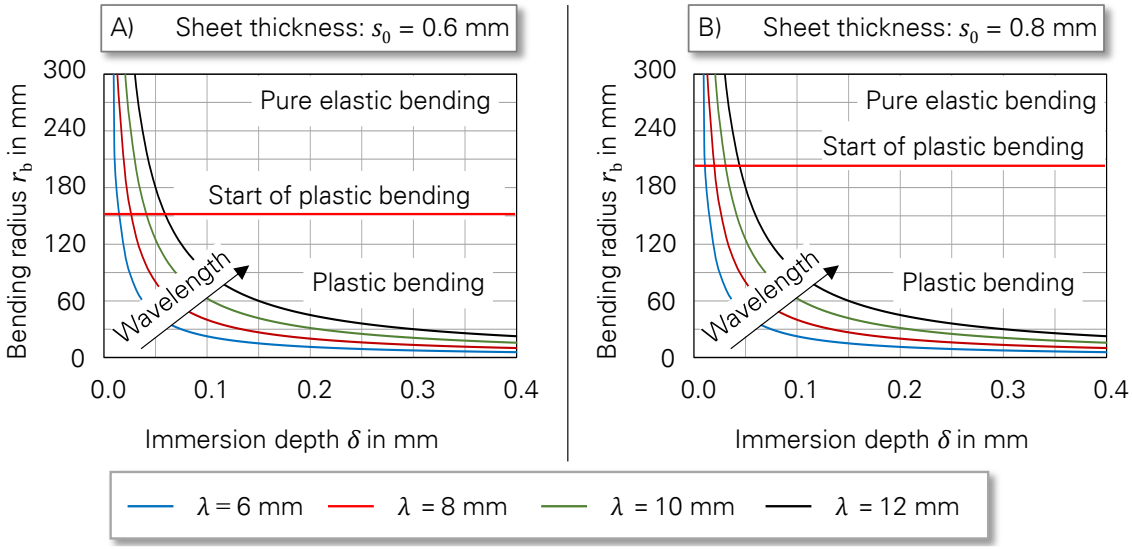

Figure 4-7: Change of the alternating bending radius as a function of immersion depth and wavelength; A) s_0 = 0.6 mm and s_0 = 0.8 mm

In other words, in the deep drawing process with macro-structured tools the frictional forces will be reduced, but in contrast the bending energy will be increased. The energy to induce the alternating bending supersedes the frictional energy in the process and makes the lubricant-free process possible. Therefore, in order to reach the same process window of conventional deep drawing for the macro-structured process, the energy to induce the alternating bending should be smaller than the energy to overcome the friction. This can be achieved through a proper tool design. Figure 4-8 compares the energy terms in the conventional and macro-structured processes.

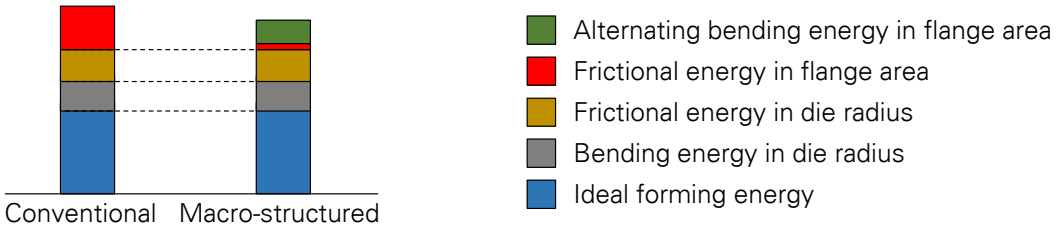

Figure 4-8: Energy terms in the conventional and macro-structured deep drawing processes

4.3 SUMMARY OF CHAPTER 4

In order to realise a lubricant-free deep drawing process, the present frictional forces in critical frictional areas of the tools, namely the flange area and the die edge radius, should be minimised to ensure the large process window. There are a number of techniques to reduce the friction coefficient at the die edge radius by means of surface treatment methods. But, friction reduction in the flange area of deep drawing tools has not been comprehensively studied so far. The integrative approach to minimise the frictional forces during the process is based on macro-structuring of the flange area with different tooling arrangements. The variant Tip to Tip can minimise the frictional shear stress through the reduction of the contact area. Nonetheless, this increases the risk of wrinkling which is caused by compressive tangential stress in the free, non-contact areas of the sheet metal. To avoid wrinkling, the sheet metal in the flange area should be stabilised by increasing its geometrical moment of inertia. This can be achieved by immersing the blankholder slightly into the drawing die, inducing an alternating bending mechanism (variant Tip to Hutch). Therefore, the friction in the deep drawing process with macro-structured tools will be reduced while the bending energy increases. Therefore, for a deep drawing process with a large possible process window, an optimum tool design is required.

5. EXPERIMENTAL SETUP

The realisation of a lubricant-free deep drawing process and verification of the approaches require a comprehensive experimental test. In this chapter, press machines, tooling and workpiece material are used, as well as conventional and macro-structured tools are introduced for the experimental tests.

5.1 PRESS MACHINES

The experimental tests are carried out with two different hydraulic machines, which are introduced in this section.

5.1.1 Hydraulic press BUP 600

The hydraulic press BUP 600 sheet metal testing machine by *Roell Amsler* makes it possible to test sheet metal materials for complex deformation conditions, or to carry out standardised and approved sheet metal test methods such as the Bulge test, the cupping test, or the recordings of FLC curves. The machine is equipped with a *ViALUX*-camera system, which permits visual evaluation of the local deformation changes by means of visio-plastic tracking. The machine provides a maximum punching and clamping force of 600 kN, with a maximum testing speed of 20 mm/s over the maximum ram stroke of 120 mm. The machine can control the travel of a deep draw piston, its load and the speed of the draw piston continuously with its hydraulic drive. Figure 5-1 shows the fundamental components of the sheet metal testing machine.

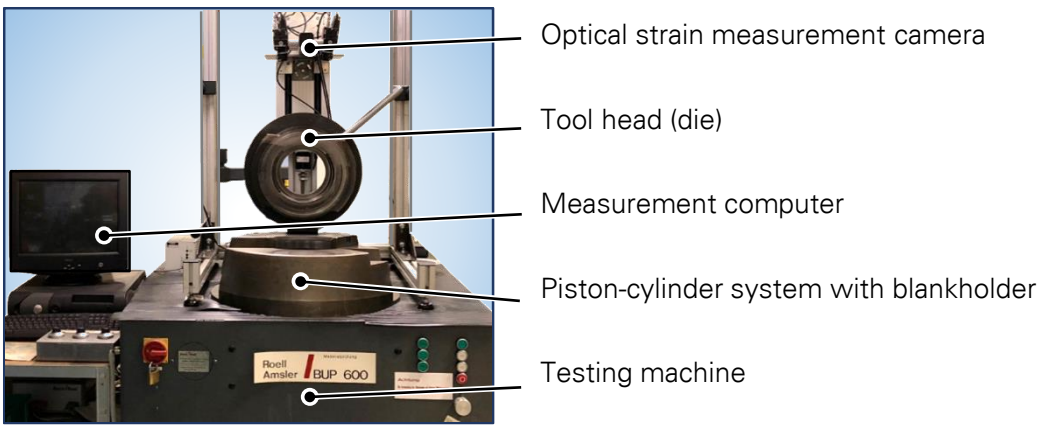

Figure 5-1: Hydraulic press machine BUP 600

For the deep drawing process, the sheet is clamped between the blankholder and the die. The punch moves upwards against the clamped sheet metal and draws it into the forming die. The measurement computer is provided for the evaluation and analysis of the measured forces and resultant driven forming energy. Regarding the measurement technology, there is a

hydraulic pressure sensor integrated in the testing machine, and the pressure will be converted into force by means of an integrated measuring board.

5.1.2 Hydraulic press Röcher RZP 250

The second hydraulic press which will be used for deep drawing of complex part geometries is RZP 250 from *Röcher Maschinenbau* and is shown in Figure 5-2. This press will be used for deep drawing of complex big size geometries because of its high nominal force (2500 kN). The table to the right of Figure 5-2 shows the properties of the press. The punch force from experimental tests is measured indirectly from the hydraulic pressure of the press machine. The hydraulic cylinder of the press machine has two pistons with mutual hydraulic pressure and known surface. Measuring the acting hydraulic pressure on each piston, it is possible to calculate the plunger force. Obviously, there are some disturbance variables like friction between the cylinder and the pistons, friction on guides (tool and press machine), the weight of the plunger, tool, etc. In order to eliminate these disturbance variables and obtain the pure forming force, the measured value should be calibrated based on a comparison with an idle operation. Through subtracting the measured force of an idle operation from the total force, it is possible to measure the forming force with a very good accuracy.

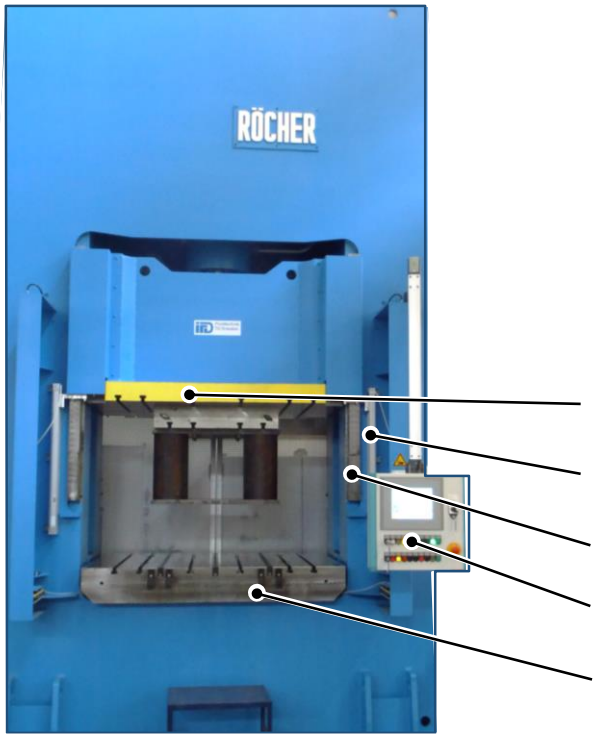

Plunger nominal force	2500 kN
Plunger hub	600 mm
Working velocity	max. 41 mm/s
Rapid traverse speed	300 mm/s
Die caution	4 x 250 kN
Die caution hub	200 mm

Figure 5-2: RÖCHER RZP250 Press

5.2 TOOLING MATERIAL

High-duty, cold work tool steel 1.2379 (EN X153CrMoV12) is widely used in industrial tool making applications such as deep drawing, punching and blanking of stainless steel, brass, copper, zinc and hard abrasive materials, generally due to its excellent properties like high yield stress, high hardness, very good dimensional stability, high compressive strength, good tempering resistance and high abrasive and adhesive wear resistance. Furthermore, it is a very good base material for PVD and CVD coating, as well as nitriding due to its secondary hardening properties [131]. Therefore, it is chosen as the tooling material for experimental tests in this thesis. The chemical composition of 1.2379 is shown in Table 5-1.

Table 5-1: Chemical composition of the studied tool steel (in wt. %) [132]

Designation to	C	Cr	Mo	V
1.2379	1.5 - 1.6	11.0 – 12.0	06 - 0.8	0.9 – 1.0

Tools made by tooling steel 1.2379 can be hardened up to a hardness level of 60-62 HRC through heat treatment.

5.3 WORKPIECE MATERIALS

Steels and aluminium alloys are widely used materials in today's industrial applications involving simple to complex deep drawing processes which require very high formability, mainly ductility and drawability. In the automobile industry, exterior components such as doors (frames and panels), front fenders, hoods (frames and panels), roof panels, trunk lids, and rear side panels are made up of steel and aluminium alloys [133]. Cold-rolled low-carbon steels as one of the most common forms of steel for forming applications, with the European standard EN 10130: 2006, are being produced for industrial applications in a broad spectrum of grades, meeting the specifications as listed in Table 5-2 [134].

The mechanical properties of the individual cold-rolled low-carbon steel grades are characterised by the yield point and tensile strength, as well as by a guaranteed minimum fracture strain. Because of the very low carbon content, minimal alloying elements and a relatively simple ferritic microstructure, they have excellent formability, relatively low strength and also some of the best weldability of any metal. Therefore, these grade of steels with a usual thickness ranging from 0.5 to 3.0 mm [135] have long been used for many applications in the automotive industry, including the body structure, closures, and other ancillary parts. Among these grades, the fracture strain of DC01 and DC03 is lower than DC04, DC05 and DC06 (see Table 5-2). Besides that, DC05 and DC06 have lower yield stresses compared to DC04. Furthermore, the formability of DC06 is highly dependent on the strain rate [136].

Therefore, DC04 was chosen as the workpiece material for the experimental tests in this thesis because of its excellent formability properties.

Table 5-2: Low-carbon steel grades with mechanical properties and chemical components [134]

Designation to		Mechanical properties			Chemical composition			
EN 10130	EN 10027-2 Material No.	σ_{y0} in MPa	R_m in MPa	A_{80} min %	C %	P %	S %	Mn %
DC01	1.0330	280	270-410	28	0.12	0.045	0.045	0.60
DC03	1.0347	240	270-370	34	0.10	0.035	0.035	0.45
DC04	1.0338	210	270-350	38	0.08	0.030	0.030	0.40
DC05	1.0312	180	270-330	40	0.06	0.025	0.025	0.35
DC06	1.0873	170	270-330	41	0.02	0.020	0.020	0.25

Steel apart, the usage of aluminium in automobiles has been gradually increasing so that nowadays it is the second-most used material in automobiles and it has the potential to be used to substitute steel in car body sheet components and become the most-used material [137]. Among the aluminium alloys, both the 5000 and 6000 series show very excellent formability and have very good surface quality, though the 6000 series lose their formability because of their aging effect [138]. Magnesium is one of the most effective and widely used alloying elements for aluminium, and is the principal element in the 5000 series alloys [139]. When it is used as the major alloying element or combined with manganese, the result is a moderate to high strength, non-heat-treatable alloy. It is a readily weldable material used in a wide variety of applications, including pressurised vessels, buildings, transport and the automotive industry. EN AW-5182 and EN AW-5754 are the principal 5000 series alloys and are primarily used in the automobile industry [140]. Furthermore, they are also the key alloys utilised in the production of beverage cans, as well as electrical and computer components due to its good deep drawing and stretch behaviour [14]. Although both of them have very similar mechanical properties, EN AW-5754 is usually recommended for relatively high temperature applications [141]. Therefore, besides DC04, the aluminium alloy EN AW-5182 is chosen as the second workpiece material for the tests. This material is called AA5182 in this thesis. The most important mechanical properties and chemical components of AA5182 are listed in Table 5-3 and Table 5-4, respectively.

Table 5-3: Mechanical properties of AA5182 [142]

Designation to		Mechanical properties		
Material Nr.	Chemical symbol	σ_{y0} in MPa	R_m in MPa	A_{80} min. in %
EN AW-5182	EN AW-Al Mg4,5Mn0,4	125	275	28

Table 5-4: Chemical components of AA5182 in wt% [143]

Si	Fe	Cu	Mn	Mg	Cr	Zn	Ti
0.25	0.35	0.15	0.20-0.50	4.0-5.0	0.10	0.25	0.10

For the numerical simulations and analytical calculations, both testing materials should be characterised regarding their flow curve by means of uniaxial tensile tests at room temperature, which corresponds approximately to the same temperature as in the experimental tests. In order to take the effects of anisotropy and the rolling direction into account, tensile samples were cut in three directions (0°, 45° and 90° to the rolling direction) according to DIN 50125 [144]. Each test was repeated five times and the average flow stressed for DC04 and AA5182 are plotted with a red line in Figure 5-3-A and B, respectively.

Although the tensile test can be used to evaluate the flow curve of the materials, the range of the equivalent true strain in this test is limited. However, in reality, the materials undergo higher deformation, so that an equivalent true strain up to 1.0 is required for analysing the process. In order to extend the flow curves determined from the tensile tests, the curve must be extrapolated. Therefore, there are various approaches to extrapolate the flow curve [145]. Unlike material models which overestimate the flow stress at a high strain level, VOCE postulated the existence of a saturation stress at which the rate of hardening should be zero. Due to its intrinsic saturation character, this model gives a good flow stress description [146]:

$$\sigma_y = \sigma_\infty - (\sigma_\infty - \sigma_{y0}) \cdot e^{(-m\varepsilon_{pl})} \quad 5\text{-}1$$

Where σ_∞ is the asymptotic value for saturation strength (ultimate strength), σ_{y0} is the initial value of isotropic hardening, m and ε_{pl} are the characteristic strain constant and equivalent true strain, respectively. Although this model might underestimate the yield stress at very high strain levels, since the strain level in the sheet metal forming process is usually around 0.5, it can better describe the material behaviour than other models [147]. Moreover, in contrast to many other material models that rely on purely analytical curve fitting, each parameter of this model has physical significance and can be determined by a simple curve fitting [148]. The matched VOCE formulation parameters for testing both materials DC04 and AA5182 are listed in Table 5-5.

Table 5-5: Parameters of the VOCE model for testing both materials

Material	σ_∞ in MPa	σ_{y0} in MPa	m
DC04	420	155	7.5
AA5182	390	150	10

Based on fitting these parameters, the flow curves of DC04 and AA5182 are extrapolated regarding the VOCE material model up to an equivalent true strain of 1.0. Figure 5-3-A and B shows that there is a good correlation between the experimental data and the extrapolated curve for both materials.

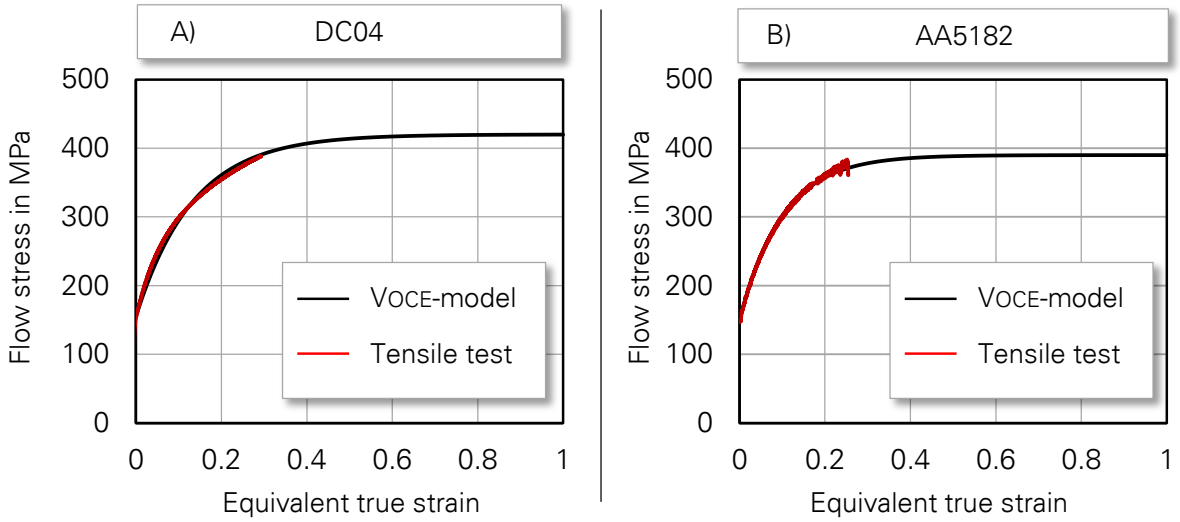

Figure 5-3: Flow curve of workpiece materials; A) DC04 and B) AA5182

5.4 CONVENTIONAL AND MACRO-STRUCTURED TOOLS

Within the scope of the experimental tests, different deep drawing tools with diverse objectives were considered. In order to investigate the effect of macro-structuring on friction reduction as well as the effect of alternating on the springback behaviour of specimens, the deep drawing tools for draw bending of the U-Channel were used, while to study about the process stability tools for deep drawing of closed-form geometries like rotationally symmetric or rectangular cups were chosen.

5.4.1 Tools for draw bending of U-Channels

Draw bending of U-Channels is considered in this thesis to examine the influence of the contact area on friction reduction in a deep drawing process and the effects of alternating bending during deep drawing with macro-structured tools on the geometrical quality of the

parts. Draw bending of U-Channels is chosen for two main reasons: Firstly, there is no ideal forming as a result of tensile-compressive stress in the flange area, and the total forming energy consists of bending and friction. Therefore, the effect of the contact area, as well as alternating bending on the forming energy can be determined directly with this test. Secondly, this process allows fast responses due to its simplicity, which is suitable for performing a large number of parameter studies. For this purpose, conventional and macro-structured drawing tools were constructed from tool steel 1.2379. Figure 5-4 shows the top and side views of conventional and macro-structured tools with corresponding dimensions schematically. Here, in the test series, where a calculation of the surface pressure is required (i.e. variant Tip to Tip), the peaks of macro-structured tools are flattened with a width of 0.5 mm in order to avoid the HERTZIAN pressure and to be able to gain an analysable condition. Furthermore, the contact area of both tools were polished to reach a roughness of R_a = 0.3 µm and R_z = 0.5 µm for comparable testing conditions and to assure the reproducibility of results.

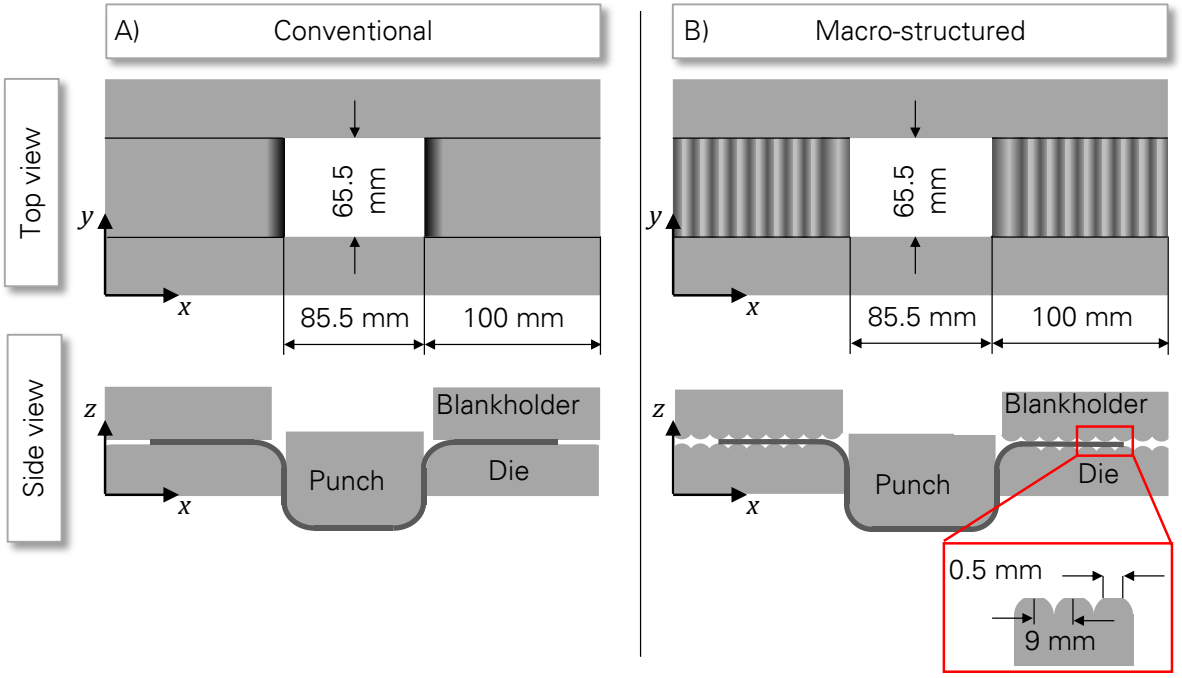

Figure 5-4: Geometry and dimensions of A) conventional and B) macro-structured draw bending of U-Channel forming tools

5.4.2 Tools for deep drawing of axial symmetric parts

In order to verify the applicability of the macro-structured deep drawing process and its influence on process stability regarding wrinkling, conventional and macro-structured rotationally symmetric tools from tooling material 1.2379 were manufactured for experimental tests. Because of structural reasons, the outer radius of the tools was limited to 113 mm. In order to reach drawing ratio greater than 2, the inner radius of the tools selected was r_i = 52 mm. Based on preliminary investigations, the die edge radius chosen for both

conventional and macro-structured tools was R_M = 10 mm. Moreover, a constant wavelength of λ = 8 mm was considered for the macro-structured tool. Additionally, in order to verify the transferability of the approach into the non-rotationally symmetric parts, a rectangular tool was constructed with inner and outer dimensions of 85 mm × 85 mm and 205 mm × 205 mm, respectively. In order to be able to ensure comparability, a constant wavelength of λ = 8 mm and a die edge radius of R_M = 10 mm were considered for the rectangular tool. In order to prevent very small straight parts in the rectangular tool, the corner radius should not be very large. From the other side, a very small corner radius and considering the draw ratio, leads to a reduction of the outer radius of the sheet metal, and consequently the alternating bending mechanism cannot take place. Because of these limitations, a corner radius of R_C = 20 mm was chosen for the rectangular tools. Furthermore, the contact areas of all three tools were polished to get an equivalent surface roughness of R_a = 0.3 µm and R_z = 0.5 µm. Figure 5-5 shows the top view of conventional and macro-structured rotationally symmetric tools, as well as the macro-structured rectangular tool with corresponding dimensions.

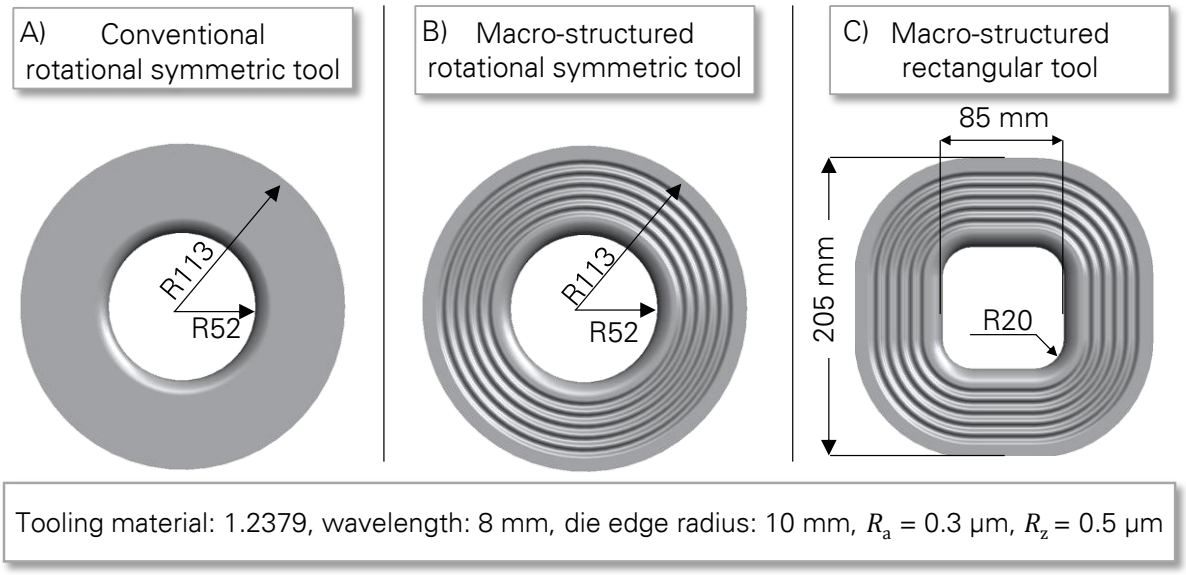

Figure 5-5: Tools for deep drawing of axial symmetric parts; A) Conventional, rotationally symmetric, B) macro-structured, rotationally symmetric and C) macro-structured, rectangular

6. PROCESS MODELING AND DETERMINATION OF PROCESS CRITERIA

In the deep drawing process with macro-structured tools, the process stability strongly depends on the selection of process inputs, i.e. wavelength and immersion depth. Therefore, to design a tool with the greatest possible process window, the process should be analysable regarding the correlation of influencing factors. This can be achieved through a combination of analysing methods i.e. trial and error, FEM or developing an analytical model which can predict the best proper setting parameters. Trial and error methods of testing should be used only as a final choice, because the process has many drawbacks that make it an unwise choice in certain situations. Besides that, FEM's main advantage is that it produces a comprehensive set of results. However, verification of the results can be sensitive to boundary conditions, and therefore the model usually needs to be refined repeatedly to give assurance that the results are reasonably accurate. Subsequently, the results should be verified and optimised with experimental testing through trial and error methods. Therefore, it is a time-consuming procedure regarding the tool design in sheet metal forming operations. However, despite these techniques, an analytical model can be developed for understanding the process behaviour regarding its response by changing the input parameters in a time-efficient manner. However, FEM simulation based on the preliminary results of the analytical model might be required for the final tool design, but it takes much less time. Figure 6-1 compared both procedures regarding the required time needed for tool design.

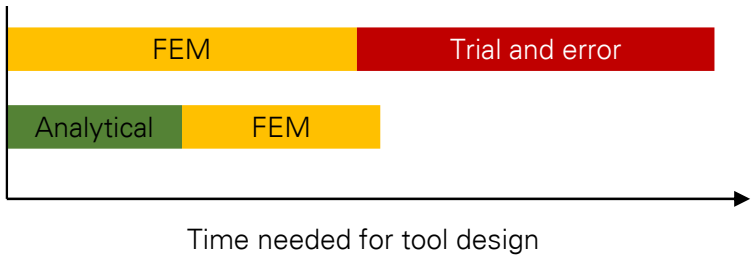

Figure 6-1: Comparison of time needed for tool design between two procedures

Because of that, the physical characteristics of the deep drawing process with macro-structured tools need to be modelled analytically (or semi-analytically). Consequently, based on the information gained from the model, the criteria for prediction of the process limits should be developed. The criteria should be able to predict the onset of wrinkling in rotationally symmetric areas of the deep drawn parts and also to determine the maximum allowable punch force for prevention of bottom cracks. Furthermore, a criterion is necessary to make a statement about the geometrical properties and the dimensional accuracy of the specimens after the forming operation. In the following, the process is modelled and the proposed criteria are introduced.

6.1 PROCESS MODELLING: BUCKLING STABILITY

Since in the deep drawing process with a macro-structured tool, the usually utilised blankholder force is not applicable, understanding the influence of parameters for buckling stiffness of the sheet metal plays an important role for a stable process. For this purpose, an analytical model has to be developed to describe the buckling stability of the sheet metal as a function of geometry and material properties in the most critical areas.

6.1.1 Identification of the most unstable part of the flange area

As discussed in Chapter 2, the tangential compressive stresses cause wrinkling in the rotationally symmetric parts of the deep drawing process, while the radial tension and the normal compression stress from the blankholder have a compensating effect. In deep drawing with macro-structured tools, the induced alternating bending increases the buckling stiffness of the sheet and prevents the buckling. However, this process provides so far a special case, in which the peripheral area of the flange (the red area in Figure 6-2) in contrast to the inner areas (the green area in Figure 6-2) is supported only on one side by the tool and forms a free end part. Consequently, the free end part of the sheet in deep drawing with the macro-structured tool is the most critical area regarding wrinkling since (see element 1 in Figure 6-2): i) the tangential compressive stress (cause of wrinkling) in this area is maximum, ii) the radial tangential stress (wrinkling compensator) in this area is minimum (compare elements 1 and 2 in Figure 6-2), iii) this part is supported only on one side, while the other parts have two supporting points, and iv) there is no alternating bending in this area, while the other parts have a wave structure which increases their buckling stiffness.

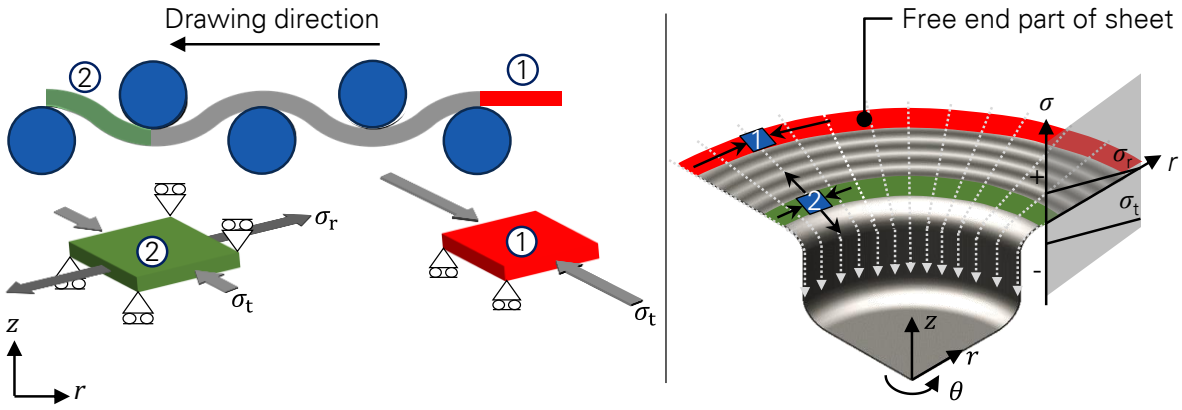

Figure 6-2: Stress state on the flange area of the deep drawing process with macro-structured tools.

That is why this part is the most critical part of the sheet metal regarding wrinkling, i.e. if the process is unstable, wrinkling will initiate from the free end part. Therefore, it is necessary to control the stability only in this area. In the following, the conditions for stability shall be studied in the free part of the sheet metal.

6.1.2 Buckling analysis of the free end part of the sheet

By taking into account that area 1 in Figure 6-2 undergoes no alternating bending, σ_r and σ_t are the present stresses in this region. Considering the force equilibrium condition, the radial tensile stress σ_r can be written as [9]:

$$\sigma_r(r) = \sigma_y(r) \cdot \int \frac{dr}{r} = \sigma_y(r) \cdot \ln\left(\frac{r_0}{r}\right) \qquad 6\text{-}1$$

Where $\sigma_y(r)$ is the corresponding yield stress at any arbitrary radius r, and r_0 is the initial radius of the sheet. Regarding the TRESCA yield criteria, the tangential compressive stress $\sigma_t(r)$ can be written as:

$$\sigma_t(r) = \sigma_r(r) - \sigma_y(r) \qquad 6\text{-}2$$

Having the flow curve of the material, it is possible to calculate the current stress state at the free end part of the sheet. Modelling the free end of the sheet with a rectangular plate, supported on one side (simply supported) and free in movement at the other side which sustain high tangential compressive and low radial tensile stresses, it is possible to perform a buckling analysis. The first theoretical examination of plate buckling was by BRYAN [149], who obtained a solution to the problem of a simply supported plate under uniform compression in 1890. Since then, numerous researchers have investigated the local instability in plates under a wide variety of loading and boundary conditions using many different methods of analysis. When a compressed plate buckles, it develops out-of-plane ripples, or buckles, along its length. In the elastic range, the buckled portions of the plate lose their loading, and become ineffective at resisting further loading, while in the portions of the plate close to the supports, out-of-plane buckling is diminished, and these parts have post-buckling reserves of strength and stiffness. The plate as a whole sustains increases in load after buckling, but the axial stiffness reduces [149]. The post-buckling behaviour of individual thin plates is governed by two simultaneous non-linear differential equations originally set up by VON KÁRMÁN [150]. For this aim, a rectangular perfectly flat plate with thickness s_0, length and width dimensions a and b, respectively, was subjected to uniform compressive stress σ_t and tensile stress σ_r, which is supported on one side and free in movement at the other side, and is considered in Figure 6-3:

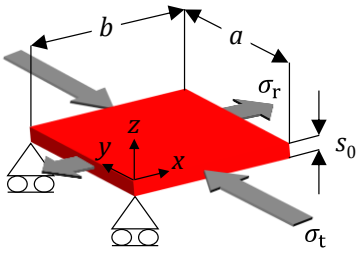

Figure 6-3: Buckling of rectangular plate under uniaxial compression and tension

The equilibrium equation for the flat plate under uniaxial tension and compression can be written as:

$$\frac{\partial^4 w}{\partial x^4} + \frac{2\partial^4 w}{\partial x^2 \partial x^2} + \frac{\partial^4 w}{\partial y^4} = \frac{12(1-v^2)}{E s_0^3}\left(\sigma_t \frac{\partial^2 w}{\partial x^2} - \sigma_r \frac{\partial^2 w}{\partial y^2}\right) \qquad 6\text{-}3$$

Where, w denotes the deflection in the z-direction, v and E are POISSON's ratio and the YOUNG modulus, respectively. Substituting σ_r and σ_t from Equations 6-1 and 6-2 into the Equation 6-3 and taking into account that x and y correspond to the width and perimeter of the free end part of the sheet in the flange area, this equation make a statement about the buckling strength of this part. Therefore, this investigation leads to understanding the correlation between the material properties and structural geometry, and their influence on the stability of the sheet metal in the flange area. Besides that, for better understanding the influence of process parameters on the forming energy, this is followed with the analytical method.

6.2 PROCESS MODELLING: FORMING ENERGY

Generally, the load-displacement progress in the deep drawing process is of importance, because a high level of loading leads to process instability in the form of bottom cracks. The calculation of the total punch force for the conventional deep drawing process based on the investigation of SIEBEL was already introduced in section 2.1.1. However, in the deep drawing process with macro-structured tools, it differs from the conventional process because of additional alternating bending. In this section, the required forming force is modelled for deep drawing with a macro-structured tool.

There are several methods to calculate the forming force for the deep drawing process. DOEGE has compared in [9] the method of SIEBEL [151], BAUER [152] and the "principle of virtual work". As Figure 6-4 shows, there is a very good agreement between the experimental results and the results from the method principle of virtual work.

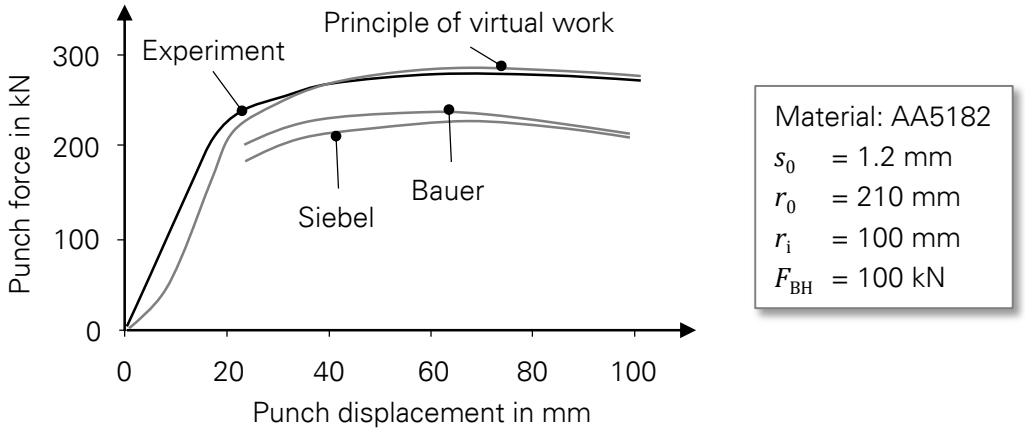

Figure 6-4: Comparison between the calculated punch force from the method of Siebel, Bauer and the principle of virtual work with experimental results according to [9]

Since the semi-analytical method based on the principle of virtual work can predict the forces in the deep drawing process more accurately compared with the SIEBEL formulation (approx. 20% [4]), this method is used in this thesis to calculate the punch force.

The total energy for deep drawing with macro-structured tools E_t, consists of the ideal energy in the flange area E_{id}, the energy to realise the alternating bending, as well as the bending at the radius of the drawing die E_b, and the energy to overcome the friction on the contact area E_f, see Figure 6-5 (compare with Figure 2-2).

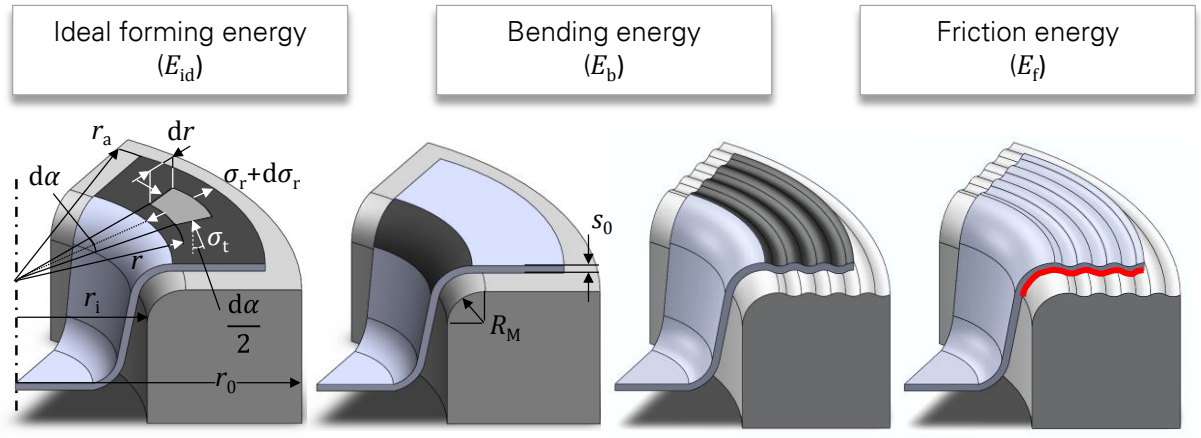

Figure 6-5: Individual components of the total forming energy for deep drawing of a rotationally symmetric cup with a macro-structured tool

The summation of all the energy terms results in the total energy E_t:

$$E_t = \int F_t \cdot dh = E_{id} + E_b + E_f \qquad 6\text{-}4$$

F_t and dh represent the punch force and punch displacement. Based on the principle of virtual work, it is possible to calculate the ideal energy for axial symmetric geometries. The principle of virtual work implies that the external work corresponds to the inner work, i.e.

$$\delta W_{int} = \delta W_{ext} \qquad 6\text{-}5$$

Equation 6-5 indicates that the virtual external work, which results from the external forces, is equal to the virtual internal work, which is calculated from the existing internal stresses and the virtual strains. Therefore, in a forming process, the virtual energy for plastic deformation of a certain volume has to be equal to the product of the according applied force and the virtual punch displacement. To establish the progress of ideal energy during the process numerically, it is required to consider the process incrementally. The incremental process evaluation allows the consideration of the process time and the relevant non-linearities. For this, the whole process should be divided into small time intervals. To calculate the ideal forming energy E_{id}, the frictional and bending energy are not considered, but only the available energy inside the

sheet metal in the flange area. Furthermore, the sheet metal forming process is considered quasi-static, i.e. the inertial forces are neglected. By an appropriate cut-out volume of the sheet metal, it is possible to find out the relevant forming forces. Therefore, the principle of virtual work can be written as follows [153]:

$$\delta E_{\mathrm{id}} = \int \Sigma \cdot \delta u \, \mathrm{d}A = \int \sigma_{\mathrm{ij}} \cdot \delta \varepsilon_{ij} \mathrm{d}V \qquad 6\text{-}6$$

Here, Σ represent the external stress of the considered cut-out volume, δu the virtual displacement on the cut-out location, and σ_{ij} and $\delta\varepsilon_{ij}$ the internal stress and virtual strain of the volume, respectively. Figure 6-6 illustrates the considered flange volume, virtual displacements and also the corresponding radius.

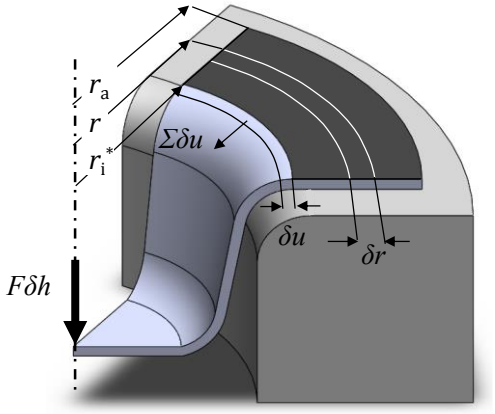

Figure 6-6: Principle of the analytical calculation of ideal forming energy in the flange area according to the principle of virtual work [153]

Considering the mean vertical anisotropy $\bar{r}$ according to HILL [154] and by neglecting the change of sheet thickness during the process, the ideal forming energy in the flange area can be calculated as [9]:

$$E_{\mathrm{id}} = \sqrt{\frac{\bar{r}+1}{\bar{r}+\frac{1}{2}}} \cdot \frac{\delta V}{\delta h} \cdot \int_{r_{\mathrm{i}}^*}^{r_{\mathrm{a}}} \sigma_{\mathrm{y}}(r) \cdot \frac{1}{r} \mathrm{d}r \qquad 6\text{-}7$$

Here, δV and δh are the virtual volume change and virtual punch displacement respectively; r_{i}^* is the inner radius of the flange, while r_{a} is the current outer radius of the sheet metal. The instantaneous yield stress $\sigma_{\mathrm{y}}(r)$ of any point in the flange area of the rotationally symmetric blanks, with an initial radius of $r_{0,}$ can be determined as a function of the current outer flange radius r_{a} and the corresponding radius of the point r [155]:

$$\sigma_{\mathrm{y}}(r) = a \left[\frac{2}{\sqrt{3}} \ln \left(\frac{\sqrt{r_0^2 + r_{\mathrm{a}}^2 + r^2}}{r} \right) \right]^n \qquad 6\text{-}8$$

Where a and n are the material constants and can be determined through material characterisation tests. As Figure 6-5 shows, the sheet metal undergoes an additional alternating bending in the flange area, besides the double bending over the die edge radius. The energy for the alternating bending in the structured surface, as well as the bending at the die edge radius, can also be calculated with the help of the principle of virtual work as follows:

$$E_{\mathrm{b}} = \left(r_{\mathrm{M}} + \frac{s_0}{2}\right) \cdot \sqrt{\frac{\bar{r}+1}{\bar{r}+\frac{1}{2}}} \cdot \delta V \cdot \int_0^{\theta} \frac{\cos(\theta)}{r(\theta)} \sigma_{\mathrm{y}}(\theta)\mathrm{d}\theta \qquad 6\text{-}9$$

Here s_0 is the initial sheet thickness and r_{b} and θ are the bending radius and bending angle, respectively. The current yield stress $\sigma_{\mathrm{y}}(r)$, depending on the radius and the virtual punch displacement, can be determined through Equation 6-8. Figure 6-7 illustrates the considered volume for bending over the die edge radius, as well as the present internal and external loads on the sheet metal in this area. Obviously, the model can be used to compute the required bending energy for alternating bending in the structured area of the flange through applying the corresponding bending radius and bending angle.

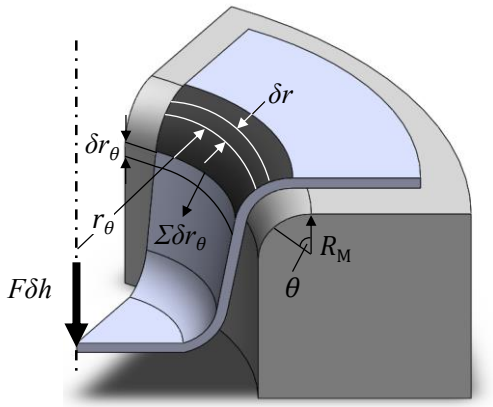

Figure 6-7: Principle of the analytical calculation of the bending energy, according to the principle of virtual work [153]

The calculation of frictional energy between the part and the tools is based on the explicit use of the local pressure and the local frictional force present along the contact length, as originally pursued by EULER and EYTELWEIN [156]. But, on the die edge radius occur high local stress peaks, which cannot be considered in that model. Accordingly, in the half-analytical model based on the principle of virtual work, the frictional energy can also be calculated from the present stresses [9]:

$$E_{\mathrm{f}} = \left(\frac{\mu}{\mu-1}\right) \cdot \sqrt{\frac{\bar{r}+1}{\bar{r}+\frac{1}{2}}} \cdot \delta V \cdot \left(\left(\frac{1}{2}\theta + \frac{1}{\mu-1}\right) \cdot \sigma_{\mathrm{y},1} + \theta \cdot \sigma_{\mathrm{y},2}\right) \qquad 6\text{-}10$$

Where, μ is the friction coefficient, θ is the bending angle and $\sigma_{\mathrm{y},1}$ and $\sigma_{\mathrm{y},2}$ are the yield stress before and after the bending, respectively. With the ability to calculate all the individual energy

terms for deep drawing with macro-structured tools and superposing them, the correlation between all the influencing parameters and the forming force can be studied in advance.

6.3 EXTENSION OF THE MODEL FOR DEEP DRAWING OF NON-ROTATIONALLY SYMMETRIC PARTS

In contrast to rotationally symmetrical parts, there is no uniform stress distribution in the flange area of irregularly shaped parts along the drawing contour. For example, in the deep drawing of rectangular cups, the tangential compressive stresses appear significantly in the rotationally symmetric area, while on the straight parts, act almost exclusively radial tensile and almost no tangential compressive stresses. In reality, however, the tangential stress in transition from the rotationally symmetric part to a straight area does not suddenly drop to zero, but it is reduced continuously in a transition zone. This is show schematically in Figure 6-8-A.

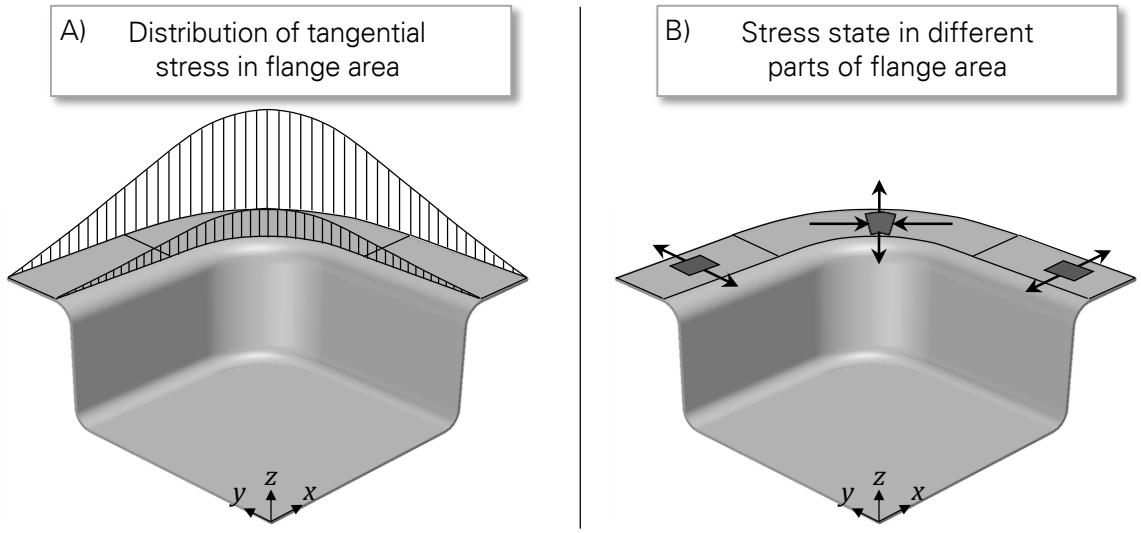

Figure 6-8: Stress state in the flange area of the rectangular cup; A) Distribution of tangential stress in the flange area according to [157] and B) the stress state in rotationally symmetric and straight parts of the flange area

During the deep drawing of irregular sheet metal parts, the individual parts of the sheet metal part undergo different stresses, which can also change during the forming process. Thus, there should be a distinction between areas where tensile stress states exist and areas where tensile-compression stress occurs. Therefore, in a first approximation, the flange area can be subdivided into the rotationally symmetric and straight areas [157], as shown in Figure 6-8-B. Based on this consideration, the 2D-analytical model developed in this thesis can be extended for deep drawing of non-rotationally symmetric parts. For this aim, the model can be used to describe the buckling stiffness of the flange area in the deep drawing of the rectangular cups with a simplified assumption, in which the rotationally symmetric and straight part of the flange can be individually analysed. Consequently, the straight zones can be assumed as a

rotationally symmetric part with an infinite radius. However, due to the absence of tangential stress in the straight area, buckling stiffness is less relevant. Despite buckling stiffness having less relevance in the straight area, the energy calculation to determine the load-displacement progress of the process in this area is of importance. In order to make an accurate statement about the required forming energy for the deep drawing of rectangular cups with macro-structured tools, it is required to exclude the ideal forming energy from the calculation, i.e. Equation 6-6.

6.4 DEVELOPMENT OF A CRITERION FOR THE PREDICTION OF WRINKLING

In order to be able to make a statement about the onset of wrinkling in the deep drawing process with macro-structured tools, the model developed in section 6.1 can be used. Based on this model, a criterion to predict the onset of wrinkling is developed within the scope of this section.

Generally, considering the buckled mode of the plate shown in Figure 6-3, the deflection geometry of the plate w in the z-direction can be written as:

$$w = \sum_{m=1,2,3,\dots} \sum_{n=1,2,3,\dots} w_{mn} \sin\frac{m\pi x}{a} \sin\frac{n\pi y}{b} \qquad 6\text{-}11$$

Here m and n are the number of half sine waves in the buckled mode. It should be taken into account that, $w = 0$ at $x = 0$, $y = 0$ and $y = a$. Considering these boundary conditions, the substitution of Equation 6-11 into Equation 6-3 gives:

$$\left(\frac{m^4\pi^4}{a^4} + 2\frac{m^2n^2\pi^2}{a^2b^2} + \frac{n^4\pi^4}{b^4}\right) = \frac{12(1-v^2)}{Es_0^3}\left(\sigma_t \frac{m^2\pi^2}{a^2} - \sigma_r \frac{n^2\pi^2}{b^2}\right) \qquad 6\text{-}12$$

Solving the differential equation, the compressive stress σ_t can be written as:

$$\sigma_t = \frac{\pi^2 E s_0^2 \left(\left(\frac{m}{a}\right)^2 + \left(\frac{n}{b}\right)^2\right)^2}{12(1-v^2)\left(\left(\frac{m}{a}\right)^2 - \left(\frac{\sigma_r}{\sigma_t}\right)\left(\frac{n}{b}\right)^2\right)} \qquad 6\text{-}13$$

The lowest value of the plate buckling stress $\sigma_{t,cr}$ in this equation can be obtained when the plate buckles only in one direction, i.e. in the case of wrinkling $n = 1$. Therefore, the critical tangential stress $\sigma_{t,cr}$ can be written as:

$$\sigma_{\mathrm{t,cr}} = \frac{\pi^2 E s_0^2 \left(\left(\frac{m}{a}\right)^2 + \left(\frac{1}{b}\right)^2 \right)^2}{12(1-\nu^2)\left(\left(\frac{m}{a}\right)^2 - \left(\frac{\sigma_\mathrm{r}}{\sigma_\mathrm{t}}\right)\left(\frac{1}{b}\right)^2 \right)} \qquad 6\text{-}14$$

This equation gives the critical value of the tangential compressive stress for the onset of elastic buckling in a plate with given dimensions under uniaxial compression and tension stress, σ_t and σ_r. In relation to wrinkling, m indicates the number of initiated wrinkles. However, since in the deep drawing process, wrinkling forms a plastic buckling, Equation 6-14 should be modified for plastic buckling. VON KÁRMÁN [158] has shown that the conventional elastic bending theory can be extended to cover plastic bending by the substitution for YOUNG's modulus E of a plastic buckling modulus, E_0:

$$E_0 = \frac{4EP}{\left(\sqrt{E}+\sqrt{P}\right)^2} \qquad 6\text{-}15$$

Where, P being the slope of the stress–strain curve of the material in simple tension at a given value of strain; it follows that E_0 is a function of strain. In order to apply Equation 6-14 for the prediction of process stability, the parameter m, which indicates the number of wrinkles in an unstable process, has to be calculated.

Besides that, In order to transfer this criterion to a deep drawing process with macro-structured tools, it is required to know the number of wrinkles at the onset of buckling when the critical stress is reached (m in Equation 6-14). The number of wrinkles in a deep drawing process depends on the blankholder force. There is no conventional blankholder force by the free end part of the sheet in the deep drawing process with macro-structured tools. SENIOR used the energy method in [159] to solve the stability problem in the deep drawing process for both cases with and without the blankholder. Considering stable equilibria, if the total energy tending to restore the conditions for equilibrium in a system is greater than the energy for displacing it, the system remains stable. Equating the two energy values gives the critical conditions. In the wrinkling of a deep drawn flange due to lateral collapse under the induced tangential compressive stress, the energy terms involved are of three main types:

- E_B, the energy due to bending into a half sine wave segment of the wrinkled flange,
- E_t, the energy due to the tangential compressive forces,
- E_L, the energy due to the lateral loading of the flange surface.

Due to lateral elastic bending, the energy stored in a half sine wave segment can be written as:

$$E_\mathrm{B} = \frac{1}{2}\int_0^l E_0 I \frac{\mathrm{d}^2 y}{\mathrm{d}x^2}\,\mathrm{d}x \qquad 6\text{-}16$$

Here, E_0 is the plastic buckling modulus, I is the moment of inertia and l is the length of a half sine wave segment and can be determined as follows:

$$l = \frac{r_\mathrm{m}}{m} \tag{6-17}$$

Where r_m is the mean flange radius and m the total number of waves formed. The energy due to the tangential compressive forces can also be written as:

$$E_\mathrm{t} = \frac{\sigma_\mathrm{t} b s_0}{2} \int_0^l \left(\frac{\mathrm{d}y}{\mathrm{d}x}\right)^2 \mathrm{d}x \tag{6-18}$$

Where b is the flange width. Considering the flange surface as q, the third energy component E_L can be calculated as follows:

$$E_\mathrm{L} = \int_0^l \int_0^y bq \, \mathrm{d}y \, \mathrm{d}x \tag{6-19}$$

The critical condition is reached when:

$$E_\mathrm{B} + E_\mathrm{L} = E_\mathrm{t} \tag{6-20}$$

SENIOR solved in [159] the differential equation with respect to the upper and lower limits of the integral and showed that the number of waves m which the flange would wrinkle is:

$$1.65 \frac{r_\mathrm{m}}{r_0 - r_\mathrm{i}} \leq m \leq 2.33 \frac{r_\mathrm{m}}{r_0 - r_\mathrm{i}} \tag{6-21}$$

Here, r_m is the mean flange radius, r_0 and r_i are the initial radius of the sheet and inner radius of the drawing die, respectively.

Substituting the upper and lower limits of m from Equation 6-21 into Equation 6-14 leads to define a safety limit for the tangential stress. The upper and lower limits of the critical tangential stress $\sigma_\mathrm{t,cr}$ are plotted in Figure 6-9-A, and this is compared with the tangential stress at the free end part. As long as the tangential stress during the process lies below the critical tangential stress $\sigma_\mathrm{t,cr}$, no wrinkling is expected and the process will be stable. If the tangential stress exceeds the critical value and enters into the uncertain zone, the process will be unstable and wrinkling will be initiated. In order to use this investigation as a criterion for the prediction of wrinkling in the deep drawing process with macro-structured tools, the progress of the tangential compressive stress at the free end part of the sheet should be evaluated. This can be achieved using Equation 6-2. Here, it should be noted that the maximum length of the free end part is half of the wavelength λ. Because of the strain hardening of the sheet during the process, the amount of tangential stress increases by each time step. Figure 6-9-B shows schematically the development of tangential stress, especially at the free end part of the sheet as a function of sheet radius and time.

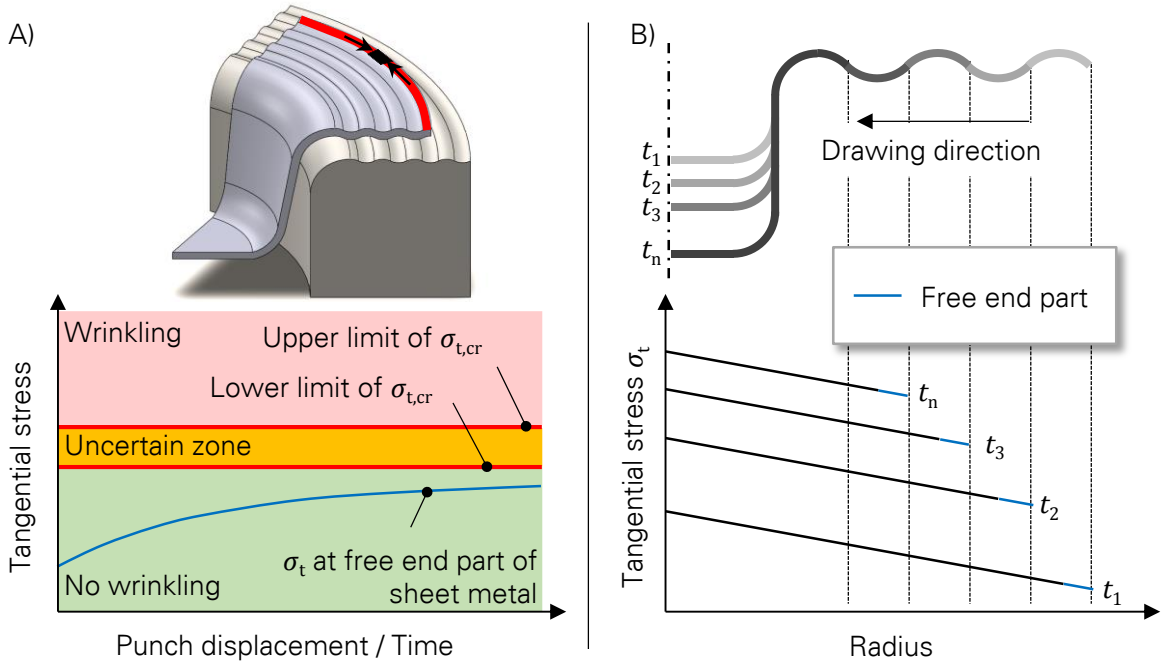

Figure 6-9: Free end part of the sheet metal; A) Controlling the stability of the process regarding wrinkling and B) Progress of the tangential stress at the free end part of the sheet during deep drawing

6.5 DEVELOPMENT OF A CRITERION FOR PREDICTION OF BOTTOM CRACKS

Generally, fractures occur in the deep drawing process in the bottom corner of the part, since the material undergoes less plastic deformation and strain hardening, and therefore its strength is less than other parts. Regarding the theoretical calculation of the maximum drawing ratio, the forming force which is required to perform the plastification in the forming area should be compared with the maximum allowable force transmission in the bottom area of the cup. The greatest possible drawing ratio results from the consideration of equilibrium. For this purpose, the total forming force based on the developed model in section 6.2 should be compared with the maximum allowable punch force.

Considering the fracture locus of stainless steel as presented in Figure 6-10, in the space of the stress triaxiality and the equivalent plastic strain to fracture, it can be observed that the equivalent plastic fracture strain for plane stress conditions is very close to the uniaxial tension condition. Therefore, since the stress state in the cylindrical wall of a drawn part is very similar to the uniaxial stress state, it is possible to use it as a simple failure criterion by comparing it with the tensile strength of the material.

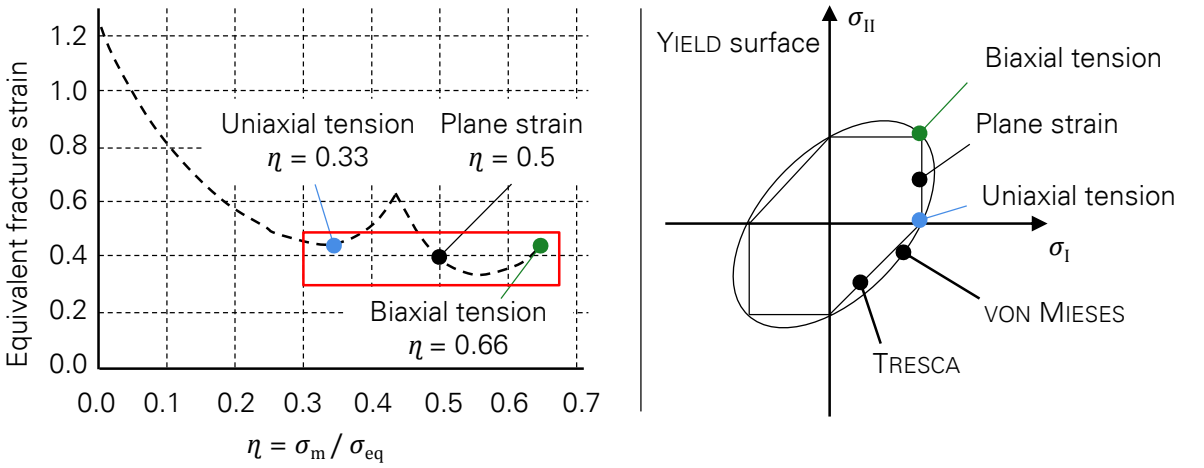

Figure 6-10: Fracture locus in the space of the stress triaxiality and the equivalent plastic strain to fracture

Considering R_m as the ultimate tensile strength of the sheet, the maximum transferable punch or bottom crack force F_{bc} can be roughly calculated by means of the following equation:

$$F_{bc} = A_0 \cdot C_R \cdot R_m \qquad 6\text{-}22$$

Here, A_0 is the cross sectional area of the drawn part and C_R is a dimensionless crack factor for the correction. To identify the crack factor, the model from DOEGE can be used [9]. This factor can vary from 0.9 to 1.5 as a function of the material and process properties. In order to determine this factor analytically, it must be assumed that neither the bending, nor the tangential compressive stress, nor material slippage, nor the friction above the punch edge radius, influence the transferable force. However, it is to be expected that the punch edge radius, the sheet thickness, the drawing ratio and above all the current stress state influence the crack factor. This relationship can be derived using the natural exponential function as follows [160]:

$$C_R = e^{\varphi_t} \qquad 6\text{-}23$$

Here φ_t is the tangential compression factor at the outlet of the punch edge radius and can be determined as follows [160]:

$$\varphi_t = \ln \frac{\sqrt{\frac{r_p A}{s_0}\left(\frac{r_i}{r_p}-1\right)(A^2-1)+(1-\cos\alpha)\frac{2}{3}\frac{r_p}{s_0}(a^3-1)+\left(\frac{r_i}{r_p}-1\right)^2}}{\frac{r_i}{r_p}-1+\sin\alpha} \qquad 6\text{-}24$$

with

$$A = \left(\frac{s_0}{r_p} + 1\right) \qquad 6\text{-}25$$

Where, r_p and α are the punch edge radius and the deflection angle of the punch edge radius, respectively. Comparing the bottom crack force F_{bc} as a criterion for the fracture with the calculated punch force, which is computed through the energy method, it is possible to make a precise and explicit statement about the stability of the process regarding bottom cracks. Obviously for a stable process, the punch force must not exceed the maximum transformable force or the bottom crack force F_{bc}.

6.6 DEVELOPEMENT OF A CRITERION FOR PREDICTION OF DIMENSIONAL ACCURACY OF THE PARTS

The deep drawing of sheet metal induces complex deformations, which in different regions of the sheet metal can have vastly different accumulated plastic strains [161]. Upon unloading by removing the tools, springback occurs which can change the shape accuracy of the part [162]. Springback is caused by non-uniform residual stresses, through the sheet thickness of the formed part, that create a bending moment, which causes a distortion of the workpiece upon unloading. Springback strains are almost completely elastic; non-linear recovery strains are usually small but, in extreme cases, they can amount up to 10% of the total recovery [163]. Therefore, reliable prediction of springback is of importance during the tool design. Nowadays, engineering guidelines and finite element software are used in the design process to predict the amount of springback in sheet metal forming. Based on this prediction, the tools' geometry and process parameters are modified to obtain the desired product shape [164]. However, the current accuracy of springback prediction is not sufficient [165].

The fact that materials are subjected predominantly to tangential compression as long as they are in the flange area, followed by radial tension for the inward cup side and radial compression for the outward cup side during the bending over the die edge radius, results in complex strain path changes in the sheet. Additionally, in the deep drawing process with macro-structured tools, further strain hardening as a result of alternating bending decreases the amount of elastic strains within the sheet thickness. Moreover, for some materials, the load change during the alternating bending leads to a kinematic hardening, see Figure 6-11. Due to the closed-form shapes and accordingly high structural stiffness, the deep drawn parts contain high residual stresses, which are strongly dependent on the material hardening behaviour. Since most of them will be cut out for the follow-on operations, the residual stresses lose their balance, which leads to a dimensional inaccuracy in the form of springback in the part.

The positive effect of the increased retention force for the compensation of springback through increasing the blankholder force in the conventional deep drawing process is known from the literature [166]. However, since in the lubricant-free deep drawing process the usually utilised blankholder force is not applicable, it can be performed geometrically through retention

force results from alternating bending. Based on this consideration, developing a criterion to predict the amount of springback due to the release of the residual stresses after cutting out the specimen in the deep drawing process with a macro-structured tool is essential. For this purpose, a half-analytical criterion is developed in this section.

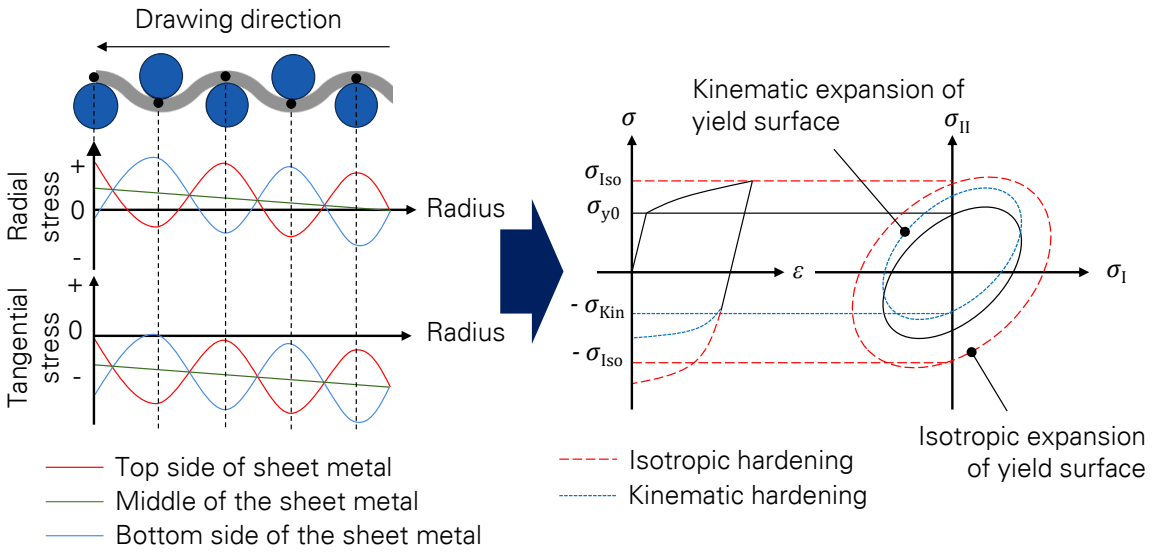

Figure 6-11: Influence of alternating bending on the kinematic hardening behaviour of the workpiece

A way to quantify the circumferential residual stress in deep drawing cups is called ring splitting (Figure 6-12), a method introduced by SIEBEL and MÜHLHÄUSER in [167]. Ring splitting is one of the most common springback-measurement tests for the deep drawing of symmetrical parts, which offers an opportunity to evaluate the amount of residual stress in the specimen. In this test, a ring (see Figure 6-12-A) will be cut out from the wall part of a deep drawn cup and subsequently split open. The tangential residual stress can then be determined from the ring opening chord upon splitting.

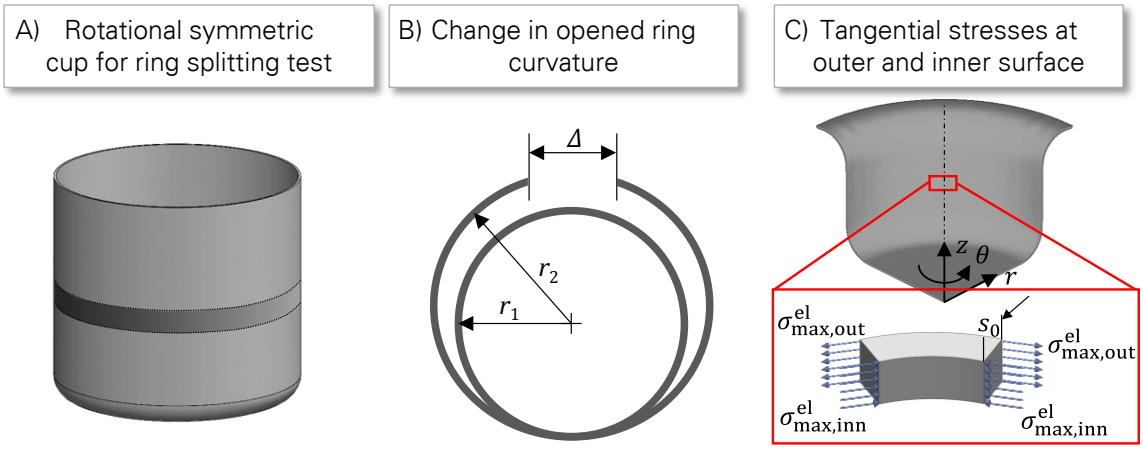

Figure 6-12: The ring splitting method to determine circumferential residual stress in deep drawing cups; A) Cutting area in a rotationally symmetric deep drawing cup for the splitting test, B) springback in the split ring and C) tangential residual stress at the inner and outer cup surfaces

To determine the tangential residual stress in the wall of the cup, the ring opening gap Δ can be approximated with a circular arc, as shown in Figure 6-12-B:

$$2\pi r_2 = 2\pi r_1 + \Delta \qquad 6\text{-}26$$

or:

$$r_2 - r_1 = \Delta/2\pi \qquad 6\text{-}27$$

Here r_1 and r_2 are the mean radius of the intact and split ring. The maximum tangential elastic bending strain due to the springback at the outer and inner surfaces of the intact ring $\varepsilon^{\mathrm{eb}}_{\mathrm{max,out}}$ can be determined from the bending theory as follows:

$$\varepsilon^{\mathrm{eb}}_{\mathrm{max,out}} = \frac{s_0}{2r_1} - \frac{s_0}{2r_2} = \frac{s_0}{2}\left(\frac{r_2 - r_1}{r_1 r_2}\right) \qquad 6\text{-}28$$

While the maximum tangential elastic bending strain at the inner surface $\varepsilon^{\mathrm{eb}}_{\mathrm{max,inn}}$ is:

$$\varepsilon^{\mathrm{eb}}_{\mathrm{max,out}} = \frac{s_0}{2r_2} - \frac{s_0}{2r_1} = \frac{s_0}{2}\left(\frac{r_1 - r_2}{r_1 r_2}\right) \qquad 6\text{-}29$$

By substituting the Equations 6-28 and 6-29 into 6-26, the elastic bending strain can be written as:

$$\varepsilon^{\mathrm{eb}}_{\mathrm{max,out}} = \frac{s_0}{2}\left(\frac{\Delta}{r_1 r_2}\right) \qquad 6\text{-}30$$

and

$$\varepsilon^{\mathrm{eb}}_{\mathrm{max,inn}} = -\frac{s_0}{2}\left(\frac{\Delta}{r_1 r_2}\right) \qquad 6\text{-}31$$

Since $\Delta/2\pi \ll r_1$, it can be assumed that $r_1 \approx r_2$, therefore:

$$\varepsilon^{\mathrm{eb}}_{\mathrm{max,out}} = \frac{s_0}{4\pi}\left(\frac{\Delta}{{r_1}^2}\right) \qquad 6\text{-}32$$

and

$$\varepsilon^{\mathrm{eb}}_{\mathrm{max,inn}} = -\frac{s_0}{4\pi}\left(\frac{\Delta}{{r_1}^2}\right) \qquad 6\text{-}33$$

Considering the Equations 6-32 and 6-33, the maximum tangential elastic bending stress at the outer and inner surfaces can be calculated as follows:

$$\sigma_{\max,\text{out}}^{\text{el}} = \frac{E \cdot s_0}{4\pi}\left(\frac{\Delta}{r_1^2}\right) \quad 6\text{-}34$$

$$\sigma_{\max,\text{inn}}^{\text{el}} = -\frac{E \cdot s_0}{4\pi}\left(\frac{\Delta}{r_1^2}\right) \quad 6\text{-}35$$

As the Equations 6-34 and 6-35 show, the residual stresses are tensile at the cup outer surface and compressive at the inner surface. Figure 6-12-C shows these stresses schematically. As long as there is no springback in the workpiece, because of equilibrium conditions, the bending moment should be zero due to tangential stresses over the sheet thickness in the wall part of the cup (intact ring) [168]:

$$M_{\text{b}} = M_{\text{b}}^{\text{res}} - M_{\text{b}}^{\text{eb}} = 0 \quad 6\text{-}36$$

Here, $M_{\text{b}}^{\text{res}}$ is the bending moment because of the residual stress in the intact ring and M_{b}^{eb} is the induced elastic bending moment which is necessary to close the split ring. Since M_{b}^{eb} is an elastic bending moment, considering the equilibrium conditions, it is symmetric about the natural axis, i.e. over the sheet thickness and can be written as a function of its maximum value $\sigma_{\max}^{\text{eb}}$:

$$M_{\text{b}}^{\text{eb}} = b \cdot \int_{-\frac{s_0}{2}}^{\frac{s_0}{2}} \sigma_{\max}^{\text{eb}} \cdot \frac{2x}{s_0} \cdot x \cdot dx \quad 6\text{-}37$$

$$M_{\text{b}}^{\text{eb}} = \frac{4}{3} b \cdot \sigma_{\max}^{\text{eb}} \cdot \left(\frac{s_0}{2}\right)^3 \quad 6\text{-}38$$

Substituting Equation 6-38 in 6-36 and using the Equation 6-34 or 6-35, the opening gap Δ due to springback can be derived as follows [168]:

$$\Delta = \frac{24 \cdot \pi \cdot r_1^2 \cdot M_{\text{b}}^{\text{res}}}{E \cdot s_0^4} \quad 6\text{-}39$$

To find the opening gap for a given deep drawn part, the residual bending moment in the intact ring $M_{\text{b}}^{\text{res}}$ has to be calculated by means of FEM-simulations. This way it is possible to evaluate the amount of residual stress in a part deep drawn by a macro-structured tool and compare it with the reference samples.

6.7 SUMMARY OF CHAPTER 6

For better understanding the physical behaviour of the deep drawing process with macro-structured tools, and also to find out the cause-and-effect relationship between the process parameters, an analytical model was developed within the scope of this chapter. The model describes the buckling stability of sheet metal in the flange area and also can determine the

load-displacement progress of the process as a function of the process input parameters. In this chapter, it was shown that the 2D model can be extended so that the deep drawing of non-rotationally symmetric parts can also be analysed. For this purpose, the flange area should be subdivided into rotationally symmetric and straight areas, and they should be subjected to analysis individually. Additionally, for a time efficient prediction of the process limits, some criteria were devised based on the developed model. With the help of the developed criteria, the process limits, i.e. bottom cracking and wrinkling, can be predicted based on the energy method and buckling analysis, respectively. Moreover, a criterion was developed to evaluate the amount of springback in the wall part of the deep drawn specimens.

7. RESULTS

In order to control the applicability of the proposed approach and verify the developed model and criteria, several experimental as well as numerical tests were carried out and their results are shown within the scope of this chapter. Experimental tests were performed with the experimental setups as introduced in Chapter 5, while all numerical simulations were carried out with the commercial FEM-Software *simufact.forming*. The results show an overview about the effects of macro-structuring on process characteristics, e.g. friction, stability and springback behaviour. Consequently, the developed process model will be verified, as well as the analytical criteria to determine the process limits and predict the dimensional accuracy of the part.

7.1 INVESTIGATION ABOUT THE EFFECTS OF MACRO-STRUCTURING ON PROCESS CHARACTERISTICS

As mentioned above, in this test series the influence of the contact area on friction reduction is examined. Furthermore, the influence of alternating bending on the process stability and compensation of springback is investigated. For this end, numerical as well as experimental tests are performed.

7.1.1 Investigation about friction reduction through macro-structuring

In Chapter 4, it was discussed how the macro-structuring of tools can reduce the integral of the surface pressure over the contact area. In order to control the feasibility of this approach for real applications, the draw bending of the U-channel as a forming process is considered in this section. Here the conventional and macro-structured tools are used, which were introduced in section 5.4.1. The tests are carried out with the hydraulic press machine BUP 600 at room temperature, with a constant drawing velocity of 10 mm/s, which corresponds to the deep drawing process. The conventional and macro-structured tools were subjected to lubricant-free, as well as lubricated conditions. For the lubrication, the industrial mineral oil-based lubricant "WISURA ZO 3368" was used. This lubricant, which has some additional additives like phosphor, is commonly used in the field of metal forming, especially for the deep drawing of aluminium and stainless steel alloys [169]. Workpiece strips were cut from DC04 steel of 1 mm thickness and 60 mm width to have a good manageability and 280 mm length to realise a relatively big drawing depth with the existence of the remaining flange area. Each strip was cleaned using a citrus-based cleaner and finally treated with acetone to remove all traces of pre-lubricants. All tests were repeated five times in order to get consistent information about the statistical repeatability of the results. In order to investigate the effect of the contact area on friction properties, an experimental matrix was defined. Within this

matrix, two constant initial surface pressures P_{Total} = 5.1 and 6.8 MPa were considered for the draw-bending of the U-Channels, which correspond to the deep drawing process. The results of the tests are presented in Figure 7-1. As the results show, 28.1 kN is required for the draw-bending of a U-Channel with a conventional tool in lubricant-free conditions under the initial surface pressure of P_{Total} = 5.1 MPa. By increasing the surface pressure to 6.8 MPa, the increased frictional force prevents the material flow on the flange area, which finally leads to necking and consequently the tearing of specimens. Lubricating the specimen with WISURA ZO 3368 improves the frictional behaviour of the process and decreases the punch force to 23.5 kN under P_{Total} = 5.1 MPa (approx. 16% reduction compared with lubricant-free conditions). However, the results show that through lubricating, the specimen will not tear under the initial surface pressure of 6.8 MPa. Although reducing the contact area by means of macro-structured tools (from 5850 mm^2 for a conventional tool to 327 mm^2 for a macro-structured tool, i.e. approx. 94% reduction) leads to an increase of local surface pressure in the contact zones, based on Equation 4-2, this results in a drastic reduction of frictional forces. This statement can also be verified with the experimental results. As shown in Figure 7-1, the average punch force for the draw-bending of U-Channels in lubricant-free conditions with macro-structured tools under the initial surface pressure P_{Total} = 5.1 and 6.8 MPa is 6.1 and 6.6 kN, respectively (approx. 74% and 77% reduction compared to the conventional process in lubricated conditions). Furthermore, using the macro-structured tools in lubricated conditions reduce the punch force even further, i.e. to 4.9 and 5.1 kN under an initial surface pressure of P_{Total} = 5.1 and 6.8 MPa, respectively. As the diagram shows, the deviation of the results is almost proportional to the average values. This reveals that there are no systematic errors in the test and measurement procedures.

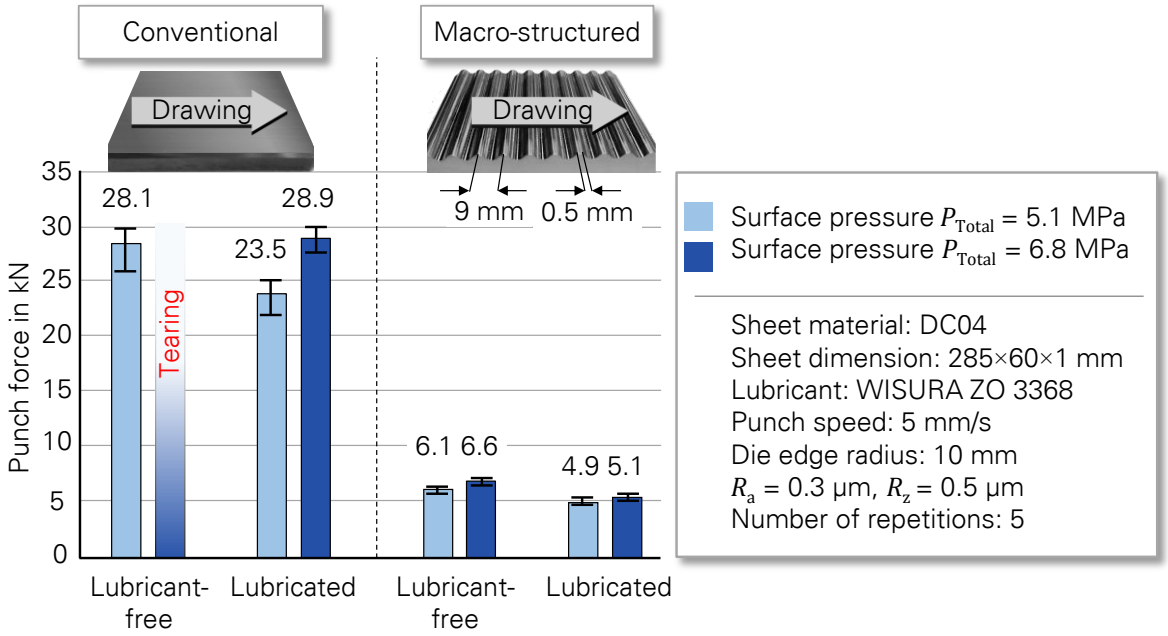

Figure 7-1: The required punch force for forming the U-Channel with conventional and macro-structured tools in lubricant-free as well as lubricated conditions

The results reveal that macro-structured tools can be used to reduce the contact area between tools and the workpiece, and this leads to a decrease in the amount of frictional shear stresses, and as a result the total frictional force in the process. In the next section, the effects of alternating bending on the process stability for the deep drawing of rotationally symmetric and rectangular cups are studied.

7.1.2 Investigation about process stabilisation through macro-structuring

In Chapter 4, with the help of Equation 4-2, it was shown that macro-structuring tools reduce the frictional shear stress, and as a result the total punch force in the sheet metal forming process. It was also discussed that the amount of the immersion depth and the wavelength as two important process input parameters, which define the geometry of alternating bending, have a great influence on the process stability regarding wrinkling and bottom cracking. In order to investigate the sensitivity of the process window regarding the process input, various numerical simulations were performed. For this purpose, the blanks from DC04 were subjected to numerical simulations. For this end, sheet metal with a 90 mm radius and 1.0 mm thickness was chosen for 3D simulation of a rotationally symmetric deep drawing process. In order to reduce the calculation time, a quarter of the workpiece with two symmetric planes was subjected to the FE-simulation. The inner radius of the tool is 50 mm so that a drawing ratio of β = 1.8 can be realised. Here, solid shell elements (element size: 1 mm with 5 integration layers per thickness and one integration point per layer) were used. The variant matrix studied comprises 4 different wavelengths and five different immersion depths. The parameter limits of the simulation matrix were chosen regarding the process window, so that the intended wrinkling and bottom cracking occurred. For comparison, a series of simulations were also carried out with a sheet thickness of 0.6 mm. The calculations were performed with and without friction in order to be able to analyse the frictional component and the bending component separately from each other. The numerical results shown in Figure 7-2 confirm basically the hypotheses of the analytical considerations regarding the influences of wavelength and immersion depth.

Red marked areas indicate the occurrence of bottom cracks, orange areas indicate the appearance of wrinkles. Due to the lower buckling stiffness, the 0.6 mm sheet has a higher sensitivity to wrinkling than the 1.0 mm sheet, which reduces the process window (green area). Furthermore, as expected, the simulations show that friction increases the risk of bottom cracks and therefore reduces the process window.

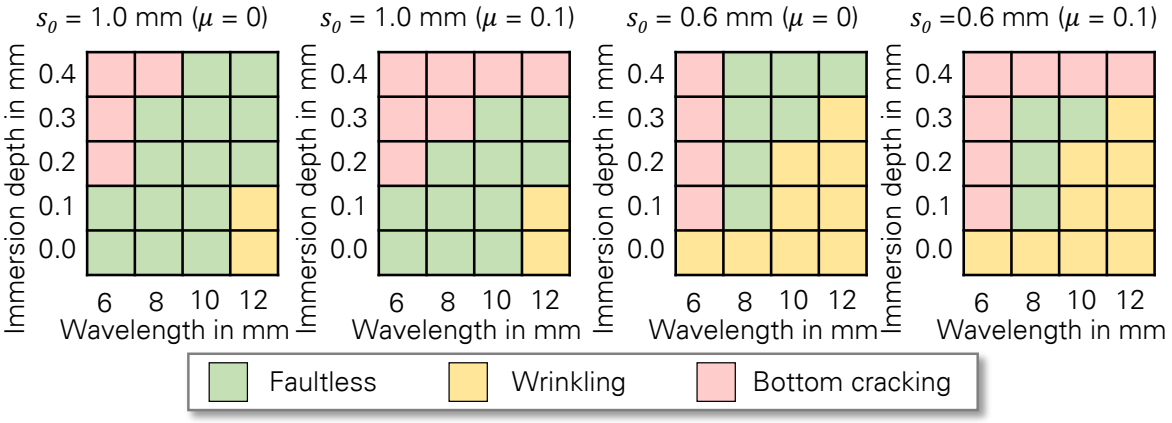

Figure 7-2: Results of the numerical parameter analysis of the process window

Moreover, in order to verify this state and control the applicability of the macro-structured deep drawing process, similar test series were performed experimentally. For this purpose, the tools introduced in section 5.4.2 were used. Sheet metals from the workpiece material DC04, which was introduced in section 5.3 with two different thicknesses of s_0 = 0.6 and 1.0 mm, were cut for the deep drawing process. Figure 7-3 shows the geometry and dimensions of the tools and the workpieces.

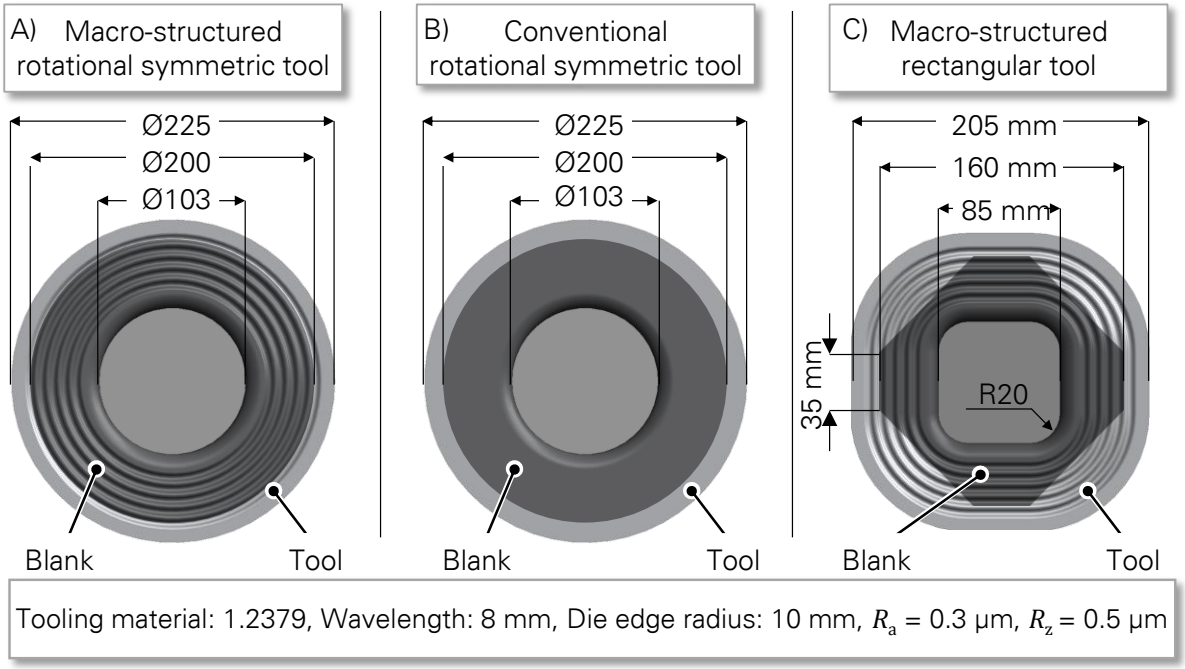

Figure 7-3: Geometry of the sheet metals used for the control of process stability

Within the scope of the experimental matrix, the stability of the rotationally symmetric deep drawing process with macro-structured tools was compared to the conventional process. Both macro-structured and conventional processes were carried out with the use of a spacer ring.

The ring can be used to adjust the amount of the immersion depth, i.e. δ = 0.2 and 0.4 mm in the macro-structured process. In the conventional process, the height of the ring was set to be equal to the sheet thickness. Pressing the blankholder with a full load to the spacer ring keeps the space between the blankholder and the drawing die constant during the process. Consequently, in order to control the feasibility of the new developed process for more complex geometries, the deep drawing of rectangular cups was performed with immersion depths of δ = 0.2 and 0.4 mm. As Figure 7-4-A and Figure 7-4-B show, no wrinkling can be seen in the workpiece made by the macro-structured process, which reveals that alternating bending can stabilise the sheet metal against wrinkling.

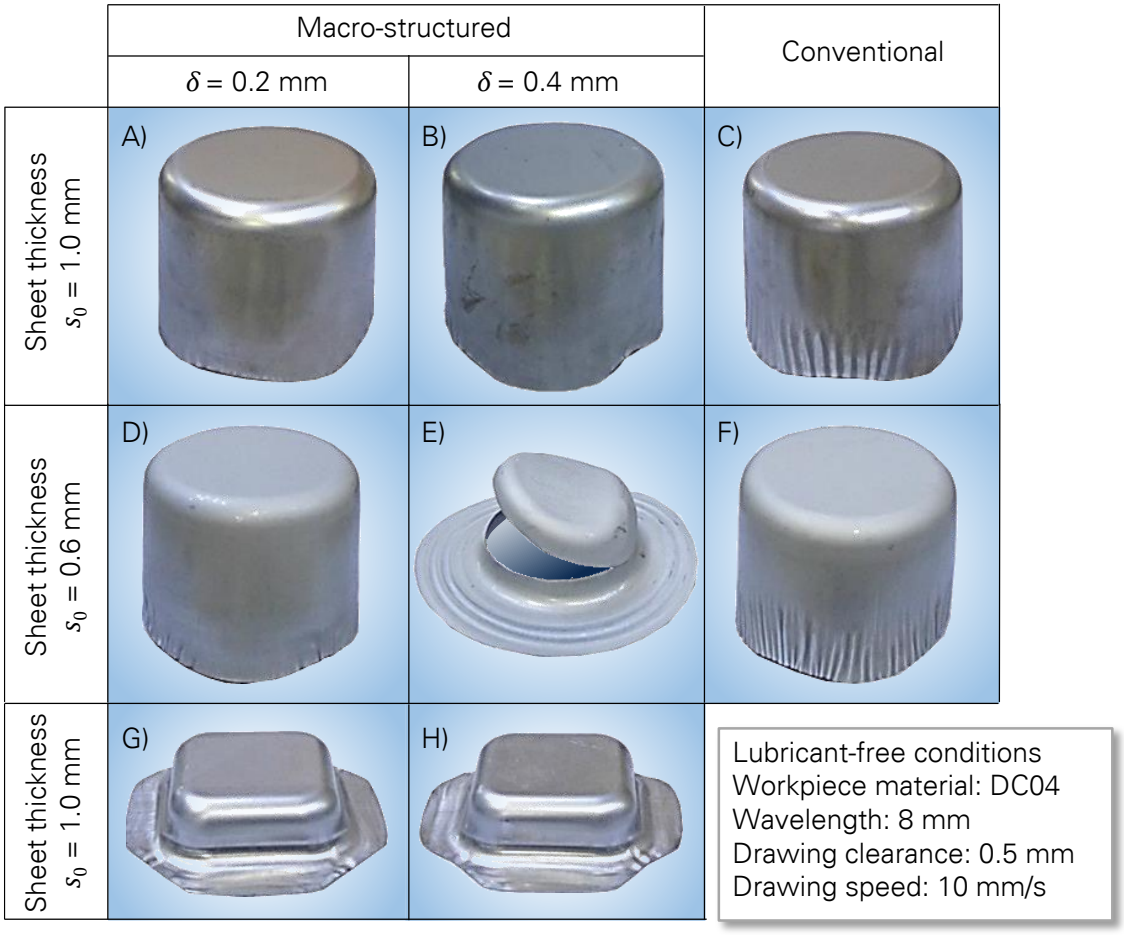

Figure 7-4: Results of the experimental tests for the control of process stability regarding wrinkling by deep drawing with macro-structured tools

Unlike the macro-structured process, there was some wrinkling in the workpiece made by the conventional process, as shown in Figure 7-4-C. Obviously, thinner materials are more unstable against wrinkling in the deep drawing process. Therefore, in the next step, sheet metals with a thickness of s_0 = 0.6 mm were chosen for the tests to control the applicability of the process for thin sheets. The results show that there was almost no wrinkling in the workpiece made by the deep drawing process with macro-structured tools and an immersion depth of δ = 0.2 mm, as shown in Figure 7-4-D. However, increasing the immersion depth to

δ = 0.4 mm leads to bottom cracks, as shown in Figure 7-4-E. It is because of the increased alternating bending energy in the flange area and consequently the increasing total punch force, which should be transferred to the bottom part of the workpiece. The stress caused by the punch force over the cross sectional area of the thin part exceeds the ultimate tensile strength of the workpiece, and this leads to the fracture of the material. Testing the same material with the conventional process, results in a number of wrinkles in the part, as shown in Figure 7-4-F. As mentioned above, to test the more complicated geometries with the macro-structured deep drawing tool, rectangular tools are considered. Here, the stress state in the transition area, where the tangential stress decreases in the corners toward the straight parts is more complicated and the risk of wrinkling is higher. For that end, the sheets with a thickness of s_0 = 1.0 mm were subjected to deep drawing with macro-structured tools. The results, which are depicted in Figure 7-4-G and Figure 7-4-H, show that there is no significant wrinkling in the workpiece and that the stability of the process is guaranteed. Summarising the results of the experimental tests, it can be concluded that the induced alternating bending, during deep drawing with macro-structured tools, increases the process stability through increasing the geometrical moment of inertia. Therefore, in this way, it is possible to enlarge the process window even more than with the conventional process. However, it should be noticed that excessive immersion depths can lead to bottom cracks in the workpiece. Therefore, process stability strongly depends on the process input parameters. Hence, to have the greatest possible process window, the optimum values of wavelengths and immersion depths should be chosen based on the criteria developed in Chapter 6.

7.1.3 Investigation about springback reduction through macro-structuring

As already discussed in section 6.6, the alternating bending mechanism in the deep drawing process with macro-structured tools can lead to a kinematic hardening effect of some materials. Because of this effect, there is a need to investigate the effects of process parameters on the springback behaviour of the workpiece in the newly developed deep drawing process. In this section, the effect of alternating bending is studied, as well as the resulting kinematic hardening on the springback behaviour of the deep drawn parts in the axial and tangential directions. To get information about the effects of materials on springback in deep drawing with macro-structured tools, two different types of industry-relevant materials, the alloy steel DC04 and the aluminium alloy AA5182, were subjected to numerical and experimental tests. For this purpose, draw bending of a U-Channel was considered. This method is attractive for these test series, because the level of springback due to the 90° bending in the axial direction is relatively large and it can easily be measured. The sensitivity of springback to basic parameters, such as tool radius, sheet thickness, geometric parameters of the tools, mechanical properties of the sheet materials and friction parameters, is usually studied by means of this technique [170]. Furthermore, the U-Channel parts are common elements in industrial sheet metal forming. They appear in many auto-body cover panels like

side members and beams. To achieve that, the process without alternating bending (δ = 0.0 mm) is compared to the process with alternating bending and an immersion depth of δ = 0.2 mm in draw bending of the U-Channel. The immersion depth of 0.2 mm is chosen because it corresponds to the stable deep drawing process. Furthermore, in order to examine the effects of kinematic hardening on springback of the workpiece during the process, the materials are considered with pure isotropic, pure kinematic and also a combined hardening behaviour in the numerical simulation. The BAUSCHINGER coefficients of each material for the combined hardening rule with a plastic strain of 0.3 are taken from literature [171] and listed in Table 7-1.

Table 7-1: BAUSCHINGER coefficients of testing materials [171]

Material	BAUSCHINGER coefficient
DC04	0.60
AA5182	0.85

Here, in the case of 100% isotropic hardening, the BAUSCHINGER coefficient is equal to 1 and by 100% kinematic hardening it is equal to zero. The process was simulated with a 2D FEM-Model with plane strain solid elements (7 elements across the sheet thickness of 1.0 mm) and a constant friction coefficient of μ = 0.15 using the COULOMB friction model. The friction coefficient was chosen based on the investigations introduced in Chapter 2. For the experimental tests, the setup applied in section 7.1.1 with the Tip to Hutch arrangement was used. All the tests were repeated five times in order to get sufficient information about the statistical repeatability of the results. The springback behaviour of U-Channels can be characterised regarding the final part geometry with three parameters: the angle between the bottom and the wall β_1, the angle between the wall and the flange β_2, and the radius of curvature of the sidewall ρ. As β_1 and β_2 increase and ρ decreases (the curvature of sidewall increases), springback increases. Figure 7-5 shows the springback geometry of a U-Channel cross section.

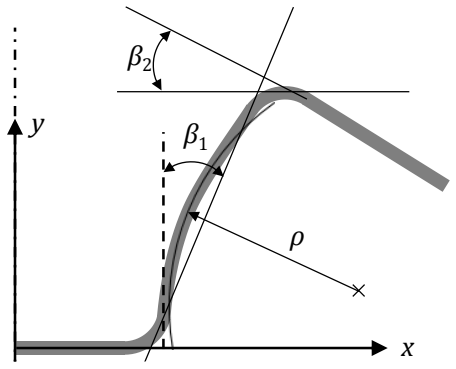

Figure 7-5: Schematic Overview for springback geometry for a U-Channel [172]

Since β_1 and β_2 are usually very close together and there is almost a linear relation between the sidewall curvature and deflection angles, β_1 was chosen as a scale to study the effects of the process parameters on springback in this section.

Experimental results reveal that the springback of workpieces will be reduced through generating an alternating bending mechanism, because of the induced tensile force in the flange area. The geometries of the formed parts which are depicted in Figure 7-6 show that regardless of the material, the springback in the process with alternating bending (δ = 0.2 mm) is always less than the process without alternating bending (δ = 0.0 mm).

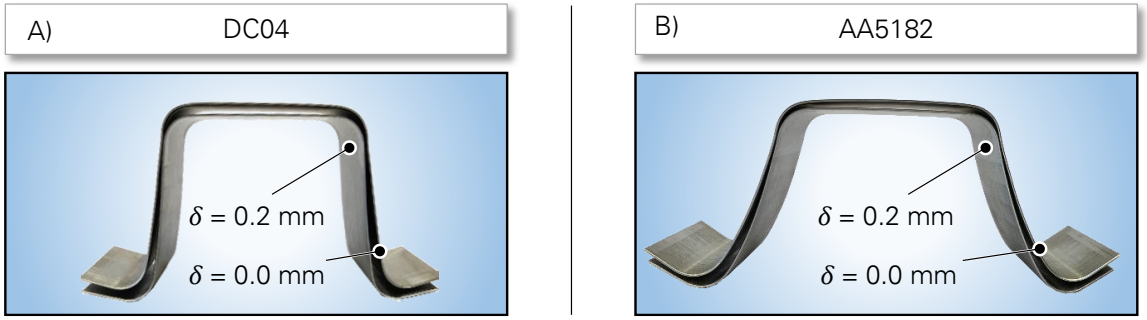

Figure 7-6: Springback behaviour of the workpieces with and without alternating bending for A) DC04 and B) AA5182 [148]

Based on the measured springback angle for both materials, it can be concluded that the amount of springback reduction through alternating bending for DC04 and AA5182 is approximately 23% and 32%, respectively. Furthermore, the results reveal that the springback of the aluminium alloy is higher than DC04 because of its smaller value of YOUNG modulus. To investigate the effects of kinematic hardening as a result of alternating bending on the springback of workpieces, numerical simulations were performed. The numerical results based on FEM-simulation for draw bending of the U-Channel with macro-structured tools confirm that the retention force caused by alternating bending in the flange area compensates for the springback of the workpiece in both hardening models. As Figure 7-7 shows, the springback will be reduced by generating alternating bending for pure isotropic, pure kinematic, and also combined hardening types in both testing materials. Based on the results of the simulations, the amount of springback by the pure isotropic hardening model is slightly higher than the pure kinematic model. This is due to the larger level of the stored energy density predicted by the simulation with the isotropic hardening model [173]. Furthermore, the springback reduction through alternating bending in the pure kinematic hardening model is more than the pure isotropic model (see the values below the diagram). This is because of the induced BAUSCHINGER effect as a result of alternating bending. In other words, the BAUSCHINGER effect has an additional influence on the compensation of springback. In summary, the retention force induced through alternating bending reduces the amount of springback during deep drawing with macro-structured tools. Moreover, the BAUSCHINGER effect because of alternating bending can reduce further the springback behaviour of materials with predominately a kinematic hardening effect.

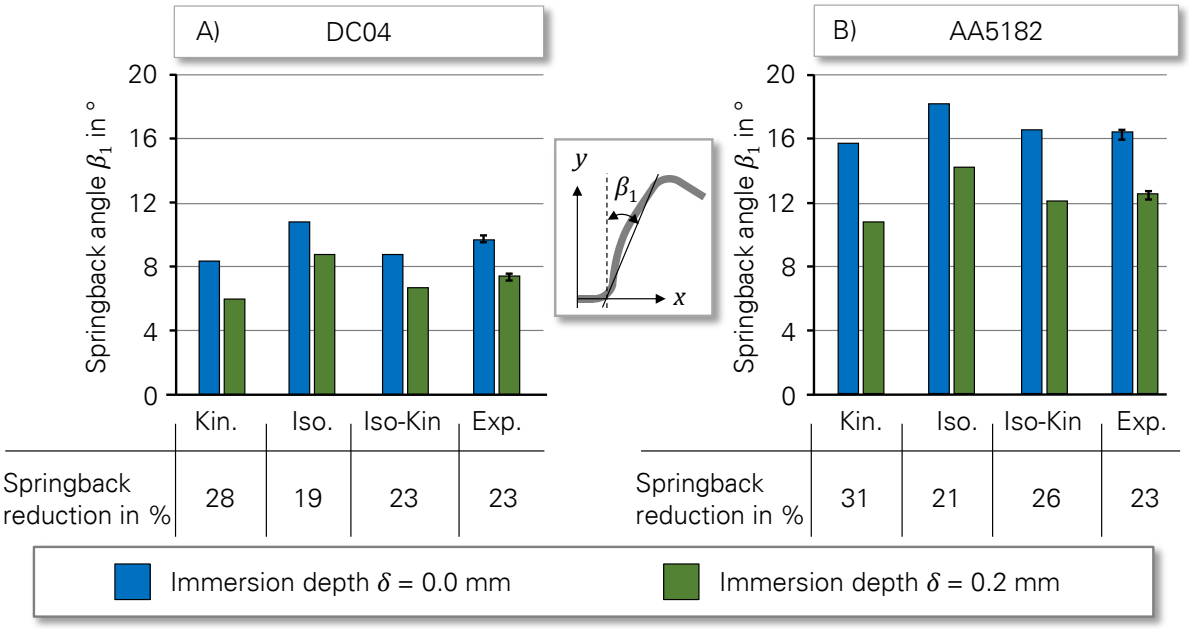

Figure 7-7: Springback angle of U-Channels under different hardening types for A) DC04 and B) AA5182

7.2 VERIFICATION OF THE DEVELOPED ANALYTICAL METHODS

In this section, the developed analytical methods to describe the process, as well as the criteria for the prediction of process limits and dimensional accuracy of the parts, are verified through experimental tests and numerical simulations.

7.2.1 Verification of the developed process model: forming energy

To verify the analytical model for calculation of the total energy for deep drawing of rotationally symmetric geometries, the analytical results are compared with FEM results and experimental tests. In these test series, samples from DC04 with two different initial outer radius of r_0 = 90 and 100 mm, two different sheet thicknesses of s_0 = 1.0 and 0.6 mm under two different immersion depths of δ = 0.2 and 0.04 are considered. Based on the experimental draw-bend test, the friction coefficient between the tools and the workpiece is set to be μ = 0.15 for both analytical and numerical calculations. The experimental tests are repeated five times in order to get reliable information about the statistical repeatability of the results. Figure 7-8 compares the calculated total energy E_t from Equation 6-6 with measured values from experimental tests and also FEM results. The diagrams reveal that the analytical and numerical results exhibit a very good agreement with the experimentally determined for forming energy in the whole matrix of the study. The error indicators in both diagrams show a very small deviation from the five repetitions per parameter set in the experiments.

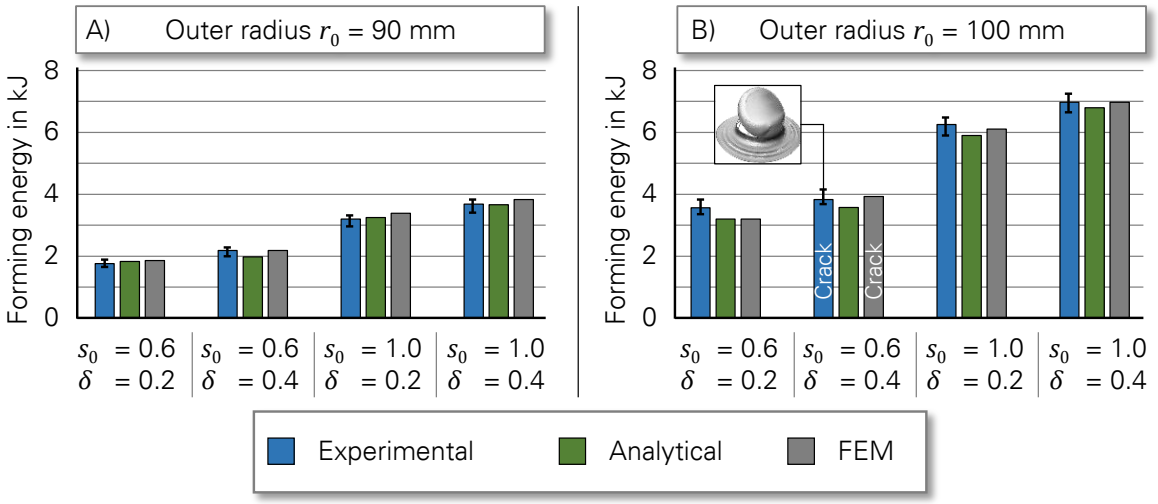

Figure 7-8: Comparing the analytical calculated total forming energy with experimental and FEM results for deep drawing of rotationally symmetric cups with outer radius of A) 90 mm and B) 100 mm [130]

The results verify the model for the calculation of total energy. However, as depicted in Figure 7-8-B, a bottom crack occurs in deep drawing of the part with an initial outer radius of r_0 = 100 mm, a thickness of s_0 = 0.6 mm, and an immersion depth of δ = 0.4 mm. In order to verify the applicability of the analytical model developed for more complex geometries by means of the assumptions mentioned in section 6.3, the rectangular macro-structured tools are used. In order to use the energy method for the rectangular cups, it should be divided into four rotationally symmetric corners and four straight sections. In the straight sections there is no compressive tangential stress and as a result the ideal forming energy E_{id} will be eliminated from the total forming energy E_t. For the other equations, the tool radius will be assumed to be infinite. With these simplified assumptions, the total energy can be calculated. As the diagram in Figure 7-9 shows, there is also a very good agreement between the calculated energy and the experimentally and numerically determined values.

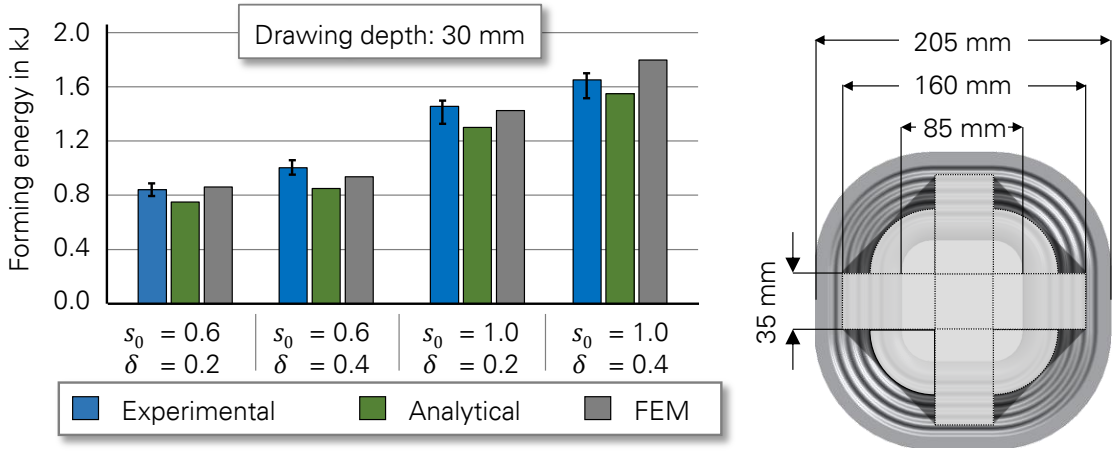

Figure 7-9: Comparing the analytically calculated total forming energy with experimental and FEM results for the deep drawing of rectangular cups

However, the diagram shows the analytical determined energies are always slightly lower than the experimentally determined energy since the in-plane shearing in the transition area between the corner areas and the straight regions is not considered in the calculations. Furthermore, small unconsidered parts of the sheet metal between the corners and the straight parts (dark parts of the sheet metal in Figure 7-9) are not subjected to the calculation because of their indefinable geometry. These results show that with the ability to calculate all the individual energy terms for deep drawing with macro-structured tools, it is possible to design the most energy-efficient process regarding the process input parameters.

7.2.2 Verification of the developed criterion: prediction of wrinkling

In order to control the accuracy of the criterion developed for the prediction of wrinkling, experimental deep drawing processes with macro-structured tools were performed. For this end, macro-structured tools with a constant wavelength of λ = 8.0 mm were used. Since the thickness plays an important role on the buckling stiffness of the sheet metal, and thereby the critical tangential stress $\sigma_{t,cr}$ for wrinkling, blanks with an initial outer radius of r_0 = 100 mm in three different thicknesses of s_0 = 0.3, 0.5 and 0.6 mm were subjected to the tests. In the following, the critical stress $\sigma_{t,cr}$ for wrinkling (see Equation 6-14) will be compared with the present tangential stress on the free end part of the sheet metal (Equation 6-2). As mentioned in the section on the Development of a criterion for the prediction of wrinkling, for a stable process, the tangential stress σ_t must always be below the critical tangential stress $\sigma_{t,cr}$. This criterion is controlled in this section. Figure 7-10 shows the results of the experimental tests for the verification of the criterion developed regarding the prediction of wrinkling. Here all the tests were repeated five times in order to get adequate information about the statistical repeatability of the results. The results of the tests with a sheet thickness of s_0 = 0.6 mm are depicted in Figure 7-10-A. Here, the progress of the tangential stress at the free end part of the sheet (most unstable part of the flange area, see section 6.1.1) over the punch displacement is shown with a green line. The critical tangential stress for the onset of buckling $\sigma_{t,cr,}$ which is shown with a red line is almost 480 MPa. As the figure shows, the present tangential stress on the free end part of the flange is always below the critical stress. Therefore, there is no wrinkling expected in this case. The experimentally deep drawn cup reveals that there is no wrinkling up to a punch displacement of h_2 = 45 mm. However, repeating the test with a thinner sheet metal (s_0 = 0.3 mm) leads to dropping off of the critical tangential stress $\sigma_{t,cr}$ up to 120 MPa. As Figure 7-10-B shows, from the beginning of the process (by punch displacement of h_1 = 35 mm), the present tangential stress of the sheet metal is always above an allowable value in the uncertain zone. As a result, it is expected that wrinkling will be initiated at the beginning of the process. The experimentally deep drawn part shown in Figure 7-10-B verifies this prediction. However, the critical situation should be for the sample with a sheet thickness of s_0 = 0.5 mm. As the Figure 7-10-C shows, at the beginning of the process, the tangential stress at the free end part of the sheet is below the critical stress ($\sigma_{t,cr}$ = 310 MPa), and therefore no wrinkling should be expected at the beginning. Continuing the process, the tangential stress reaches the critical value and enters

into the uncertain zone by a punch displacement of 43 mm. It means that the wrinkling should be initiated at the free end part of the sheet. This statement is verified through the experiment. As shown on the figure, by a punch displacement of h_2 = 45 mm, small wrinkling can be seen on the free end part of the sheet. The experimental results show a good agreement with the analytical criterion for the prediction of wrinkling in the deep drawing process with a macro-structured tool. In the next section, the validity of the criterion developed for the prediction of bottom cracks will be examined.

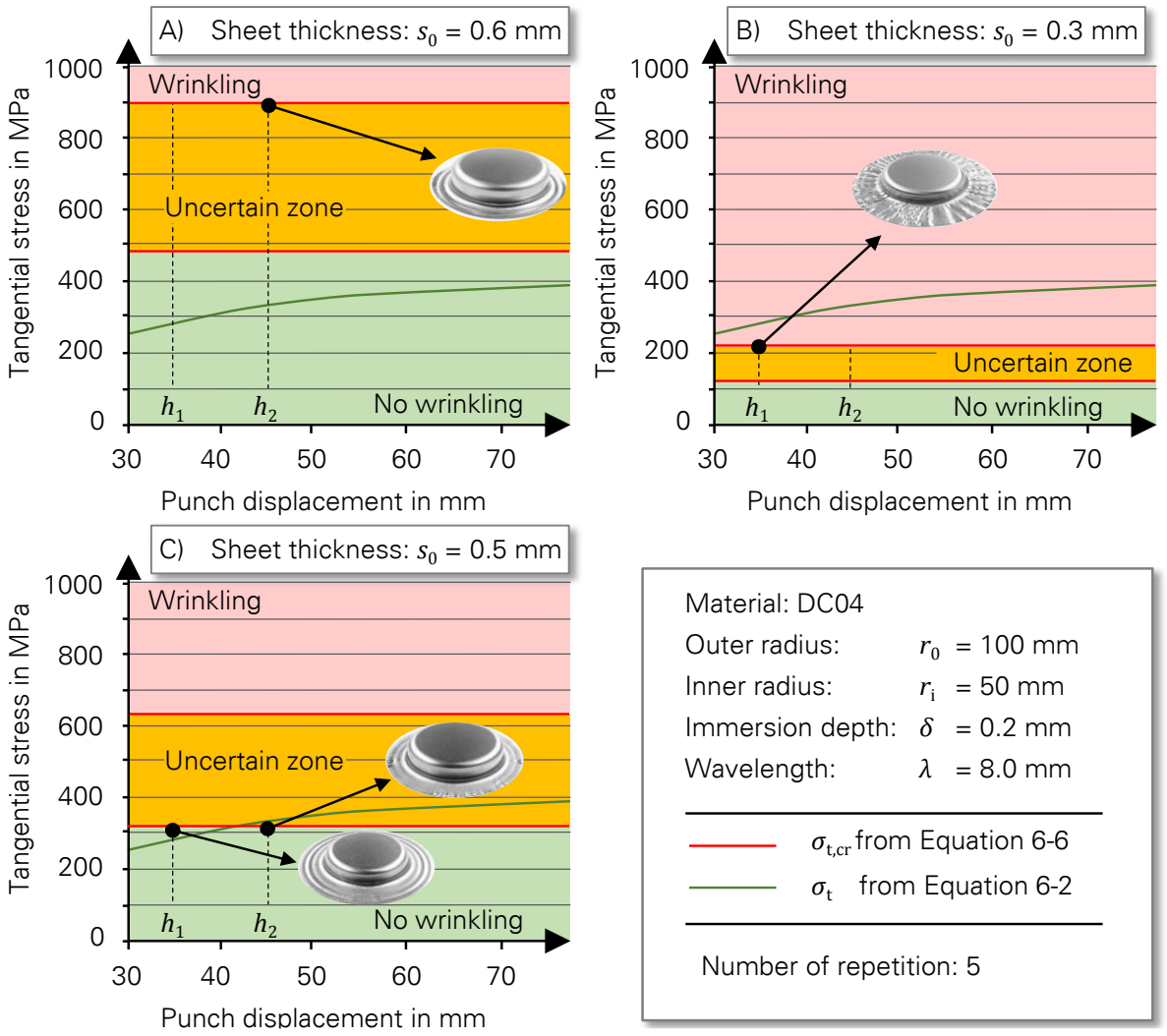

Figure 7-10: Prediction of wrinkling for samples with a sheet thickness of A) s_0 = 0.6 mm, B) s_0 = 0.3 mm and C) s_0 = 0.5 mm

7.2.3 Verification of the developed criterion: prediction of bottom cracks

As discussed in section 6.4, for a stable process, the total forming force F_t (see Equation 6-4) should be less than the critical bottom crack force F_{bc} (see Equation 6-22). In order to verify

the criterion developed regarding the prediction of bottom cracks, the critical bottom crack force for all the test series are calculated using the Equations 6-22 to 6-25. Figure 7-11 compares the measured maximum punch forces from the test series introduced in section 7.2.1 with the analytically calculated forces and also the corresponding bottom crack forces F_{bc}.

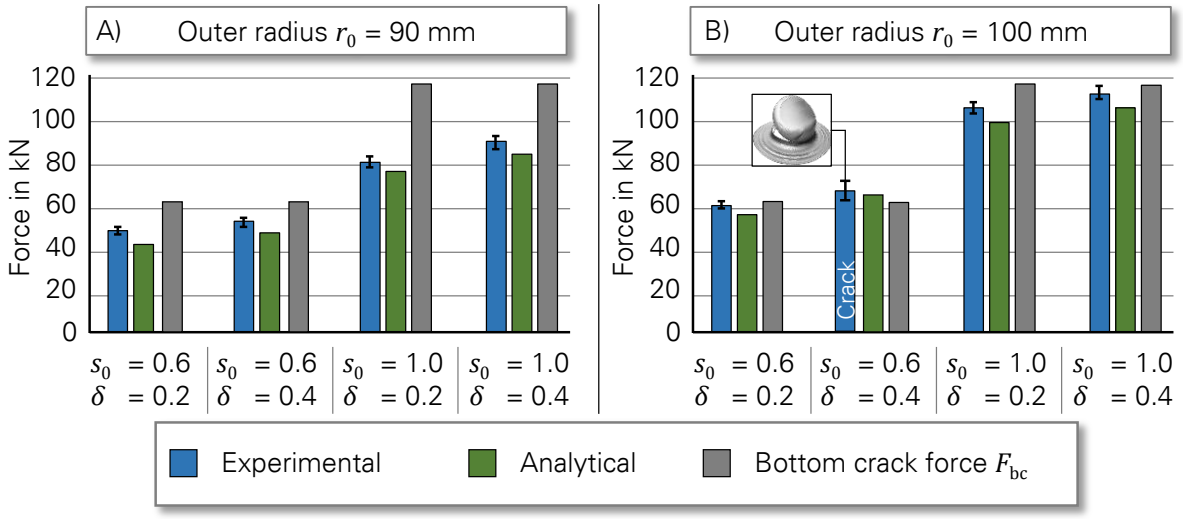

Figure 7-11: Prediction of bottom cracks through the critical punch force for sheet metals with outer radius of A) 90 mm and B) 100 mm

Figure 7-11-A shows that the forming force for the sample with an initial outer radius of r_0 = 90 mm is always below the critical force. Therefore, no bottom cracks are expected in this test series while the experimental tests verify this prediction. However, as shown in Figure 7-11-B, for the samples with an initial outer radius of r_0 = 100 mm, the critical punch forces from Equation 6-22 are always slightly higher than the analytically calculated and experimentally measured forces, except for the sample with a thickness of s_0 = 0.6 mm and an immersion depth of δ = 0.4 mm. Therefore, bottom cracks can be expected in this case and the corresponding experiment verifies this prognosis. These results approve the adequacy of the criterion for the prediction of bottom cracks in the deep drawing process with macro-structured tools.

7.2.4 Verification of the developed criterion: prediction of dimensional accuracy

To control the influence of alternating bending on the residual stress of the parts during the deep drawing process with a macro-structured tool, this process should be compared with a conventional process. Furthermore, in order to take the dependency of the material into account, the mild steel DC04, as well as the aluminium alloy AA5182, were subjected to investigation. To use the half-analytical method described in section 6.6, the processes were

simulated by means of FEM. In the simulation sets, the deep drawing process with conventional tools was considered as a reference and is compared with the macro-structured deep drawing process with two different immersion depths of δ = 0.2 and 0.4 mm, respectively, and a constant wavelength of λ = 8.0 mm. The results of the FEM are based on 2D FEM-simulations with an isotropic hardening assumption. The workpiece consists of eleven elements over its thickness with a maximum element size of 0.1 mm. The blanks with an initial outer radius of r_0 = 90 mm and a sheet thickness of s_0 = 0.6 mm were chosen for the analysis. As mentioned in previous sections, based on experimental determinations, the friction coefficient was set to be μ = 0.15 for the simulations. The conventional processes are simulated using a spacer ring with a height equal to the sheet thickness in order to realise a uniform surface pressure in the flange area. The simulations consist of two steps: deep drawing up to the predefined height and consequently unloading the workpiece to simulate the springback of the parts. To evaluate the opening gap of the split rings from Equation 6-39, it was necessary to determine the bending moment as a result of the residual stress M_b^{res}. For this purpose, the progress of the tangential residual stress σ_t^{res} over the sheet thickness on the wall of the part (where a ring will be cut out), should be determined based on the FEM results. Figure 7-12 shows these stresses at the height of 35 mm from the bottom of the parts. Consequently, the opening gap Δ from Equation 6-39 can be evaluated based on numerical integration of the shown residual stress curves. In order to verify the results of the developed criterion, the results should be compared with real values from the experimental test. The experimentally deep drawn parts are cut out by means of an electrical discharge machining (EDM) process to prevent the external residual stresses through the cutting process, because it does not require high cutting forces for removal of the material.

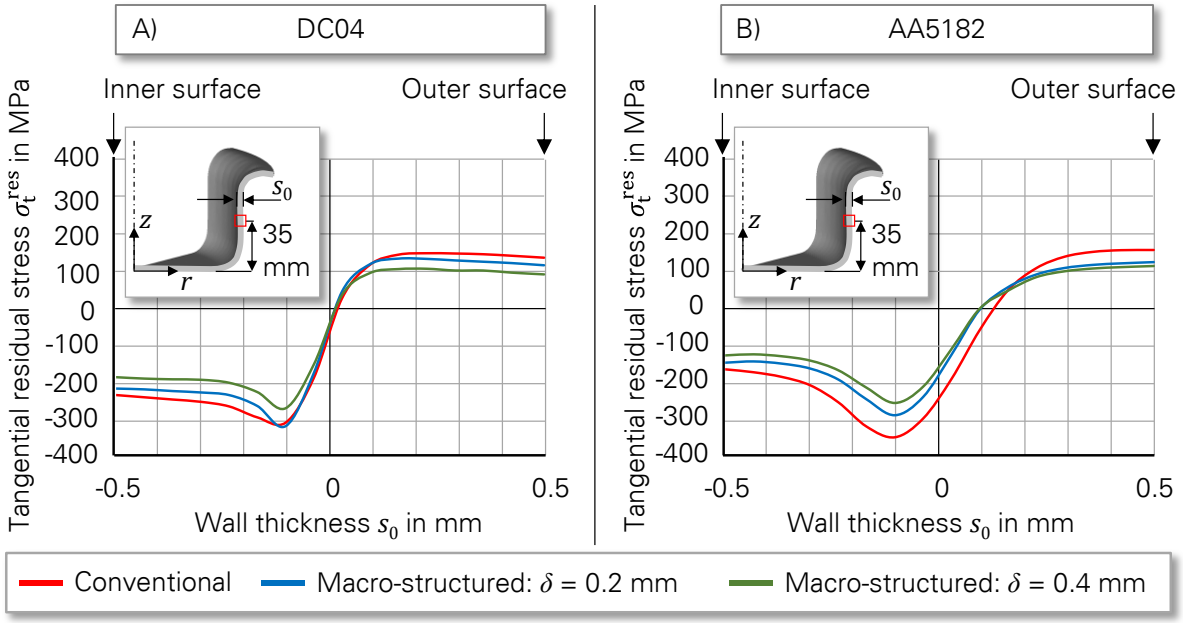

Figure 7-12: Tangential residual stress over the sheet thickness in the cup made by conventional and macro-structured processes from A) DC04 and B) AA5182.

The opening gap of each ring after splitting was measured and is listed in Table 7 2. Moreover, the calculated values for the opening gap, based on the half-analytical method, are also presented in the same table in order to compare with the experimental results. The experimental results exhibit a very good agreement with the half-analytically determined opening gap of the split rings. The results reveal that regardless of the material, by increasing the immersion depth in the macro-structured deep drawing process, the amount of residual stresses can be reduced. It is because of the superimposed tensile stress as a result of alternating bending, which is transferred from the punch to the material. This superimposed tensile stress changes the proportion of the residual tensile and compression stress through the sheet thickness. As a result, the stored elastic energy and consequently the springback of the rings after cutting will be decreased. The same effect is also seen in [174].

Table 7-2: The opening gap of split rings based on experimental tests and calculated values.

Material	Opening gap in mm (conventional)		Opening gap in mm (macro-structured)			
			δ = 0.2 mm		δ = 0.4 mm	
	Measured	Calculated	Measured	Calculated	Measured	Calculated
DC04	50	48.7	45	44.1	37	36.9
AA5182	95	99.2	73	81.1	64	71.8

In other words, the created non-frictional retention force can be used positively to compensate the springback behaviour of the workpiece. Furthermore, the additional plastic deformation due to the alternating bending decreases the elastic strains. This can also lead to a reduction of springback in the deep drawn parts with macro-structured tools. Figure 7-13 shows the top view of the split rings and gives an overview regarding the effects of the material and the process on residual stress in the deep drawing process.

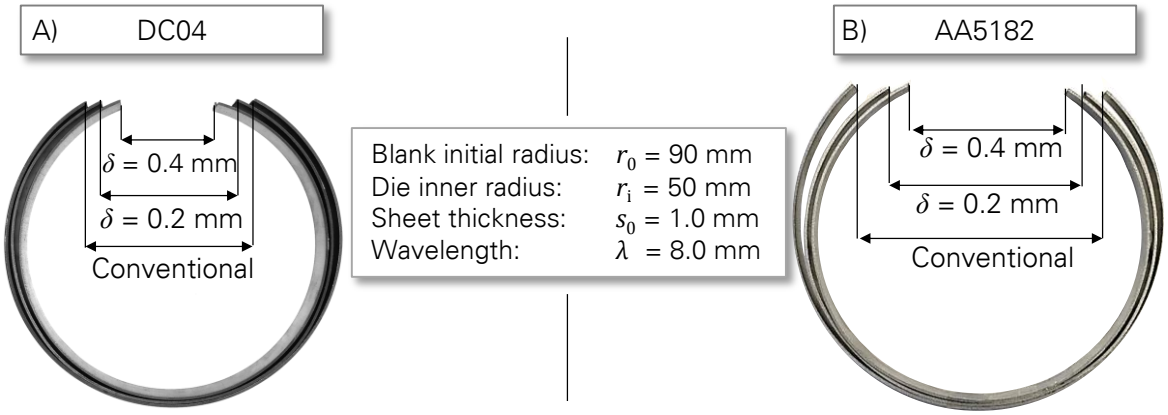

Figure 7-13: Results of the ring splitting test for cups made by conventional and macro-structured tools from A) DC04 and B) AA5182.

7.3 SUMMARY OF CHAPTER 7

Within the scope of this chapter, the analytical model and criteria developed in the previous chapter were verified by means of the FEM, as well as experimental tests. Regarding process stability, it was confirmed that the onset of wrinkling can be predicted analytically based on the in-plane buckling theory. It was shown that as long as tangential stress at the free end part of the sheet is below the critical tangential stress, no wrinkling is expected in the process. The results verified also that the developed criterion can predict the process stability regarding bottom cracks based on the energy method. For this purpose, the maximum allowable punch force is a good benchmark for comparison with the forming force.

Moreover, there was a good agreement between the experimentally measured and analytically calculated values, regarding the residual stresses in the workpiece. It was also shown that the residual stresses in the deep drawing process with macro-structured tools are generally smaller than by the conventional process.

8. TRANSFER OF THE METHODOLOGY INTO THE COMPLEX GEOMETRIES

Deep drawing of complex geometries is widely used in sheet metal forming processes to produce irregularly shaped components. The formed asymmetric cups are needed in a variety of industrial uses. It is required for automotive applications and aerospace parts, as well as a wealth of other products. Rectangular and elliptic cups with large aspect ratios are used for electrical parts such as battery containers, semi-conductor cases, and crystal vibrators. In this chapter, the transferability of the developed approach into complex geometries is investigated.

8.1 CONSTRUCTION OF A DEEP DRAWING TOOL TO FORM A T-CUP

In order to control the transferability of the already proposed technology into complex geometries for industrial applications, a modular deep drawing tool with a relatively complex geometry, a so called "T-Cup", was constructed in the scope of this thesis. Figure 8-1 shows a detailed view of the tool. The form entails concave and convex shapes, as well as straight parts to have a variety of stress states in the part. The modularity of the tool allows all functional surfaces to be changed, like the die edge radius and the flange area, regarding their forms and dimensions. The modular die edge from the cold work tool steel 1.2379, with a radius of 10 mm, was hardened up to 60 HRC and afterwards grinded and polished to reach a surface roughness of R_a = 0.1 and R_z = 3.2 µm. The segments of the flange area also from tool steel 1.2379, with a delivered hardness of 25 HRC, were milled to fabricate the macro-structures with a constant wavelength of λ = 10 mm, based on preliminary investigations by means of the FE and the analytical method. These segments were also ground and polished manually to reach a surface roughness of R_a = 0.6 and R_z = 6.5 µm. Here, polishing the macro-structures using a classical polishing machine was not applicable. These parts were assembled from several segmented pieces on the fixing plate. To compare the macro-structured deep drawing with the conventional process, conventional flange segments with the same inner and outer geometries were also constructed and manufactured. These segments have the same hardness and surface roughness as the die edge radius. The surface properties of both conventional and macro-structured tools are listed in Table 8-1.

Table 8-1: Surface-related properties of the modular deep drawing tool

Part	Hardness (HRC)	R_a (µm)	R_z (µm)
Die edge radius	62	0.1	3.2
Conventional flange	62	0.1	3.2
Macro-structured flange	25	0.6	6.5

The differences between the roughness and the hardness values were because of their manufacturing processes. To apply the blankholder force, six pneumatic springs were used. The nitrogen medium (N_2) used in each spring, with the maximum filling pressure of 15 MPa, realises a quasi-steady working spring stiffness of 625 N/mm. The 80 mm nominal stroke of springs determines the traveling distance of the tool and also its maximum drawing depth. The tool is cleaned with a proper cleaning agent before being used to ensure a total lubricant-free deep drawing process. The hydraulic press machine RZP 250 from *Röcher Maschinenbau* (see section 5.1.2) was used to form the T-Cups because of its high power performance and room capacity.

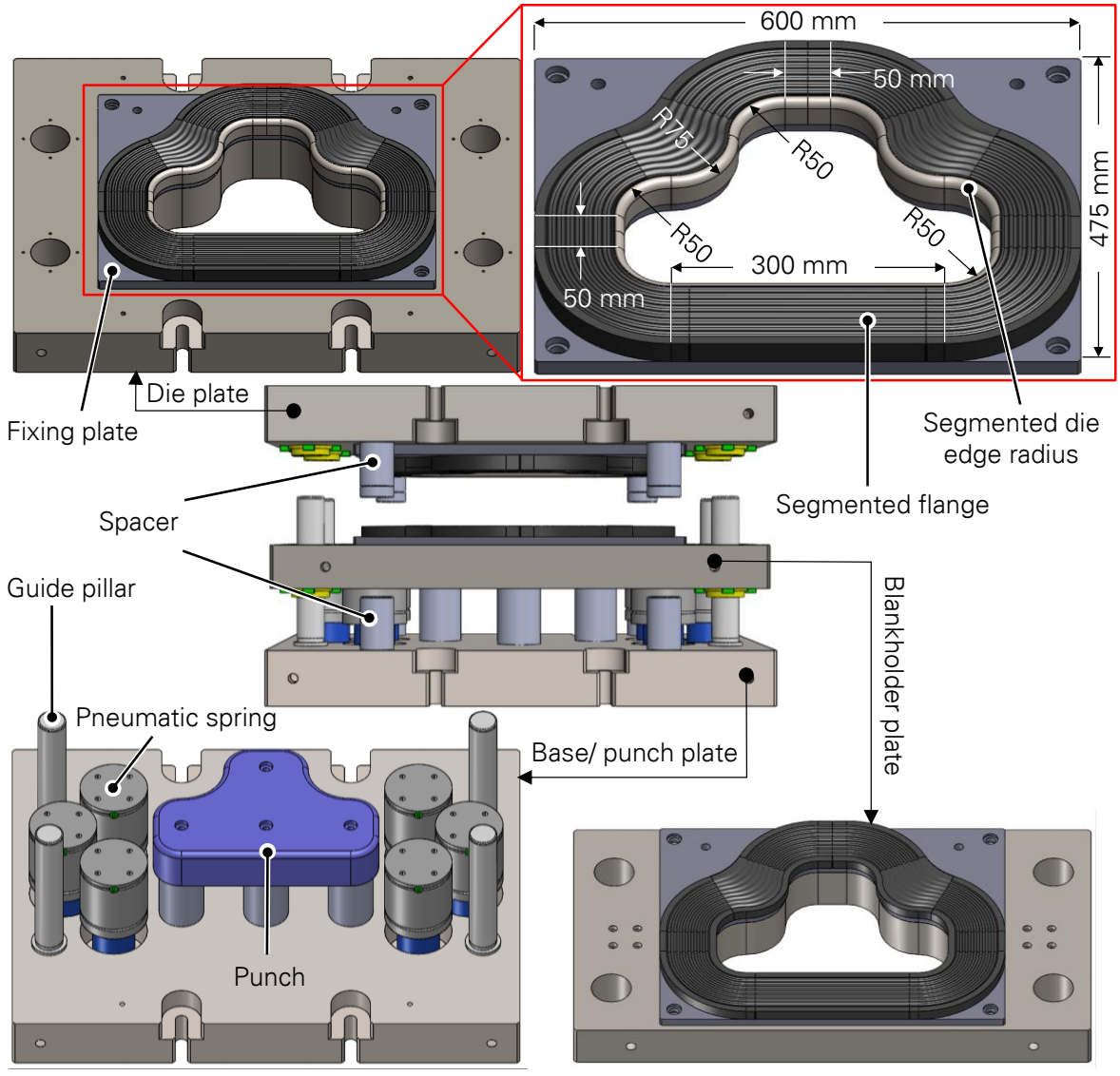

Figure 8-1: Detailed view and components of the T-Cup deep drawing tool

8.2 DETERMINATION AND EVALUATION OF OPTIMUM INITIAL BLANK GEOMETRY

Deep drawing of complex parts requires several intermediate steps to avoid any defects and to achieve the final desired geometry successfully. Using the optimum initial blank geometry has many advantages in the deep drawing process. The optimum initial blank geometry not only reduces the material costs of the produced part, but also improves the deep drawing quality, thickness distribution and formability of the part, and minimises forming defects. However, finding the optimum blank geometry could be difficult and time consuming. Since experimental trial-and-error methods for achieving the initial blank geometry are time consuming and expensive, other methods were sought for optimum blank design in the sheet metal forming operations. Different approaches for blank geometry design have been reported in the literature [175]. These methods can be classified as the slip-line field method [176], geometrical mapping [177], the analogy method [178], ideal forming [179], the inverse approach [180], backward tracing [181], and the sensitivity analysis method [182]. The blank shape design in this thesis was carried out using the slip-line field method. Slip-line field theory is based on the analysis of a deformation field that is both geometrically self-consistent and statically admissible. Slip lines are planes of maximum shear stress and are therefore oriented at 45° to the axes of principal stress [183]. Using this graphical-analytical approximation method, the initial blank geometry was determined for deep drawing of the T-Cup as shown in Figure 8-2.

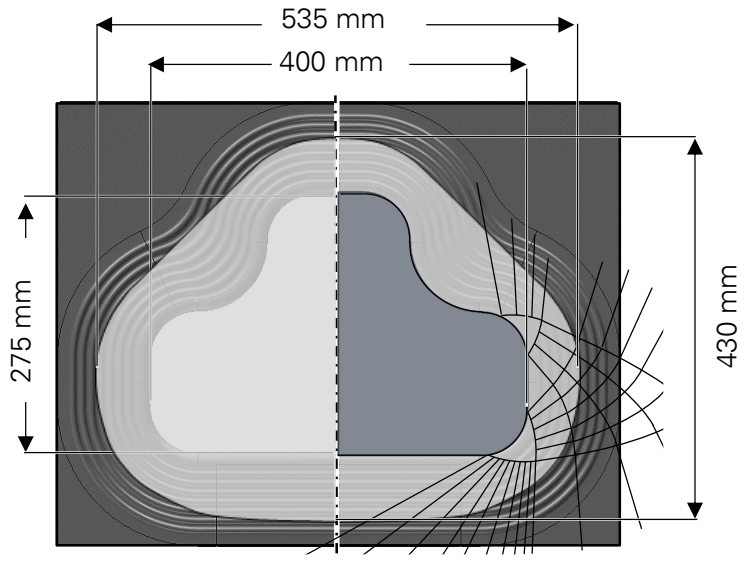

Figure 8-2: Determination of the optimum initial blank geometry using Slip-line field theory

To prognosticate the process stability regarding bottom cracking and wrinkling, the analytical method which was introduced in section 6.3 can be applied for the T-Cup. For this purpose, the sheet metal determined can be divided into several geometrical analysable parts with definable dimensions as shown in Figure 8-3. Through superposing the forming force of all

parts, it is possible to find out the required punch force. Subsequently, it can be compared with the bottom crack force F_{bc} and used to predict the process stability regarding bottom cracks. Moreover, considering the stress states in each part which are labelled with directional arrows in Figure 8-3, it is possible to specify the most unstable areas regarding wrinkling. Parts 2, 4 and 6, with a quarter circle geometry and 100 mm radius, undergo tensile-compressive stress with superimposed alternating bending. Because of the existing tangential compressive stress in these areas, these parts are the most probable wrinkling zones of the sheet metal. Therefore, the model for analysing the rotationally symmetric deep drawing process can be applied to these parts. Straight parts 1, 5 and 7 sustain alternating bending with superimposed tensile stress.

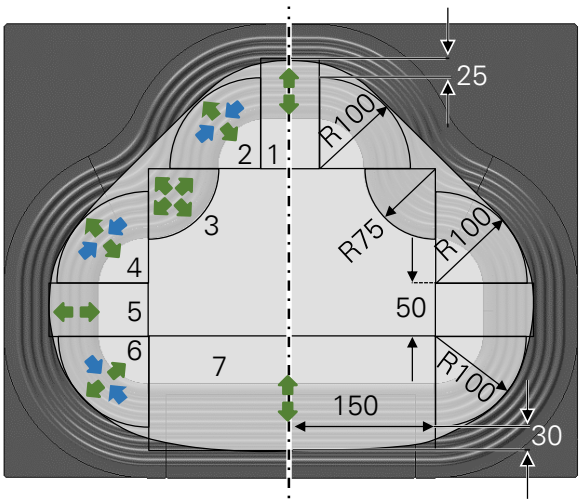

Figure 8-3: The superposing method for analysing the deep drawing of the T-Cup

Hence, the corresponding forming force can be calculated by excluding the ideal forming force from the punch force calculation of the rotationally symmetric parts. In part 3, a tensile-tensile stress state leads to stretch forming conditions. The stretch of the sheet with a thickness of s_0 = 1.0 mm can be estimated by the formulation of OEHLER und KAISER [184], which is verified by LANGE in [166] as following:

$$F_{sf} = \frac{A_1}{\eta_F} \sigma_{ym} \ln \frac{A_1}{A_0} \qquad 8\text{-}1$$

Here, A_0 is the original area of the sheet, A_1 is the increased area after stretch drawing, and σ_{ym} is the mean yield stress. The forming efficiency is x = 0.5 to 0.7. If the stresses are distributed uniformly over the entire surface, this factor should be η_F = 0.7, and for unequal load distribution the forming efficiency should be η_F = 0.5 [166].

8.3 TEST PROCEDURE AND INTERPRETATION OF RESULTS

In order to investigate the usability of macro-structured tools, as well as verification of the analytical model for a T-Cup, experimental tests were performed. For this purpose, sheet metals from DC04 with 1.0 mm thickness were cut out through the laser-beam cutting method, corresponding to the already determined optimum shape. The sheet metals were cleaned after deburring with acetone to remove the initial corrosion-preventing oil on the sheet metal. Subsequently, the cleaned and deburred sheet metals were subjected to the deep drawing process with macro-structured tools with an immersion depth of δ = 0.2 mm. The exact immersion depth can be adjusted by using a contouring spacer ring. Figure 8-4 shows the progress of the drawing process in three stages. As the Figure shows, there is a stable process regarding both the failure cases of bottom cracking and wrinkling.

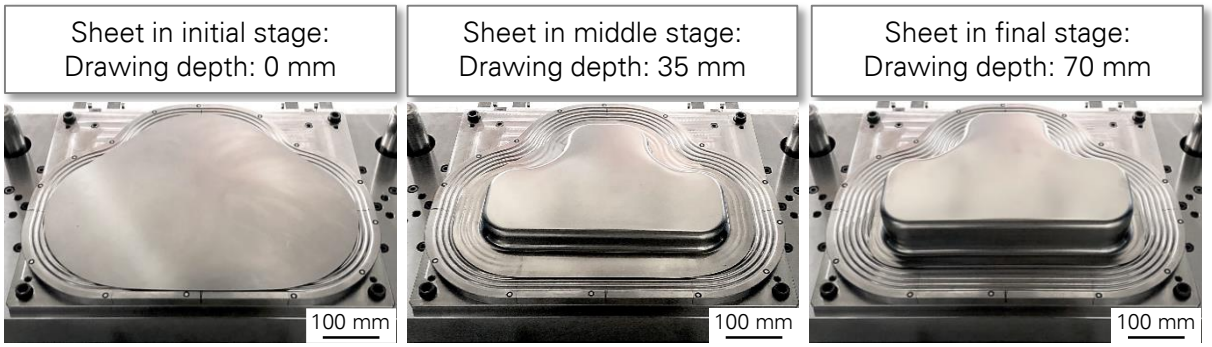

Figure 8-4: Progress of the deep drawing of the T-Cup with macro-structured tools

In order to make a statement about the accuracy of the analytical criterion to predict the occurrence of bottom cracks, the required punch force to form the T-Cup, calculated from the analytical model, was compared with the FEM and experimental results. The process was simulated in 3D with the FEM. For the simulation, solid shell elements with 2 mm element size which consist of 5 integration layers (1 integration point on each layer) were used. To increase the accuracy of the simulation, the anisotropic yield function of HILL was applied, with the corresponding *r*-values determined from uniaxial tensile tests. The frictional force based on the COULOMB model with a friction coefficient of μ = 0.15 for the whole tool was considered. Figure 8-5 shows the load-displacement curve for deep drawing of the T-Cup, regarding the experimental, FEM and analytical results. The results show that the progression of forces over the punch displacement tended to be similar. However, for determination of bottom crack by means of developed criterion only the maximum value of the punch force is relevant, therefore this is considered for the calculations.

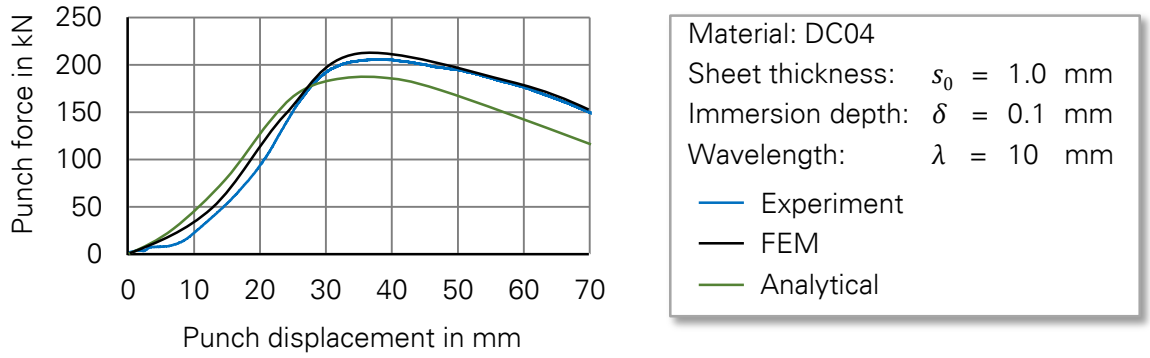

Figure 8-5: Load-displacement curve for the deep drawing of the T-Cup

To quantify the punch force and also to be able to assess the process window regarding bottom cracks, the critical bottom crack force from Equation 6-22 was calculated. All results regarding the maximum punch force from the experimental tests, FEM calculations and the analytical model are summarised in Figure 8-6 and compared with the relating bottom crack force F_{bc}.

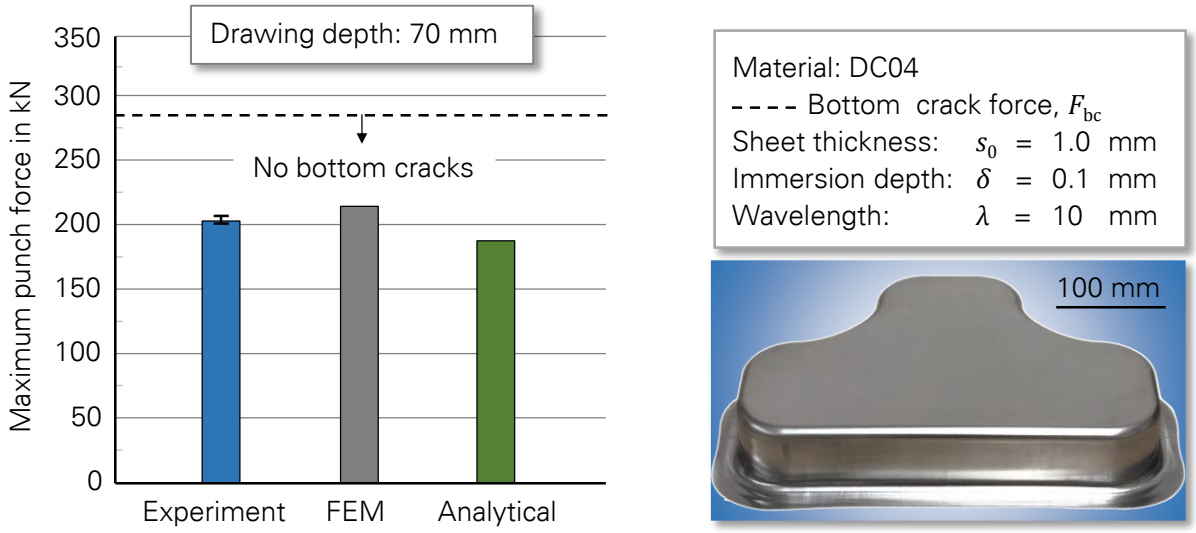

Figure 8-6: Comparison between the maximum punch force from the experimental tests, FEM calculations and the analytical model

In the experimental tests, the average punch force was 205 kN, for the deep drawing of the T-Cup from DC04 with a 1.0 mm thickness, 10 mm wavelength and 0.2 mm immersion depth. Comparing this value with the corresponding result from the FEM simulation shows that there is approximately only a 7% difference. This good agreement, between the numerical results and the experimental tests, reveals the accuracy of the applied material model and the boundary conditions. However, the analytical model predicts a punch force of 180 kN, which is 12% and 18% less than the experimental and FEM results, respectively. These deviations from the real measured values and the FEM-based calculated punch force are because of

ignoring the in-plane shearing in the transition area between the corner areas and the straight regions. Moreover, the small parts of the sheet metal between the geometrically definable segments were not considered in the calculations (see Figure 8-3). Comparing the punch force from the analytical model with the bottom crack force (F_{bc} = 285 kN, see the dashed line in Figure 8-6), it can be noted that no bottom cracks was expected. Obviously this statement was verified with the experimental tests.

To investigate the stability of the process regarding wrinkling, the analytical criterion based on buckling analysis which was proposed in section 6.4 should be used for the corners with high probability of wrinkling (the green marked parts of the sheet metal in Figure 8-7). As shown in Figure 8-7, the corners approaching a quarter circle and an outer radius of 100 mm were subjected to the analysis. Setting the corresponding parameter into Equation 6-13, results in the critical tangential stress of $\sigma_{t.cr}$ = 721MPa, which is well over the acting tangential stress. This consideration reveals that the analytical model expects no wrinkling for the deep drawing of the T-Cup, which was verified with the experimental tests.

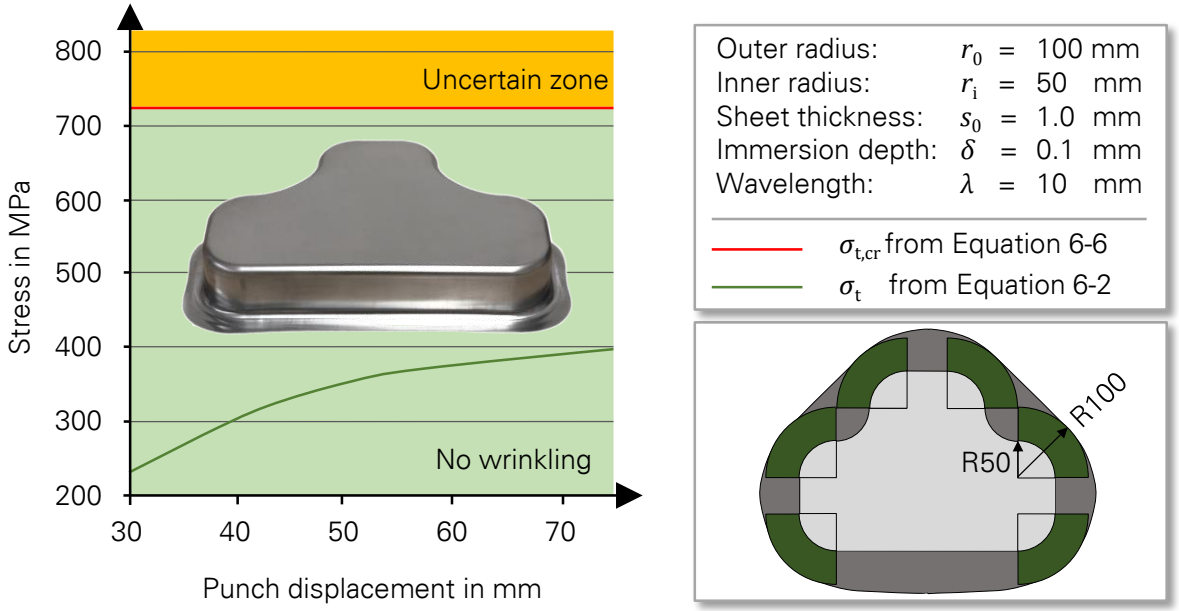

Figure 8-7: Buckling analysis to predict the process stability regarding wrinkling for the deep drawing of the T-Cup

These experimental results are in good agreement with the prediction of the analytical criteria. However, in order to compare the total punch force resulting from deep drawing with macro-structured tools with the conventional process, some further tests were carried out. Here, the conventional tools were used which were introduced in section 8.1. In order to ensure the comparability of results, the same blank geometries were used for deep drawing with macro-structured tools as for the conventional process. Here, the conventional deep drawing processes were done with use of a spacer ring, as well as the direct blankholder force. The tests were performed initially in a lubricant-free and subsequently in lubricated conditions. The

corresponding results are presented in Figure 8-8-A, and compared with results of the deep drawing process with macro-structured tools in lubricant-free conditions. The results show that for deep drawing of a T-Cup with conventional tools in lubricant-free conditions with use of space ring (with the height equal to the sheet thickness), the total punch force amounts to almost 220 kN. This is approximately 10% more than deep drawing with macro-structured tools. Here, it must also be taken into account that according to Table 8-1, the conventional tools have much better surface roughness as well as hardness, which play a very significant role on the tribological behaviour of the tools. However, repeating the test without a spacer ring and direct application of blankholder force leads to bottom cracks in the workpiece. The blankholder force which is provided from pneumatic springs varies during the test regarding their spring stiffness. Figure 8-8-B shows the change of the blankholder force and resulting surface pressure as a function of drawing depth. Changing the test conditions through lubricating the sheet metal with WISURA ZO 3368 leads to a reduction of the punch force of up to 195 kN in the deep drawing process with conventional tools and use of a space ring. This value is very close to the required punch force for the deep drawing of a T-Cup with macro-structured tools in lubricant-free conditions. Therefore, it proves that the macro-structured tools can fulfil the function of lubricants regarding the reduction of friction to realise a lubricant-free forming process even for complex geometries. Moreover, the results show that no bottom cracks occur when applying the blankholder force for the conventional process in lubricated conditions. However, the punch force increases up to 225 kN, which is approximately 12% higher than a macro-structured tool.

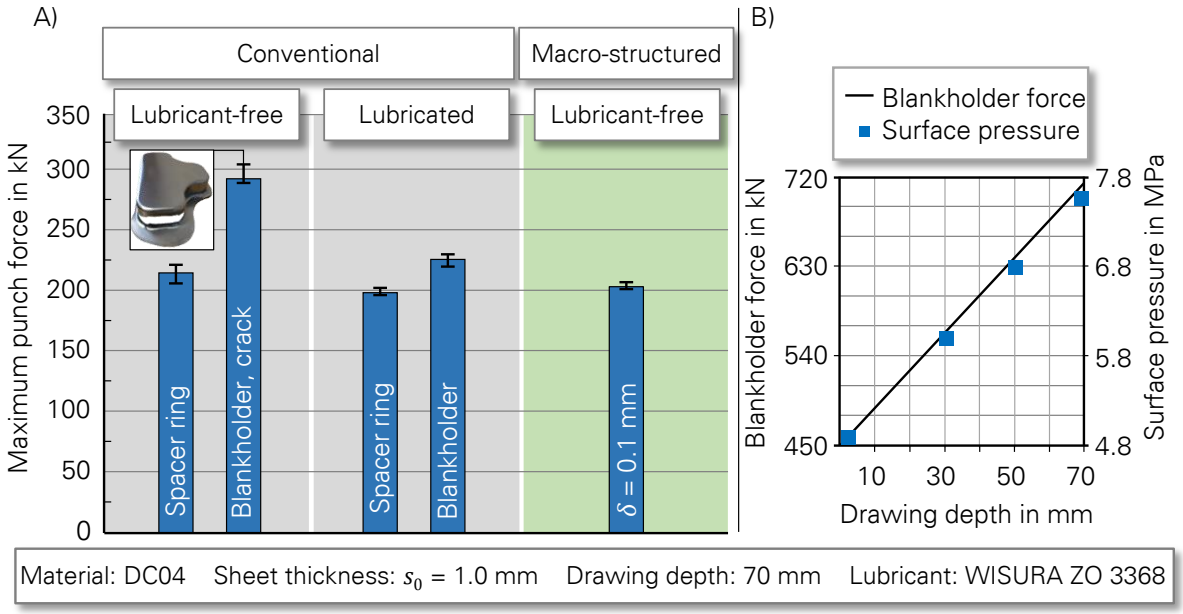

Figure 8-8: Comparison between the conventional and macro-structured deep drawing processes; A) Difference between the conventional and macro-structured deep drawing processes regarding the total punch force and B) the progress of the blankholder force as a function of drawing depth

In order to clarify the advantages of the macro-structured process over the conventional process, the parts which are formed in lubricant-free conditions are compared in Figure 8-9. As mentioned above, there is no significant difference between the forming force in macro-structured and conventional tools using the spacer ring in lubricant-free conditions (approximately 10%). However, as shown in Figure 8-9-A, the bottom area of the deep drawn part made by a conventional tool is not formed plastically, and therefore there is a bending fold in the corner of the part. Despite this, in the deep drawn part made by macro-structured tools, the bottom area is totally flat. This is because of the possibility to control the material flow in deep drawing with macro-structured tools through alternating bending mechanisms.

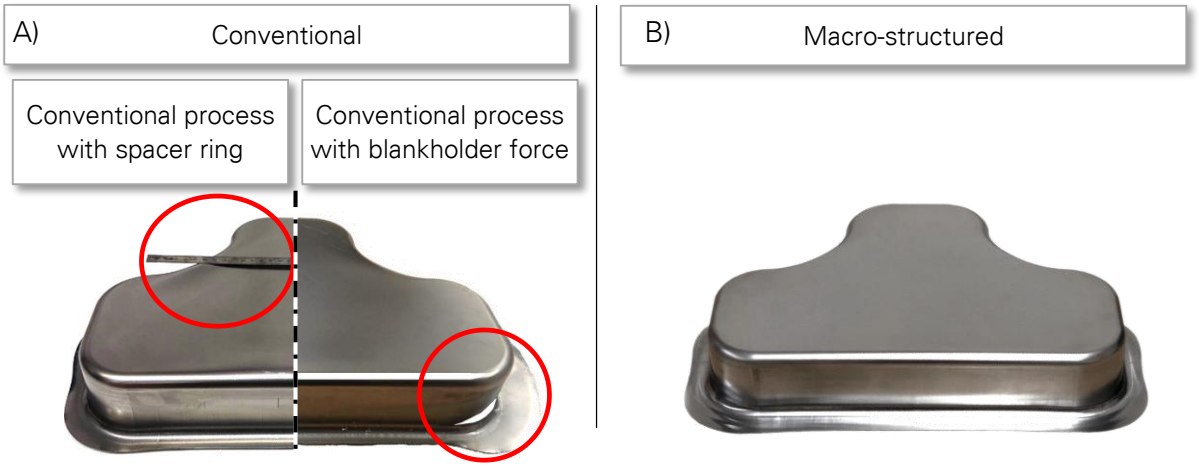

Figure 8-9: Comparison between the part properties made by conventional and macro-structured tools in lubricant-free conditions; A) Conventional tool and B) macro-structured

8.4 SUMMARY OF CHAPTER 8

Several structural parts of automobile components have complicated and very often asymmetrical geometries, which require their production to be performed by means of the deep drawing process. This fact indicates the importance of technology transfer into the industrial parts. To control the transferability of the proposed approach and also the suitability of the criteria developed to predict the process limits, a tool for deep drawing of the T-Cup was constructed. The flange area of the tool is macro-structured, based on an already developed model to have a stable process. The advantage of the T-Cup is because of its variety of stress states. Slip-line field theory was used to determine the optimum initial blank geometry. Firstly, the experimentally deep drawn parts with macro-structured tools in lubricant-free conditions had neither wrinkles nor bottom cracks. For verification of the model with the experimental observations, the required forming force for the T-Cup was determined analytically and numerically. These forces were in a very good agreement with the experimentally measured force. Therefore, it can be concluded that the model is able to predict the required forming force of the complex geometries as well. Comparing this force with the critical bottom crack force, showed that the process is in a safe working area and no bottom cracks are expected. The process was also analysed regarding wrinkling to control the

accuracy of the criterion for the prediction of wrinkling. The implemented buckling analysis showed that the critical tangential stress for the initiation of wrinkling is over the true compressive stress in corners of the part. Therefore, the analytically developed criterion predicted no wrinkling in the specimen and it was proven with real experimental tests. Furthermore, it was shown that the macro-structured deep drawing process in lubricant-free conditions requires less punch force compared to the conventional process in lubricated conditions through application of the direct blankholder force. Moreover, the results showed that using a spacer ring in the deep drawing process with conventional tools in lubricated conditions requires almost the same amount of punch force as the macro-structured process. The results revealed that macro-structured tools can be completely replaced with conventional tools to reduce the frictional force and realise a lubricant-free forming process. However, the results showed that there is no significant difference in the punch force between conventional tools using a spacer ring and macro-structured tools in lubricant-free conditions. But, in deep drawing with a macro-structured tool the material flow can be controlled, in a way which can influence the material strain in the bottom part of the T-Cup. Thereby, unlike conventional process, the material in this area can be formed plastically and consequently no bending folds occur in this area.

9. POSSIBILITIES FOR PROCESS IMPROVEMENT

It has already been shown that to eliminate the lubrication from the deep drawing process macro-structured tools can be used. Using macro-structured tools can reduce the amount of frictional forces in the flange area. As a sub-target, it is also possible to enlarge the process window compared with the conventional process. For this end, the total punch force of the lubricant-free deep drawing process with macro-structured tools should be less than the punch force of the conventional process in lubricated conditions. Therefore, in order to improve the process regarding the enlargement of the process window, a further reduction of the punch forces is necessary. Considering the energy component for deep drawing with macro-structured tools as introduced in section 6.2, the ideal forming energy and the energy for bending over the die edge radius are unchangeable for a particular process. However, a further reduction of friction on the flange area, as well as reduction of the alternating bending energy, can be considered as two improving measures for the enlargement of the process window in deep drawing with macro-structured tools. In this chapter, these measures are introduced and their influences on the reduction of punch force are examined through the FEM and experimental tests.

9.1 USE OF ROTARY ELEMENTS AS MACRO-STRUCTURED ELEMENTS

For further reduction of frictional forces, spherical elements with very small friction coefficients should be combined with line structures in the flange area of the deep drawing tools to induce alternating bending. For this purpose, rotary spherical elements (like ball casters) can be used [185]. By using these elements, the contact lines can be reduced to contact points, minimising the contact area even further. This leads to a reduction of the frictional force and changes the type of friction from sliding to rolling. However, using the spherical elements in the flange area reduces the supporting points against wrinkling. Therefore, the spherical elements should only be applied in uncritical areas regarding wrinkling, like the straight parts of a deep drawing part.

Based on the positive results achieved in Chapter 7, the amount of friction reduction for an oval-form macro-structured tool with combined forming elements compared to a conventional deep drawing tool (see Figure 9-1-A) was examined through numerical investigation [114]. To determine the non-frictional forming force, which means without any friction, a third simulation was carried out. As Figure 9-1-B shows, approximately 70 kN were required for the forming process in the idealised case without friction. Therefore, this result can be considered as the lowest forming force for deep drawing of this part. As the diagram shows, a punch force of 155 kN is required for the deep drawing process with a conventional tool, and 85 kN are solely necessary to overcome the frictional forces caused by using a sliding friction coefficient of μ = 0.15. Therefore, 55% of the total punch force is due to the frictional force. Simulation results from deep drawing processes with macro-structured tools combined with spherical elements (with a friction coefficient of μ = 0.02 based on [186]) and line structures (with a

sliding friction coefficient of $\mu = 0.15$) indicate a total punch force of 90 kN, which is equivalent to a reduction of 42% compared to the conventional process. In this case of macro-structured tools, about 10 kN are required to generate the alternating bending, but the frictional forces account for only 10 kN. This means a reduction of 88% compared to the conventional process. Comparing the macro-structured deep drawing process with a frictionless deep drawing process shows that the punch force increases by only 22% because of alternating bending and frictional forces. This can be used to enlarge the process window significantly.

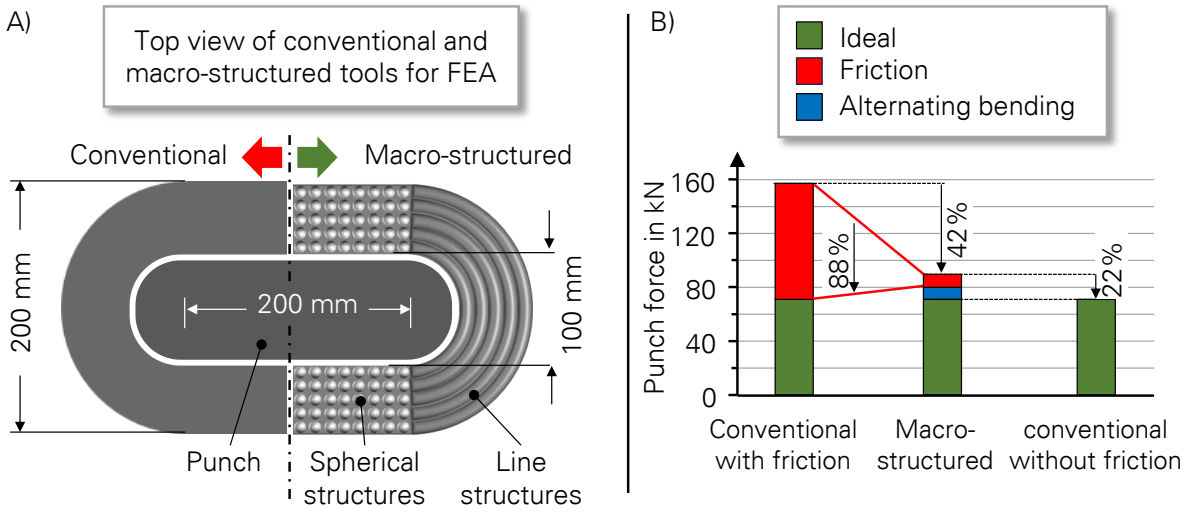

Figure 9-1: Using rotary elements as macro-structured elements; A) Schematic of conventional and macro-structured deep drawing tools, B) comparison between the conventional and macro-structured deep drawing process regarding the punch force [114]

By using the industrial ball casters available on the market as forming elements, some other advantages can be expected in terms of the process design and tool technology. Due to the locally variable adjustability of the position and the height of the elements relative to the sheet metal, a high level of flexibility can be achieved for setting the values of the wavelengths and immersion depths. The ball casters are available in numerous different designs with regard to the types of construction, diameter and permissible load suspension.

9.2 MACRO-STRUCTURED TOOLS WITH VARIABLE WAVELENGTHS

In this section, the already developed approach for the lubricant-free deep drawing process can be improved regarding the locally adapted wavelengths in order to further reduce the punch force and also the enlargement of the process window. The improving approach considers all requirements of a lubricant-free deep drawing process for the broadest possible material spectrum, based on macro-structured elements with variable wavelengths. So far, a constant wavelength λ has been used for the macro-structuring, while the value of λ at the most critical part of the flange is determined for a stable process regarding wrinkling. As shown in section 6.1.1, this corresponds to the area of the greatest tangential compressive

stress; in the rotationally symmetric case, this is the outer free end part of the blank. As a result of material flow, this area moves in a radial direction, whereby the tangential compressive stress increases continuously because of the strain hardening of the sheet metal. This effect has less importance for the low-strength materials, but it can be taken into account in the selection of the wavelength λ for the deep drawing of (super) high-strength materials. Figure 9-2-A shows how the tangential stress at the free end part of the sheet metal increases during the process. In other words, the risk of wrinkling at the free end part increases during the process. In order to compensate for this effect, the wavelength should be reduced in the direction of material flow. This way allows macro-structures to be used with a higher wavelength at the outer part of the flange, where there is no particularly high risk of wrinkling. Furthermore, in contrast to the previous consideration, the number of alternating bending mechanisms in the flange area can also be reduced since the number of macro-structures can be smaller. This strategy reduces the required energy to generate the alternating bending mechanism, which results in a reduced punch force and thus an increased process window for the lubricant-free deep drawing, especially for (super) high-strength materials.

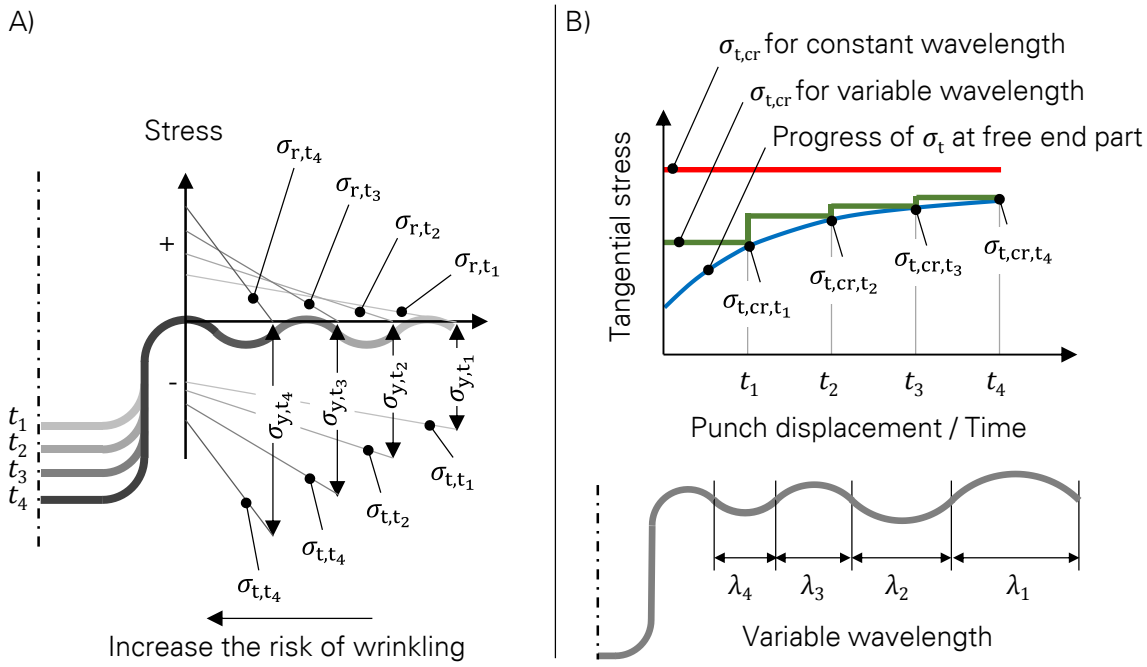

Figure 9-2: Macro-structured tool with variable wavelength; A) Increasing the amount of tangential compressive stress as a result of strain hardening, and B) developing a concept for a macro-structured tool with variable wavelength

In order to be able to take the above mentioned relationships into tool design, the already developed criterion for the prediction of wrinkling should be extended to find the locally-adapted wavelength for a stable process. The amplitude of the macro-structures that so far were assumed to be constant should be varied in the direction of the material flow during the deep drawing process. For this purpose, the tangential stress at each time step can be

considered as the critical tangential stress $\sigma_{t,cr}$ as shown in Figure 9-2-B for the four time step. Knowing the amount of critical tangential stress per each time step, the wavelength can be calculated locally based on the inverse calculation of the already developed criteria (Equation 6-14). In order to investigate the effects of the proposed approach regarding the reduction of forming energy and punch force, as well as the enlargement of the process window, new rotationally symmetric macro-structured deep drawing tools with variable wavelengths from the tooling material described in 5.2, were provided for the experimental tests. As it depicted in Figure 9-3, the wavelength varies from 11 mm to 8 mm in a radial direction of material flow based on the extended analytical approach which is discussed above. For experimental verification of the approach, the same material DC04 was chosen. In order to quantify the advantages of deep drawing with variable macro-structured tools, the same experimental test series which were carried out with a constant wavelength tool (section 7.2.3), are repeated with a new tool design.

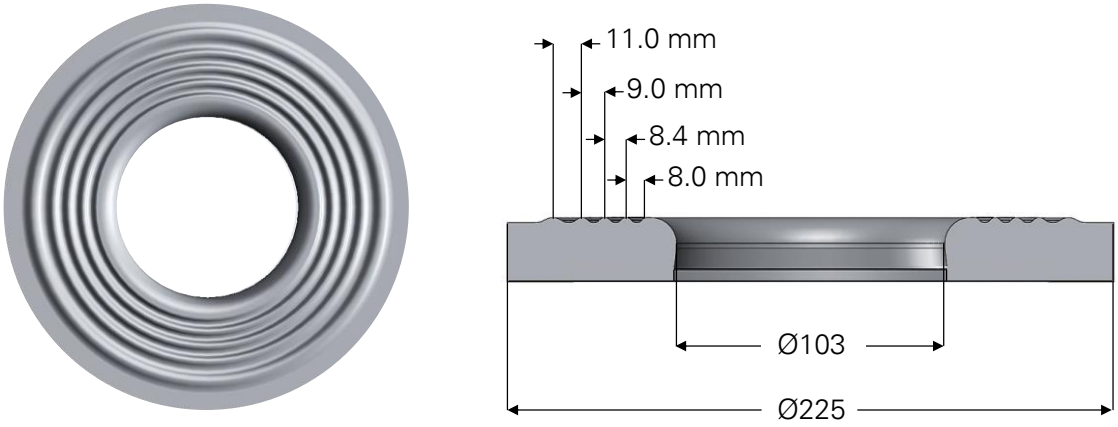

Figure 9-3: Macro-structured deep drawing tool with variable wavelength

As mentioned above, the experimental test matrix used in section 7.2.1 is repeated with a new macro-structured tool. Here the blanks, with outer radius of r_0 = 90 and 100 mm and two different sheet thicknesses of s_0 = 0.6 and 1.0 mm, were subjected for the test series. The immersion depth varies from δ = 0.2 to 0.4. The measured punch forces for deep drawing with variable macro-structured tools are compared with the previous results and shown in Figure 9-4. As the diagram shows, the punch forces are always slightly reduced by using the macro-structured tools with variable wavelengths ($11\ \text{mm} < \lambda < 8\ \text{mm}$). Based on these results, it can be concluded that the modified macro-structured tool can further reduce the punch force and improve the efficiency of the lubricant-free deep drawing process. Furthermore, despite macro-structured tools with a constant wavelength, no bottom cracks occurred when using variable wavelength tools for deep drawing samples with a thickness of s_0 = 0.6 and an immersion depth of δ = 0.4 mm.

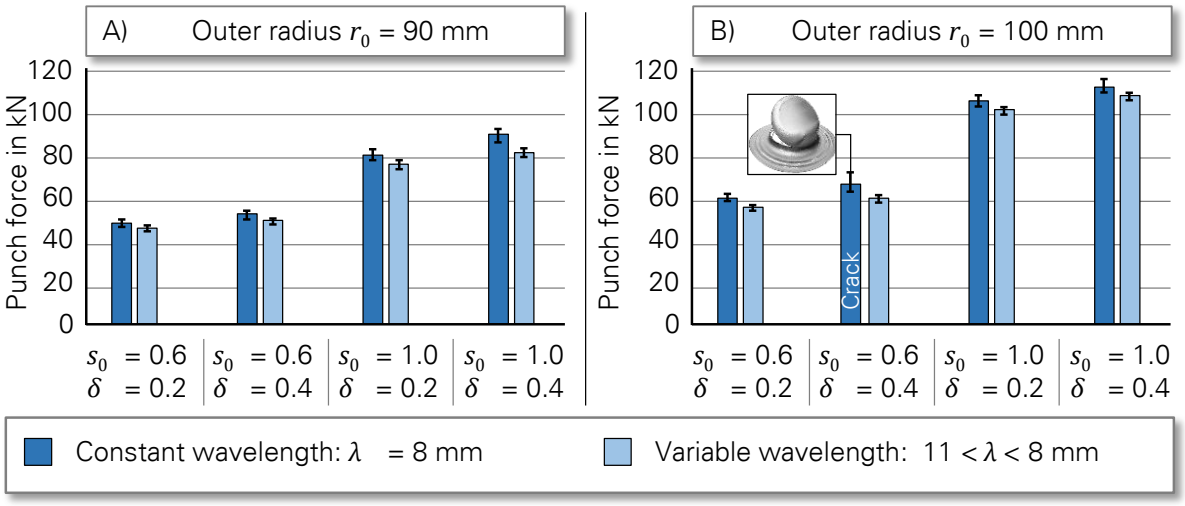

Figure 9-4: Comparison between macro-structured tools with constant and variable wavelengths regarding the punch force and enlargement of the process window for sheet metals with outer radius of A) 90 mm and B) 100 mm

9.3 SUMMARY OF CHAPTER 9

Within the scope of this chapter, two different methods were introduced to improve the process regarding reducing the forming energy which leads to enlargement of the process window. It was shown that the rotary spherical element reduces the contact lines to contact points and changes the sliding friction condition to a rolling condition. The FEM results showed that the share of friction from the total punch force can be reduced up to 88%. However, this method can be applied only in the uncritical parts of the tool regarding wrinkling, because of the loss of supporting points.

As a second method, it is possible to adjust the macro-structures to the acting tangential stress at the free end part of the sheet metal locally. Through this method, a macro-structure with a variable wavelength can be plausible. Generally, the tangential compressive stress increases continuously at the free end part of the sheet metal during the process due to the strain hardening of the material, while the radial tensile stress is always zero. Therefore, the risk of wrinkling increases during the process. Based on this investigation, locally adapted macro-structures were developed which leads to reduction of the bending energy at the outer part of the flange area, and as a result, reduction of the punch force. The experimental results showed that the punch force can be slightly reduced through this measure.

Summarising these statements, it can be concluded that by combining the improvement methods, the punch force can be further reduced for the lubricant-free deep drawing process and the process window can be enlarged regarding bottom cracks. It should also be taken into account that these methods have no negative influences on the process stability regarding wrinkling.

10. SUMMARY AND CONCLUSIONS

Friction is one of the most restricting parameters in sheet metal forming operations. In the deep drawing process, lubricants are applied with the aim of reducing the friction between the tool and the sheet metal for protection of the semi-finished products against corrosion, reduction of tool wear and also the enlargement of process window. However, from both economic and ecological points of view, it is strongly recommended to remove the lubricants within the deep drawing process. For the upcoming process steps after forming, such as joining and coating processes, which are absolutely sensitive to contaminants and oil, it is essential to clean the workpieces from lubricants. This is carried out in post-treatment processes by use of degreasing agents, which are solvent-based and therefore environmentally unfriendly and unhealthy. In addition to lubrication, there are currently a number of ways to reduce friction, like improving the surface quality (hardness as well as roughness), tool coating, and surface texturing. However, for a total lubricant-free process, the frictional forces should be reduced even further. Realising a total lubricant-free deep drawing process leads to:

- a reduction of process steps in production,
- a reduction of mineral oil needs and
- establishing a green forming technology.

The goal of this thesis was to develop a new deep drawing tool for lubricant-free applications, which ensures the process window in lubricant-free conditions. Since the largest contribution of the drawing force is the friction in the flange area, this part of the tool should be adapted for the new tool design. In order to decrease the amount of frictional force in this area for a given friction coefficient, the integral of the contact pressure over the contact area has to be reduced. To achieve that, this area is macro-structured, which has only line contacts and thus a smaller contact area with the sheet metal. This can increase the risk of wrinkling in the unsupported sheet metal areas, because the usually utilised blankholder force is not applicable. To avoid this effect, the geometrical moment of inertia of the sheet should be increased by the alternating bending mechanism of the material in the flange area through immersing the blankholder slightly into the drawing die. Figure 10-1 summarises the sequence of approaches to realise the lubricant-free deep drawing process.

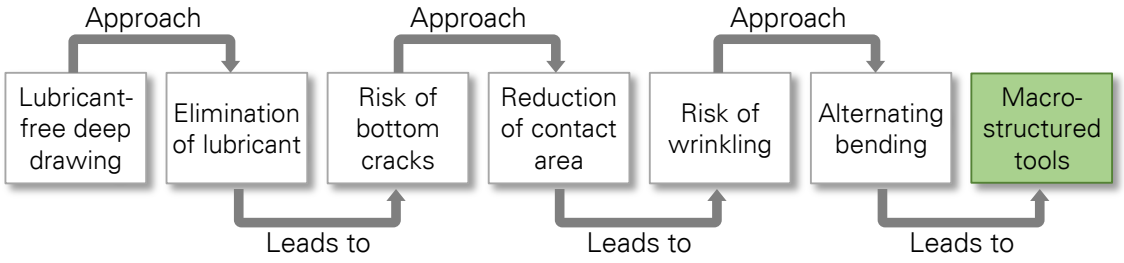

Figure 10-1: Procedural methods for realisation of the lubricant-free deep drawing process

Therefore, the developed process can, besides the reduction of the contact area and the blankholder force, also increase the resistance of the sheet metal against wrinkling. Furthermore, through adjusting the immersion depth, it is possible to control the material flow and enlarge the process window. The induced alternating bending to stabilise the sheet metal against wrinkling during deep drawing with macro-structured tools generates an additional force in the drawing direction. The created non-frictional restraining force can be used positively to compensate the springback behaviour of the workpiece. Generally, following positive effects can be achieved by deep drawing with macro-structured tools:

- reducing the contact area,
- reducing the integral of the contact pressure over the contact area,
- reducing the total punch force through minimising the frictional force,
- saving the added-cleaning time of the lubricant, as well as its disposal costs through elimination,
- enlargement of the process window regarding bottom cracks through reducing the total punch force,
- increasing the process stability regarding wrinkling through inducing alternating bending,
- compensation of the springback effect because of the induced alternating bending as a non-frictional restraining force,
- possibility to control the additional strain hardening, as well as the strain softening through alternating bending for a material with predominantly isotropic or kinematic hardening behaviour,
- possibility to control the material flow by adjusting the amount of the immersion depth and
- no die spotting is required for the new tool systems.

Since the process stability is dependent on the two input parameters, local immersion depth and local wavelength, it is necessary for a time efficient tool design to have an analytical model and criteria to predict the process stability in a fast and accurate way in advance. Therefore, a deep drawing process with macro-structured tools was modelled analytically to predict bottom cracks and wrinkling by means of the energy calculation method, as well as plastic buckling analysis, respectively. The feasibility of the process and also the accuracy of the model were verified through numerical simulations, as well as experimental tests. The results from the analytical model were in a very good agreement with both the numerical and experimental results.

In order to control the transferability of the proposed approach into a more complicated geometry, macro-structured as well as conventional tools for the deep drawing of the T-Cup were constructed within the scope of this thesis. Both criteria to predict the process limits were used for deep drawing of the T-Cup with macro-structured tools. Based on these predictions, neither bottom cracks nor wrinkling were expected during the process and the experimental results verified these prognoses. Moreover, the results showed that the

maximum punch force for deep drawing with macro-structured tools in lubricant-free conditions were very close to that of conventional tools in lubricated conditions. The results showed that using conventional tools with a blankholder force in lubricant-free conditions produces bottom cracks in the workpiece. However, using a spacer ring for deep drawing with conventional tools in lubricant-free conditions leads to a stable process with no significant difference in the punch force compared to macro-structured tools. Nevertheless, due to the ability of macro-structured tools to control material flow during the process, no bending folds occurred on the bottom part of the specimen.

Moreover, two additional approaches were introduced to reduce the punch force further. The use of rotary elements as macro-structures changes the type of friction from sliding to rolling, which can reduce the frictional force further and leads to enlargement of the process window. Although this is a complicated approach in application, it can be considered as a vision for future work. Besides that, it was shown that locally adapting the wavelength regarding the tangential stress can lead to further reduction of the punch force.

Although, the design for macro-structured tool can be relatively more time- and cost-consuming, because of its form and additional wear minimising surface treatments like coating and micro-texturing, it provides several economic and ecological advantages in production. Since the main task of macro-structuring is to reduce the amount of frictional forces, it can be used in the presence of lubrication to perform a minimum-quantity lubrication. Moreover, the newly developed tool design can in combination with a common lubricating system reduce the frictional forces further and thereby lead to increased enlargement of the process window.

II. ZUSAMMENFASSUNG

Reibung stellt einen der am stärksten einschränkenden Parameter in der Blechumformung dar. Bei Tiefziehprozessen wird deshalb Schmierstoff eingesetzt, um die Reibung zwischen Werkzeug und Blech zu verringern, Halbzeug gegen Korrosion zu schützen, den Werkzeugverschleiß zu begrenzen und das Prozessfenster zu vergrößern. Aus ökonomischen und geoökologischen Gesichtspunkten besteht die Herausforderung, auf den Einsatz von Schmierstoffen verzichten zu können. So muss beispielsweise der Schmierstoff für die Folgeoperationen nach dem Umformen, wie Fügen und Beschichten, die überwiegend sehr sensibel bezüglich Verunreinigungen und Öl sind, unbedingt entfernt werden. Die Reinigung wird mithilfe von Entfettungsmitteln durchgeführt, die Lösemittel enthalten und somit umweltunfreundlich und gesundheitsschädlich sind. Neben der Schmierung gibt es derzeit eine Reihe von Möglichkeiten, um die Reibung zu verringern, z. B. eine verbesserte Oberflächenqualität (Härte sowie Rauheit), die Werkzeugbeschichtung und die Oberflächenstrukturierung. Trotzdem muss die Reibung für einen schmierstofffreien Prozess noch weiter reduziert werden. Die Realisierung eines total schmierstofffreien Tiefziehprozesses ermöglicht

- eine Reduzierung der Produktionsschritte,
- eine Reduzierung des Mineralölbedarfs und
- die Realisierung einer „Green Technology“.

Das Ziel dieser Arbeit war die Entwicklung eines neuen Tiefziehwerkzeuges für schmierstofffreie Anwendungen, welches die Stabilität des Prozessfensters sicherstellt. Da die Reibung im Flanschbereich den größten Anteil an der Umformkraft hat, sollte dieser Teil des Werkzeuges bei der neuen Werkzeugauslegung angepasst werden. Bei gegebener Reibzahl muss das Integral der Flächenpressung über die Kontaktfläche reduziert werden, um die Reibkräfte zu reduzieren. Durch die Makrostrukturierung reduziert sich die Kontaktfläche zu einem linien- oder punktförmigen Kontakt. Dies kann zur Erhöhung der Neigung zur Faltenbildung im Flanschbereich in den nicht gestützten Bereichen führen. Allerdings ermöglicht das geringfügige Eintauchen des Niederhalters in die Struktur der Matrize eine Erhöhung des Flächenträgheitsmoments des Bleches durch die eingebrachte Wellenstruktur im Flanschbereich, was die Stabilisation des Flanschbereiches ermöglicht und somit einer Faltenbildung entgegenwirkt. Neben ökonomischen und ökologischen Vorteilen ermöglicht das Tiefziehen mit makrostrukturierten Werkzeugen die Steuerung des Materialflusses durch Einstellung der Eintauchtiefe und reduziert das Rückfederungsverhalten des Bauteils. Durch Tiefziehen mit makrostrukturiertem Werkzeug kann eine Vielzahl positiver Effekte erreicht werden:

- Reduzierung der Kontaktfläche
- Reduzierung des Integrals der Flächenpressung über die Kontaktfläche
- Reduzierung der gesamten Stempelkraft durch Minimierung der Reibkräfte

- Einsparung von Reinigungszeiten durch den Wegfall von Schmierstoffen und der Entsorgungskosten
- Erweiterung des Prozessfensters bezüglich der Bodenreißer durch Verringerung der Stempelkraft
- Erweiterung der Prozessstabilität bezüglich der Faltenbildung durch Ausnutzung des Wechselbiegemechanismus
- Kompensation des Rückfederungsverhaltens des Bauteils durch den erzeugten Wechselbiegemechanismus in Form einer nicht reibungsbehafteten Rückhaltekraft
- Möglichkeit zur Kontrolle der zusätzlichen isotropen und kinematischen Verfestigung im Flanschbereich durch den Wechselbiegemechanismus
- Möglichkeit zur Werkstoffflusssteuerung durch Einstellung der Eintauchtiefe
- Keine Tuschierung bei neuen Werkzeugen erforderlich

Da die Prozessstabilität von den Prozessparametern, d. h. Eintauchtiefe und Wellenlänge, abhängt, ist es für ein zeiteffektives Werkzeugdesign notwendig, die Prozessstabilität anhand analytischer Modelle und Kriterien schnell und präzise vorhersagen zu können. Aus diesem Grund wurde der entwickelte Tiefziehprozess analytisch mittels Energiemethode und auch Beulanalyse modelliert, um das Auftreten von Bodenreißern und Faltenbildung vorhersagen zu können. Die Machbarkeit des Prozesses sowie die Genauigkeit der analytischen Berechnungen wurden durch numerische Simulationen und experimentelle Untersuchungen überprüft. Die Ergebnisse zeigten eine hohe Übereinstimmung mit den numerischen und experimentellen Ergebnissen.

Damit die Übertragbarkeit des hier vorgestellten Ansatzes auf kompliziertere Geometrien gewährleistet werden kann, wurden im Rahmen dieser Arbeit sowohl makrostrukturierte als auch konventionelle Werkzeuge zum Tiefziehen eines T-Napfes konstruiert und gefertigt. Die beiden Kriterien zur Vorhersage der Prozessgrenzen wurden für die Werkzeugauslegung angewandt. Darauf basierend wurden keine Bodenreißer und keine Faltenbildung erwartet, was sich experimentell bestätigte. Darüber hinaus zeigten die Resultate, dass die maximale Stempelkraft beim Tiefziehen mit makrostrukturiertem Werkzeug unter schmierstofffreien Bedingungen nur marginal höher als jene beim konventionellen Tiefziehen mit Distanzring unter Einsatz von Schmierstoff ist. Des Weiteren zeigte sich, dass das konventionelle Tiefziehen ohne Einsatz von Schmierstoff durch die aufgebrachte Niederhaltekraft zum Bodenreißer kam. Allerdings führte der Einsatz eines Distanzrings beim konventionellen Tiefziehen unter schmierstofffreien Bedingungen ebenfalls zu einem stabilen Prozess ohne wesentlichen Unterschied bezüglich der Stempelkraft gegenüber dem Tiefziehen mit makrostrukturiertem Werkzeug. Jedoch treten bei letzterem Prozess durch seine Fähigkeit, den Materialfluss während des Prozesses zu kontrollieren, keine Beule im Bodenbereich des Bauteils auf.

Nachfolgend werden zwei weitere Ansätze erwähnt, um die Stempelkraft weiter zu reduzieren. Der Einsatz von gelagerten Kugeln als Makrostruktur führt dazu, dass Rollreibung statt Gleitreibung Anwendung findet, was die Reibkräfte weiter reduzieren und das

Prozessfenster vergrößern kann. Auch wenn dies in der Anwendung und Umsetzung ein komplizierter Ansatz seien mag, kann er doch als Vision für die zukünftige Forschung verstanden werden. Außerdem zeigte sich, dass eine lokal angepasste Wellenlänge bezüglich der tangentialen Spannung einen Beitrag zur weiteren Reduzierung der Stempelkraft leisten kann.

Obwohl die Auslegung und Herstellung der makrostrukturierten Werkzeuge aufgrund ihrer Form und zusätzlicher verschleißminimierender Maßnahmen, wie Beschichtung und Oberflächenstrukturierung, relativ zeit- und kostenintensiv seien kann, bietet ihr Einsatz zahlreiche ökonomische und ökologische Vorteile in der Fertigung. Da die Hauptaufgabe der Makrostrukturierung eine Reduktion der Reibkräfte ist, kann sie auch in Gegenwart von Schmierstoffen im Rahmen einer Minimalmengenschmierung zum Einsatz kommen. Das neu entwickelte Tiefziehwerkzeug kann in Kombination mit herkömmlichen Schmiersystemen die Reibung hochgradig verringern und somit zu einer signifikanten Vergrößerung des Prozessfensters führen.

.

III. LIST OF FIGURES

Figure 1-1: Structure of Audi A4 limousine with hang on parts [2] 1

Figure 2-1: Deep drawing mechanism, geometrical variables, and acting stresses [10] 4

Figure 2-2: Individual components of the total forming force in deep drawing of the rotationally symmetric cup 5

Figure 2-3: Process window in deep drawing 6

Figure 2-4: The Stribeck curve showing the onset of various lubrication mechanisms [29] 8

Figure 2-5: Comparison between bulk and sheet metal forming regarding the surface pressure and the resulting surface enlargement according to [40] 10

Figure 2-6: An overview of COULOMB [37], shear friction [38], OROWAN [41], and SHAW [42] friction models 11

Figure 2-7: Friction force as a function of normal force and the range of applications for various manufacturing processes (the ranges shown are for unlubricated cases) according to [45] . 12

Figure 2-8: Threefold diagrams of amorphous carbon types and the properties of ta-C coating [95] 17

Figure 2-9: Average of specific roughness values for the substrate, coated and brushed surfaces [98] 18

Figure 2-10: Comparison between the friction coefficient of the ta-C coated tool in lubricant-free conditions and uncoated tools in lubricant-free and lubricated conditions resulting from draw-bend tests with a range of results 18

Figure 2-11: Different micro-structuring technologies differing from the surface fabrication speed and structure size [106] 20

Figure 2-12: Direct Laser Interface Pattering; A) schematic of the interference principle, B) line-type pattern with corresponding two laser beams and C) dot-type pattern with corresponding three laser beams [111] 20

Figure 2-13: Comparison between unstructured and DLIP structured ta-C coating regarding wear reduction by the draw-bend test; A) relative wear and B) structure height differences before and after testing [114] 21

Figure 2-14: Schematic overview of a draw-bend test for the calculation of the friction coefficient under high non-uniform pressure 23

Figure 3-1: Advantages of a lubricant-free deep drawing process according to [128] 26

Figure 4-1: Reduction of punch force in deep drawing process through 50% reduction of A) friction coefficient and B) blankholder force 28

Figure 4-2: Surface pressure in A) conventional and B) macro-structured deep drawing tool 29

Figure 4-3: Tooling arrangement for macro-structured deep drawing; A) Tip to Tip and B) Tip to Hutch 30

Figure 4-4: Comparison between the A) conventional and B) macro-structured deep drawing process 31

Figure 4-5: Process window in A) a conventional deep drawing process, B) macro-structuring the tools with Tip to Tip tooling arrangement, and C) macro-structuring with Tip to Hutch tooling arrangement 32

Figure 4-6: Geometrical parameters of induced alternating bending during the process 32

Figure 4-7: Change of the alternating bending radius as a function of immersion depth and wavelength; A) s_0 = 0.6 mm and s_0 = 0.8 mm 33

Figure 4-8: Energy terms in the conventional and macro-structured deep drawing processes 33

Figure 5-1: Hydraulic press machine BUP 600 35

Figure 5-2: RÖCHER RZP250 Press 36

Figure 5-3: Flow curve of workpiece materials; A) DC04 and B) AA5182 40

Figure 5-4: Geometry and dimensions of A) conventional and B) macro-structured draw bending of U-Channel forming tools 41

Figure 5-5: Tools for deep drawing of axial symmetric parts; A) Conventional, rotationally symmetric, B) macro-structured, rotationally symmetric and C) macro-structured, rectangular 42

Figure 6-1: Comparison of time needed for tool design between two procedures 43

Figure 6-2: Stress state on the flange area of the deep drawing process with macro-structured tools 44

Figure 6-3: Buckling of rectangular plate under uniaxial compression and tension 45

Figure 6-4: Comparison between the calculated punch force from the method of Siebel, Bauer and the principle of virtual work with experimental results according to [9] 46

Figure 6-5: Individual components of the total forming energy for deep drawing of a rotationally symmetric cup with a macro-structured tool 47

Figure 6-6: Principle of the analytical calculation of ideal forming energy in the flange area according to the principle of virtual work [153] 48

Figure 6-7: Principle of the analytical calculation of the bending energy, according to the principle of virtual work [153] 49

Figure 6-8: Stress state in the flange area of the rectangular cup; A) Distribution of tangential stress in the flange area according to [157] and B) the stress state in rotationally symmetric and straight parts of the flange area 50

Figure 6-9: Free end part of the sheet metal; A) Controlling the stability of the process regarding wrinkling and B) Progress of the tangential stress at the free end part of the sheet during deep drawing 54

Figure 6-10: Fracture locus in the space of the stress triaxiality and the equivalent plastic strain to fracture 55

Figure 6-11: Influence of alternating bending on the kinematic hardening behaviour of the workpiece 57

Figure 6-12: The ring splitting method to determine circumferential residual stress in deep drawing cups; A) Cutting area in a rotationally symmetric deep drawing cup for the splitting test, B) springback in the split ring and C) tangential residual stress at the inner and outer cup surfaces 57

Figure 7-1: The required punch force for forming the U-Channel with conventional and macro-structured tools in lubricant-free as well as lubricated conditions 62

Figure 7-2: Results of the numerical parameter analysis of the process window 64

Figure 7-3: Geometry of the sheet metals used for the control of process stability 64

Figure 7-4: Results of the experimental tests for the control of process stability regarding wrinkling by deep drawing with macro-structured tools 65

Figure 7-5: Schematic Overview for springback geometry for a U-Channel [172] 67

Figure 7-6: Springback behaviour of the workpieces with and without alternating bending for A) DC04 and B) AA5182 [148] 68

Figure 7-7: Springback angle of U-Channels under different hardening types for A) DC04 and B) AA5182 69

Figure 7-8: Comparing the analytical calculated total forming energy with experimental and FEM results for deep drawing of rotationally symmetric cups with outer radius of A) 90 mm and B) 100 mm [130] 70

Figure 7-9: Comparing the analytically calculated total forming energy with experimental and FEM results for the deep drawing of rectangular cups 70

Figure 7-10: Prediction of wrinkling for samples with a sheet thickness of A) s_0 = 0.6 mm, B) s_0 = 0.3 mm and C) s_0 = 0.5 mm 72

Figure 7-11: Prediction of bottom cracks through the critical punch force for sheet metals with outer radius of A) 90 mm and B) 100 mm 73

Figure 7-12: Tangential residual stress over the sheet thickness in the cup made by conventional and macro-structured processes from A) DC04 and B) AA5182. 74

Figure 7-13: Results of the ring splitting test for cups made by conventional and macro-structured tools from A) DC04 and B) AA5182 75

Figure 8-1: Detailed view and components of the T-Cup deep drawing tool 78

Figure 8-2: Determination of the optimum initial blank geometry using Slip-line field theory 79

Figure 8-3: The superposing method for analysing the deep drawing of the T-Cup 80

Figure 8-4: Progress of the deep drawing of the T-Cup with macro-structured tools 81

Figure 8-5: Load-displacement curve for the deep drawing of the T-Cup 82

Figure 8-6: Comparison between the maximum punch force from the experimental tests, FEM calculations and the analytical model 82

Figure 8-7: Buckling analysis to predict the process stability regarding wrinkling for the deep drawing of the T-Cup 83

Figure 8-8: Comparison between the conventional and macro-structured deep drawing processes; A) Difference between the conventional and macro-structured deep drawing processes regarding the total punch force and B) the progress of the blankholder force as a function of drawing depth 84

Figure 8-9: Comparison between the part properties made by conventional and macro-structured tools in lubricant-free conditions; A) Conventional tool and B) macro-structured . 85

Figure 9-1: Using rotary elements as macro-structured elements; A) Schematic of conventional and macro-structured deep drawing tools, B) comparison between the conventional and macro-structured deep drawing process regarding the punch force [114] 88

Figure 9-2: Macro-structured tool with variable wavelength; A) Increasing the amount of tangential compressive stress as a result of strain hardening, and B) developing a concept for a macro-structured tool with variable wavelength 89

Figure 9-3: Macro-structured deep drawing tool with variable wavelength 90

Figure 9-4: Comparison between macro-structured tools with constant and variable wavelengths regarding the punch force and enlargement of the process window for sheet metals with outer radius of A) 90 mm and B) 100 mm 91

Figure 10-1: Procedural methods for realisation of the lubricant-free deep drawing process 92

IV. LIST OF TABLES

Table 2-1: Comparison between different forming process regarding their economic importance [8] 3

Table 2-2: Common equations used to calculate the friction coefficient for draw-bend test. 24

Table 5-1: Chemical composition of the studied tool steel (in wt. %) [132] 37

Table 5-2: Low-carbon steel grades with mechanical properties and chemical components [134] 38

Table 5-3: Mechanical properties of Al 5182 [140] 39

Table 5-4: Chemical components of Al 5182 in wt% [117] 39

Table 5-5: Parameters of VOCE model for both testing materials 40

Table 7-1: Bauschinger coefficient of testing materials [165]. 67

Table 7-2: Opening gap of split rings based on experimental tests and calculated values. ... 75

Table 8-1: Surface-related properties of modular deep drawing tool 77

V. REFERENCES

[1] K. Lange, "Modern metal forming technology for industrial production," *Journal of Materials Processing Technology*, vol. 71, no. 1, pp. 2–13, 1997.

[2] "Audi A4 Avant | Audi MediaCenter," 2015. [Online]. Available: https://www.audi-mediacenter.com/de/fotos/detail/audi-a4-avant-26117. [Accessed: 11-Mar-2019].

[3] F. Vollertsen and F. Schmidt, "Dry metal forming: Definition, chances and challenges," *International Journal of Precision Engineering and Manufacturing - Green Technology*, vol. 1, no. 1, pp. 59–62, 2014.

[4] K. Taube, "Carbon-based coatings for dry sheet-metal working," *Surface and Coatings Technology*, vol. 98, no. 1–3, pp. 976–984, 1998.

[5] M. Meiler, M. Pfestorf, M. Geiger, and M. Merklein, "The use of dry film lubricants in aluminum sheet metal forming," *Wear*, vol. 255, no. 7–12, pp. 1455–1462, Aug. 2003.

[6] A. Mousavi, M. Schomacker, and A. Brosius, "Macro and micro structuring of deep drawing's tools for lubricant free forming," *Procedia Engineering*, vol. 81, pp. 1890–1895, 2014.

[7] F. Klocke, *Manufacturing Processes 4: Forming*. Springer, 2013.

[8] DIN 8582, *Fertigungsverfahren Umformen – Einordnung; Unterteilung, Begriffe, Alphabetische Übersicht*. Beuth Verlag GmbH, Berlin, 2003.

[9] E. Doege and B.-A. Behrens, *Handbuch Umformtechnik*, 2nd ed. Springer, 2007.

[10] DIN 8584-3, *Fertigungsverfahren Zugdruckumformen, Teil 3: Grundlagen, Tiefziehen*. Beuth Verlag GmbH, Berlin, 2003.

[11] J. Jeswiet, M. Geiger, U. Engel, M. Kleiner, M. Schikorra, J. Duflou, R. Neugebauer, P. Bariani, and S. Bruschi, "Metal forming progress since 2000," *CIRP Journal of Manufacturing Science and Technology*, vol. 1, no. 1, pp. 2–17, 2008.

[12] Y. Harada, Y. Maeda, M. Ueyama, and I. Fukuda, "Improvement of Formability for Multistage Deep Drawing of Ti-15V-3Cr-3Sn-3Al Alloy Sheet," *Procedia Engineering*, vol. 81, pp. 819–824, 2014.

[13] Steels Atlas, "Stainless Steel Grade Datasheets," *Atlas Steels Technical Department*, 2013.

[14] W. S. Miller, L. Zhuang, J. Bottema, A. . Wittebrood, P. De Smet, A. Haszler, and A. Vieregge, "Recent development in aluminium alloys for the automotive industry," *Materials Science and Engineering: A*, vol. 280, no. 1, pp. 37–49, Mar. 2000.

[15] E. Siebel and H. Beisswänger, *Tiefziehen-Tiefziehen: Forschungsarbeiten auf dem Gebiete des Tiefziehens im Auftrage der Forschungsgesellschaft Blechverarbeitung*, 1st ed. München: Carl Hanser Verlag, 1955.

[16] M. P. Groover, *Fundamentals of modern manufacturing - Materials, Process, and Systems*, 4th ed. John Wiley and Sons Ltd, 2010.

[17] N. Kanetake and Y. Tozavan, "Crystallographical Calculation of Earing in Deep Drawing under Various Conditions," *Textures and Microstructures*, vol. 7, pp. 131–147, 1987.

[18] A. Agrawal, N. V. Reddy, and P. M. Dixit, "Determination of optimum process parameters for wrinkle free products in deep drawing process," *Journal of Materials Processing Technology*, vol. 191, no. 1–3, pp. 51–54, 2007.

[19] D. Banabic, H.-J. Bunge, and A. E. Tekkaya, *Formability of metallic materials: plastic anisotropy, formability testing, forming limits*. Springer, 2000.

[20] K. Siegert, M. Ziegler, and S. Wagner, "Closed loop control of the friction force. Deep drawing process," *Journal of Materials Processing Technology*, vol. 71, no. 1, pp. 126–133, 1997.

[21] B. D. Carleer, P. T. Vreede, P. Drent, M. F. M. Louwes, and J. Huétink, "Modelling drawbeads with finite elements and verification," *Journal of Materials Processing Technology*, vol. 45, no. 1–4, pp. 63–68, Sep. 1994.

[22] M. Meiler, M. Pfestorf, M. Geiger, and M. Merklein, "The use of dry film lubricants in aluminum sheet metal forming," *Wear*, vol. 255, no. 7–12, pp. 1455–1462, 2003.

[23] W. E. Jamison, "Introduction to tribology," *Journal of Vacuum Science and Technology*, vol. 13, no. 1, pp. 76–81, Jan. 1976.

[24] J. A. Tichy and D. M. Meyer, "Review of solid mechanics in tribology," *International Journal of Solids and Structures*, vol. 37, no. 1–2, pp. 391–400, 2000.

[25] R. Stribeck, *Kugellager für beliebige Belastungen*, 1st ed. Buchdruckerei AW Schade, 1901.

[26] W. C. Emmens, "The influence of surface roughness on friction," *International Conference on Controlling Sheet Metal Forming Processes*, pp. 63–70, 1988.

[27] B. N. J. Persson, "Theory of friction and boundary lubrication," *Physical Review B*, vol. 48, no. 24, p. 18140, 1993.

[28] T. Altan and A. E. Tekkaya, *Sheet metal forming-fundamentals*. ASM International, 2012.

[29] J. A. Schey, "Tribology in metalworking: friction, lubrication, and wear," *ournal of Applied Metalworking*, vol. 3(2), pp. 173–174, 1984.

[30] Q. Liu, "Friction in Mixed and Elastohydrodynamic Lubricated Contacts Including Thermal Effects," University of Twente, 2002.

[31] R. J. J. M. Sniekers, "Friction in Deep Drawing," Eindhoven University of Technology, 1996.

[32] B. J. Hamrock, S. R. Schmid, and B. O. Jacobson, *Fundamentals of Fluid Film Lubrication*. CRC Press, 2004.

[33] D. Dowson, *History of Tribology*, 2nd ed. Addison-Wesley Longman Limited, 1979.

[34] A. A. Pitenis, D. Dowson, and W. Gregory Sawyer, "Leonardo da Vinci's friction experiments: An old story acknowledged and repeated," *Tribology Letters*, vol. 56, no. 3, pp. 509–515, 2014.

[35] Y. Mo, K. T. Turner, and I. Szlufarska, "Friction law at the nanoscale," *Nature*, vol. 457, p. 1116, 2009.

[36] B. Feeny, A. Guran, N. Hinrichs, and K. Popp, "A Historical Review on Dry Friction and Stick-Slip Phenomena," *Applied Mechanics Reviews*, vol. 51, pp. 321–342, 1998.

[37] D. Dowson, *History of Tribology*, 2nd ed. Bury St Edmunds, United Kingdom: John Wiley and Sons Ltd, 1997.

[38] W. R. D. Wilson, "Friction and lubrication in bulk metal-forming processes," *Journal of Applied Metalworking*, vol. 1, no. 1, pp. 7–19, 1978.

[39] H.-W. Wagener, "Tribologische Untersuchungen zur Kaltmassivumformung," Shaker Verlag, 1999.

[40] B. G. Kappes, "Über den Nachweis tribologischer Effekte mit Hilfe von Modellversuchen im Bereich der umweltfreundlichen Kaltmassivumformung," Technischen Universität Darmstadt, Darmstadt, 2005.

[41] E. Orowan, "The calculation of roll pressure in hot and cold flat rolling," *Proceedings of the Institution of Mechanical Engineers*, vol. 150, no. 1943, pp. 140–167, 1943.

[42] M. C. Shaw, A. Ber, and Pierre A. Mamin, "Friction characteristics of sliding surfaces undergoing subsurface plastic flow," *Journal of Basic Engineering*, vol. 82(2), pp. 342–345, 1960.

[43] T. Wanheim and N. Bay, "A model for friction in metal forming processes," *Annals of the CIRP*, vol. 27, no. 1, pp. 189–194, 1978.

[44] F. P. Bowden, D. Tabor, and F. Palmer, "The Friction and Lubrication of Solids," *American Journal of Physics*, vol. 19, no. 7, pp. 428–429, 1951.

[45] S. Kalpakjian and R. S. Schmid, *Manufacturing Processes for Engineering Materials*, 5th ed. Pearson Education, 2008.

[46] J. W. Raedt, "Grundlagen für das schmiermittelreduzierte Tribosystem bei der Kaltumformung des Einsatzstahles 16MnCr5," RWTH Aachen, 2002.

[47] J. P. Byers, *Metalworking Fluids*, 2nd ed. CRC Press, 2006.

[48] E. Brinksmeier, D. Meyer, A. G. Huesmann-Cordes, and C. Herrmann, "Metalworking fluids - Mechanisms and performance," *CIRP Annals - Manufacturing Technology*, vol. 64, no. 2, pp. 605–628, 2015.

[49] T. Mang, *Encyclopedia of Lubricants and Lubrication*, 1st ed. Springer, 2014.

[50] T. F. Tadros, *Emulsion Formation and Stability*, 1st ed. Wiley-VCH Verlag GmbH & Co. KGaA, 2013.

[51] S. A. Lawal, I. A. Choudhury, and Y. Nukman, "Application of vegetable oil-based metalworking fluids in machining ferrous metals - A review," *International Journal of Machine Tools and Manufacture*, vol. 52, no. 1, pp. 1–12, 2012.

[52] H. E. Sliney, "Solid lubricant materials for high temperatures - a review," *Tribology International*, vol. 15, no. 5, pp. 303–315, 1982.

[53] S. Dilbag and P. V. Rao, "Performance improvement of hard turning with solid lubricants," *International Journal of Advanced Manufacturing Technology*, vol. 38, no. 5–6, pp. 529–535, 2008.

[54] K. P. Rao and C. L. Xie, "A comparative study on the performance of boric acid with several conventional lubricants in metal forming processes," *Tribology International*, vol. 39, no. 7, pp. 663–668, 2006.

[55] D. A. Dornfeld, "Moving towards green and sustainable manufacturing," *International Journal of Precision Engineering and Manufacturing - Green Technology*, vol. 1, no. 1, pp. 63–66, 2014.

[56] F. Vollertsen, H. Flosky, and T. Seefeld, "Dry Metal Forming – a Green Approach," in *60 Excellent Inventions in Metal Forming*, 1st ed., A. E. Tekkaya, W. Homberg, and A. Brosius, Eds. Springer, 2015, pp. 113–118.

[57] S. H. Ahn, "An evaluation of green manufacturing technologies based on research databases," *International Journal of Precision Engineering and Manufacturing - Green Technology*, vol. 1, no. 1, pp. 5–9, 2014.

[58] W. J. Bartz, "Lubricants and the environment," *Tribology International*, vol. 31, no. 1–3, pp. 35–47, 1998.

[59] T. Mang and W. Dresel, *Lubricants and Lubrication*, 2nd ed. Wiley-VCH Verlag GmbH, 2007.

[60] P. Nagendramma and S. Kaul, "Development of ecofriendly/biodegradable lubricants: An overview," *Renewable and Sustainable Energy Reviews*, vol. 16, no. 1, pp. 764–774, 2012.

[61] I. Madanhire and C. Mbohwa, *Mitigating Environmental Impact of Petroleum Lubricants*. Springer International Publishing, 2016.

[62] A. R. Shahani and I. Salehinia, "Analysis of wear in deep-drawing process of a cylindrical cup," *Journal of Materials Processing Technology*, vol. 200, no. 1–3, pp. 451–459, 2008.

[63] M. Masen, "Abrasive tool wear in metal forming processes," University of Twente, 2004.

[64] Organisation for Economic Co-operation and Development. Research Group on Wear of Engineering Materials, *Glossary of terms and definitions in the field of friction, wear and lubrication-tribology*. Paris: O.E.C.D. : H.M.S.O., 1969.

[65] A. Gåård, P. Krakhmalev, and J. Bergström, "Wear mechanisms in deep drawing of carbon steel – correlation to laboratory testing," *Tribotest*, vol. 14, no. 1, pp. 1–9, Jan. 2008.

[66] S. Christiansen and L. De Chiffre, "Topographic Characterization of Progressive Wear on Deep Drawing Dies," *Tribology Transactions*, vol. 40, no. 2, pp. 346–352, 1997.

[67] E. Van der Heide, "Lubricant failure in sheet metal forming processes," University of Twente, 2002.

[68] T. Yamamoto and D. H. Buckley, *Wear Mechanism Based on Adhesion*. NASA Technical Paper, 1982.

[69] M. Hanson, "On Adhesion and Galling in Metal Forming," Acta Universitatis Upsaliensis, 2008.

[70] I. Hutschings and P. Shipway, *Tribology Materials, Friction and Wear of Engineering*, 2nd ed. Butterworth-Heinemann, 2017.

[71] J. D. Gates, "Two-body and three-body abrasion : A critical discussion," *wear*, vol. 214, pp. 139–146, 1998.

[72] M. P. Pereira, M. Weiss, B. F. Rolfe, and T. B. Hilditch, "The effect of the die radius profile accuracy on wear in sheet metal stamping," *International Journal of Machine Tools and Manufacture*, vol. 66, pp. 44–53, 2013.

[73] D. D. Olsson, N. Bay, and J. L. Andreasen, "Analysis of Pick-Up Development in Punching," *CIRP Annals - Manufacturing Technology*, vol. 51, no. 1, pp. 185–190, 2002.

[74] K. Tamaoki, K. ichi Manabe, S. Kataoka, and T. Aizawa, "Electroconductive ceramic tooling for dry deep drawing," *Journal of Materials Processing Technology*, vol. 210, no. 1, pp. 48–53, 2010.

[75] A. Mitsuo, T. Akhadejdamrong, and T. Aizawa, "Self-Lubrication of Cl-Implanted Titanium Nitride Coating for Dry Metal Forming," *Materials Transactions*, vol. 44, no. 7, pp. 1295–1302, 2003.

[76] G. Reisel, S. Steinhäuser, and B. Wielage, "The behaviour of DLC under high mechanical and thermal load," *Diamond and Related Materials*, vol. 13, pp. 1516–1520, 2004.

[77] S. Kataoka, M. Murakawa, T. Aizawa, and H. Ike, "Tribology of dry deep-drawing of various metal sheets with use of ceramics tools," *Surface and Coatings Technology*, vol. 177–178, pp. 852–590, 2004.

[78] T. Arai, "Tool materials and surface treatments," *Journal of Materials Processing Technology*, vol. 35, no. 3–4, pp. 515–528, 1992.

[79] M. Murakawa, N. Koga, and T. Kumagai, "Deep-drawing of aluminum sheets without lubricant by use of diamond-like carbon coated dies," *Surface and Coatings Technology*, vol. 76–77, no. 1–3, pp. 553–558, Dec. 1995.

[80] M. de Rooij, "Tribological aspects of unlubricated deepdrawing processes," University of Twente, 1998.

[81] C. Weist and H. Westheide, "Application of chemical and physical methods for the reduction of tool wear in bulk metal forming processes (in German)," *CIRP Annals - Manufacturing Technology*, vol. 35, no. 1, pp. 199–204, 1986.

[82] K. H. W. Seah and K. S. Lee, "The effects of titanium nitride coatings on punches and dies in the deep drawing of cold-rolled mild steel," *International Journal of Machine Tools and Manufacture*, vol. 28, no. 4, pp. 399–407, 1988.

[83] S. Zhang and W. Zhu, "TiN coating of tool steels: a review," *Journal of Materials Processing Technology*, vol. 39, no. 1–2, pp. 165–177, Oct. 1993.

[84] A. Ghiotti and S. Bruschi, "Tribological behaviour of DLC coatings for sheet metal forming tools," *Wear*, vol. 271, no. 9–10, pp. 2454–2458, 2011.

[85] F. Klocke, T. Maßmann, K. Bobzin, E. Lugscheider, and N. Bagcivan, "Carbon based tool coatings as an approach for environmentally friendly metal forming processes," *Wear*, vol. 260, no. 3, pp. 287–295, 2006.

[86] A. M. Ladwig, R. D. Koch, E. G. Wenski, and R. F. Hicks, "Atmospheric plasma deposition of diamond-like carbon coatings," *Diamond and Related Materials*, vol. 18, no. 9, pp. 1129–1133, 2009.

[87] F. Klocke, T. Maßmann, and K. Gerschwiler, "Combination of PVD tool coatings and biodegradable lubricants in metal forming and machining," *Wear*, vol. 259, no. 7–12, pp. 1197–1206, 2005.

[88] Z. G. Jiang, C. J. Lu, D. B. Bogy, C. S. Bhatia, and T. Miyamoto, "Nanotribological Characterization of Hydrogenated Carbon-Films by Scanning Probe Microscopy," *Thin Solid Films*, vol. 258, no. 1–2, pp. 75–81, 1995.

[89] G. M. Pharr, D. L. Callahan, S. D. McAdams, T. Y. Tsui, S. Anders, A. Anders, J. W. Ager, I. G. Brown, C. S. Bhatia, S. R. P. Silva, and J. Robertson, "Hardness, elastic modulus, and structure of very hard carbon films produced by cathodic-arc deposition with substrate pulse biasing," *Applied Physics Letters*, vol. 68, no. 6, pp. 779–781, 1996.

[90] J. Robertson, "Requirements of ultrathin carbon coatings for magnetic storage technology," *Tribology International*, vol. 36, no. 4–6, pp. 405–415, Apr. 2003.

[91] C. Casiraghi, J. Robertson, and A. C. Ferrari, "Diamond-like carbon for data and beer storage," *Materials Today*, vol. 10, no. 1–2, pp. 44–53, 2007.

[92] T. Roch, E. Beyer, and A. Lasagni, "Surface modification of thin tetrahedral amorphous carbon films by means of UV direct laser interference patterning," *Diamond and Related Materials*, vol. 19, no. 12, pp. 1472–1477, 2010.

[93] A. C. Ferrari, A. Libassi, B. K. Tanner, V. Stolojan, J. Yuan, L. M. Brown, S. E. Rodil, B. Kleinsorge, and J. Robertson, "Density, SP3 fraction, and cross-sectional structure of amorphous carbon films determined by x-ray reflectivity and electron energy-loss spectro," *Physical Review B*, vol. 62, no. 16, pp. 11089–11103, 2000.

[94] T. Roch, L. Stepien, T. Kunze, A. Mousavi, S. Topalski, and A. Lasagni, "Tool Optimization for Dry Forming Applications – Optimized Surface Preparation of ta-C," *Dry Met. Forming OAJ FMT 3*, vol. 1, pp. 025–029, 2017.

[95] J. Robertson, "Diamond-like amorphous carbon," *Materials Science and Engineering: R: Reports*, vol. 37, no. 4–6, pp. 129–281, 2002.

[96] S. . Ahn, J. H. Lee, J. G. Kim, and J. G. Han, "Localized corrosion mechanisms of the multilayered coatings related to growth defects," *Surface and Coatings Technology*, vol. 177–178, pp. 638–644, 2004.

[97] E. R. G. Eckert and H. D. Chiang, "Effect of Surface Roughness on," vol. 4, no. 3, pp. 45–56, 2013.

[98] T. Kunze, A. Mousavi, T. Stucky, F. Böttcher, T. Roch, A. Brosius, and A. Lasagni, "Tribological Optimization of Dry Forming Tools," *Dry Met. Forming OAJ FMT 2*, vol. 1, pp. 78–82, 2016.

[99] T. Kunze, A. Mousavi, T. Stucky, F. Böttcher, T. Roch, M. Schomäcker, A. Lasagni, and A. Brosius, "Tool Optimization for Dry Forming Applications," *12th International Conference THE"A" Coating 2016*, pp. 201–207, 2016.

[100] J. Vetter, "60 years of DLC coatings: Historical highlights and technical review of cathodic arc processes to synthesize various DLC types, and their evolution for industrial applications," *Surface and Coatings Technology*, vol. 257, pp. 213–240, 2014.

[101] C. Gachot, A. Rosenkranz, S. M. Hsu, and H. L. Costa, "A critical assessment of surface texturing for friction and wear improvement," *Wear*, vol. 372–373, pp. 21–41, 2017.

[102] D. B. Hamilton, A. A. Walowit, and C. M. Allen, "A Theory of Lubrication by Microirregularities," *Journal of Basic Engineering*, vol. 88, no. 1, pp. 177–185, 1966.

[103] S.-C. Vlădescu, A. V Olver, I. G. Pegg, and T. Reddyhoff, "Texturing, Combined friction and wear reduction in a reciprocating contact through laser surface," *Wear*, vol. 358–359, pp. 51–61, 2016.

[104] V. Franzen, J. Witulski, A. Brosius, M. Trompeter, and A. E. Tekkaya, "Textured surfaces for deep drawing tools by rolling," *International Journal of Machine Tools and Manufacture*, vol. 50, no. 11, pp. 969–976, 2010.

[105] M. Geiger, U. Popp, and U. Engel, "Excimer Laser Micro Texturing of Cold Forging Tool Surfaces - Influence on Tool Life," *CIRP Annals - Manufacturing Technology*, vol. 51, no. 1, pp. 231–234, 2002.

[106] A. Lasagni, D. Benke, T. Kunze, M. Bieda, S. Eckhardt, T. Roch, D. Langheinrich, and J. Berger, "Bringing the direct laser interference patterning method to industry: A one tool-complete solution for surface functionalization," *Journal of Laser Micro Nanoengineering*, vol. 10, no. 3, pp. 340–344, 2015.

[107] R. Petruškevičius, J. Baltrusaitis, D. Kezys, M. Mikolajunas, V. Grigaliunas, and D. Viržonis, "E-beam lithography of computer generated holograms using a fully vectorial 3D beam propagation method," *Microelectronic Engineering*, vol. 87, no. 11, pp. 2332–2337, 2010.

[108] F. Meriche, E. Neiss-Clauss, R. Kremer, A. Boudrioua, E. Dogheche, E. Fogarassy, R. Mouras, and A. Bouabellou, "Micro structuring of LiNbO3 by using nanosecond pulsed laser ablation," *Applied Surface Science*, vol. 254, no. 4, pp. 1327–1331, 2007.

[109] N. Ganesh, I. D. Block, and B. T. Cunningham, "Near ultraviolet-wavelength photonic-crystal biosensor with enhanced surface-to-bulk sensitivity ratio," *Applied Physics Letters*, vol. 89, no. 2, pp. 8–10, 2006.

[110] M. Bieda, E. Beyer, and A. F. Lasagni, "Direct Fabrication of Hierarchical Microstructures on Metals by Means of Direct Laser Interference Patterning," *Journal of Engineering Materials and Technology*, vol. 132, no. 3, p. 031015, 2010.

[111] T. Kunze, F. Böttcher, V. Lang, A. Gärtner, and A. Lasagni, "Surface functionalization of forming using direct laser interference patterning for dry forming applications," *Dry Met. Forming OAJ FMT 1*, vol. 1, pp. 108–112, 2015.

[112] A. F. Lasagni, D. F. Acevedo, C. A. Barbero, and F. Mücklich, "One-step production of organized surface architectures on polymeric materials by direct laser interference patterning," *Advanced Engineering Materials*, vol. 9, no. 1–2, pp. 99–104, 2007.

[113] T. Roch, V. Weihnacht, H.-J. Scheibe, A. Roch, and A. F. Lasagni, "Direct Laser Interference Patterning of tetrahedral amorphous carbon films for tribological applications," *Diamond and Related Materials*, vol. 33, pp. 20–26, 2013.

[114] A. Mousavi, T. Kunze, T. Roch, A. Lasagni, and A. Brosius, "Deep drawing process without lubrication – an adapted tool for a stable , economic and environmentally friendly process," *International Conference on the Technology of Plasticity, ICTP*, vol. 207, pp. 48–53, 2017.

[115] A. Rosenkranz, L. Reinert, C. Gachot, and F. Mücklich, "Alignment and wear debris effects between laser-patterned steel surfaces under dry sliding conditions," *Wear*, vol. 318, no. 1–2, pp. 49–61, 2014.

[116] M. Merklein, M. Schmidt, S. Tremmel, K. Andreas, T. Häfner, R. Zhao, and J. Steiner, "Tailored modifications of amorphous carbon based coatings for dry deep drawing," *Dry Met. Forming OAJ FMT 2*, vol. 2, pp. 25–39, 2016.

[117] N. Axén, S. Hogmark, and S. Jacobson, "Friction and Wear Measurement Techniques," in *Modern Tribology Handbook*, Crc Press Inc, 2000.

[118] DIN 50324, *Tribologie; Prüfung von Reibung und Verschleiß; Modellversuche bei Festkörpergleitreibung (Kugel-Scheibe-Prüfsystem)*. Beuth Verlag GmbH, Berlin, 1992.

[119] ASTM Standard, "G99 - 95a Standard Test Method for Wear Testing with a Pin-on-Disk Apparatus," Nov. 2000.

[120] Y. S. Kim, "A draw-bend friction test applied to measurement and modeling of anisotropic friction on sheet metal," McMaster University, 2008.

[121] Y. S. Kim, M. K. Jain, and D. R. Metzger, "Determination of pressure-dependent friction coefficient from draw-bend test and its application to cup drawing," *International Journal of Machine Tools and Manufacture*, vol. 56, pp. 69–78, 2012.

[122] Y. S. Kim, M. K. Jain, and D. R. Metzger, "Non-uniform pressure distribution in draw-bend friction test and its influence on friction measurement," *AIP Conference Proceedings*, vol. 778 A, no. 1, pp. 661–666, 2005.

[123] D. W. Vallance and O. K. Matlock, "Application of the bending-under-tension friction test to coated sheet steels," *Journal of Materials Engineering and Performance*, vol. 1, no. 5, pp. 685–693, 1992.

[124] R. T. Fox, A. M. Maniatty, and D. Lee, "Determination of friction coefficient for sheet materials under stretch-forming conditions," *Metallurgical Transactions A*, vol. 20A, no. 10, pp. 2179–2182, 1989.

[125] M. Sulonen, P. Eskola, J. Kumpulainen, and A. Ranta-Eskala, "A reliable method for measuring the friction coefficient in sheet metal forming," *IDDRG Working Group Meetings*, 1981.

[126] W. R. Wilson, H. G. Malkani, and P. K. Saha, "Boundary friction measurements using a new sheet metal forming simulator," *Trans. NAMRI/SME*, vol. 19, pp. 37–42, 1991.

[127] S. S. Han, "The influence of tool geometry on friction behavior in sheet metal forming," *Journal of Materials Processing Technology*, vol. 63, no. 1–3, pp. 129–133, 1997.

[128] "BIAS GmbH - Schwerpunktprogramm." [Online]. Available: http://www.trockenumformen.de/schwerpunktprogramm/. [Accessed: 13-Mar-2019].

[129] J. A. Greenwood and J. P. Williamson, "Contact of nominally flat surfaces," *Proceedings of the Royal Society of London. Series A. Mathematical and Physical Sciences*, vol. 295, no. 1442, pp. 300–319, Dec. 1966.

[130] A. Brosius and A. Mousavi, "Lubricant free deep drawing process by macro structured tools," *CIRP Annals - Manufacturing Technology*, vol. 65, no. 1, pp. 253–256, 2016.

[131] T. V. Pirtovšek, G. Kugler, and M. Terčelj, "The behaviour of the carbides of ledeburitic AISI D2 tool steel during multiple hot deformation cycles," *Materials Characterization*, vol. 83, pp. 97–108, 2013.

[132] I. Picas, N. Cuadrado, D. Casellas, A. Goez, and L. Llanes, "Microstructural effects on the fatigue crack nucleation in cold work tool steels," *Procedia Engineering*, vol. 2, no. 1, pp. 1777–1785, 2010.

[133] D. Ravi Kumar, "Formability analysis of extra-deep drawing steel," *Journal of Materials Processing Technology*, vol. 130–131, pp. 31–41, 2002.

[134] J. E. Bringas, *Handbook of Comparative World Steel Standards*, 3rd ed. ASTM International, 2004.

[135] Thyssenkrupp, "Product information deep-drawing steels DD, DC und DX," Duisburg, 2018.

[136] D. Jocham, R. Norz, and W. Volk, "Strain rate sensitivity of DC06 for high strains under biaxial stress in hydraulic bulge test and under uniaxial stress in tensile test," 2013.

[137] I. N. Fridlyander, V. G. Sister, O. E. Grushko, V. V. Berstenev, L. M. Sheveleva, and L. A. Ivanova, "Aluminum alloys: Promising materials in the automotive industry," *Metal Science and Heat Treatment*, vol. 44, no. 9–10, pp. 365–370, 2002.

[138] F. Ozturk, A. Sisman, S. Toros, S. Kilic, and R. C. Picu, "Influence of aging treatment on mechanical properties of 6061 aluminum alloy," *Materials & Design*, vol. 31, no. 2, pp. 972–975, Feb. 2010.

[139] T. Naka and F. Yoshida, "Deep drawability of type 5083 aluminium–magnesium alloy sheet under various conditions of temperature and forming speed," *Journal of Materials Processing Technology*, vol. 89–90, pp. 19–23, May 1999.

[140] N. Abedrabbo, F. Pourboghrat, and J. Carsley, "Forming of AA5182-O and AA5754-O at elevated temperatures using coupled thermo-mechanical finite element models," *International Journal of Plasticity*, vol. 23, no. 5, pp. 841–875, May 2007.

[141] T. Mao, "Evaluation of Formability and Drawability of Al 5182-O Using a Servo Drive Press," Ohio State University, 2014.

[142] T. Sakurai, "The latest trends in aluminium alloy sheets for automotive body panels," *Kobelco technology review*, vol. 28, pp. 22–28, 2008.

[143] DIN EN 573-3, *Aluminum und Aluminumlegierungen - Chemische Zusammensetzung und Form von Halbzeug*, vol. 3. Beuth Verlag GmbH, Berlin, 2009.

[144] DIN 50125, *Prüfung metallischer Werkstoffe - Zugproben*. Beuth Verlag GmbH, Berlin, 2016.

[145] A. Mustafa-Seçkin, J. Gerlach, and L. Keßler, "Verfahren zur Extrapolation der Fließkurve aus den Daten des Zugversuches jenseits der Gleichmaßdehnung," Filderstadt, 2009.

[146] E. Voce, "The relationship between stress and strain for homogeneous deformation," *Journal of the Institute of Metals*, vol. 74, pp. 537–562, 1948.

[147] X. R. Chu, L. Leotoing, D. Guines, and J. Gao, "Comparison of Constitutive Laws on the Modeling of Thermo-Viscoplastic Behaviour of an Aluminum Alloy," *Applied Mechanics and Materials*, vol. 496–500, pp. 307–310, Jan. 2014.

[148] M. F. Horstemeyer, *Integrated Computational Materials Engineering (ICME) for Metals*. John Wiley & Sons, Inc., 2012.

[149] G. H. Bryan, "On the stability of a plane plate under thrusts in its own plane, with applications to the 'buckling' of the sides of a ship," *Proceedings of the London Mathematical Society*, vol. 1.1, pp. 54–67, 1890.

[150] V. T. Kármán, "Festigkeitsprobleme im Maschinenbau," *Encyclopädie der mathematischen Wissenschaften*, vol. IV, p. 349, 1910.

[151] E. Siebel, *Die Formgebung im bildsamen Zustand*, 1st ed. Stahleisen m.b.H., 1932.

[152] D. Bauer and S. Keller, "Genaues Berechnen der Kraft optimiert Tiefziehprozeß," *Bänder Bleche Rohre*, vol. 6, pp. 43–47, 1991.

[153] B. A. Behrens, E. Doege, and B. Springub, "Analytische Ziehkraftberechnung nach dem 'Prinzip der virtuellen Arbeit,'" *Forschung im Ingenieurwesen/Engineering Research*, vol. 69, no. 3, pp. 132–136, 2005.

[154] R. Hill, "A Theory of the Yielding and Plastic Flow of Anisotropic Metals," *Proceedings of the Royal Society of London. Series A. Mathematical and Physical Sciences*, vol. 193, no. 1033, pp. 281–297, 1948.

[155] F.-J. Lenze, "Beitrag zum Umformwirkungsgrad beim Tiefziehen," Universität Siegen, 1982.

[156] C. Spura, *Technische Mechanik 1. Stereostatik*. Wiesbaden: Springer Fachmedien Wiesbaden, 2016.

[157] H. Hoffmann, R. Neugebauer, and G. Spur, *Handbuch Umformen*. Carl Hanser Verlag GmbH & Co. KG, 2012.

[158] T. von Kármán, "Untersuchungen über Knickfestigkeit," in *Mitteilungen über Forschungsarbeiten auf dem Gebiete des Ingenieurwesens insbesondere aus den Laboratorien der technischen Hochschulen*, Springer, 1910, pp. 1–44.

[159] B. W. Senior, "Flange wrinkling in deep-drawing operations," *Journal of the Mechanics and Physics of Solids*, vol. 4, no. 4, pp. 235–246, 1956.

[160] E. Doege, "Untersuchungen über die maximal übertragbare Stempelkraft beim Tiefziehen rotationssymmetrischer zylindrischer Teile," TU Berlin, 1963.

[161] E. Brinksmeier and J. T. Cammett, "Residual Stresses - Measurements and Causes in Machining Processes," *Annals of the CIRP*, vol. 31, no. 2, pp. 491–510, 1982.

[162] M. N. A. Nasr, E.-G. Ng, and M. A. Elbestawi, "Effects of Strain Hardening and Initial Yield Strength on Machining-Induced Residual Stresses," *Journal of Engineering Materials and Technology*, vol. 129, no. 4, p. 567, 2007.

[163] J. Danckert, "The Residual Stress Distribution in the Wall of a Deep-Drawn and Ironed Cup Determined Experimentally and by FEM," *Annals of the CIRP*, vol. 43, pp. 249–252, 1994.

[164] I. Burchitz, "Springback: improvement of its predictability: Literature study report," *Project, NIMR project number MC1 2121*, 2005.

[165] S. Sumikawa, A. Ishiwatari, J. Hiramoto, and T. Urabe, "Improvement of springback prediction accuracy using material model considering elastoplastic anisotropy and Bauschinger effect," *Journal of Materials Processing Technology*, vol. 230, pp. 1–7, Apr. 2016.

[166] K. Lange, *Handbuch für Industrie und Wissenschaft, Band 3: Blechbeaarbeitung*, 2nd ed. Springer, 1990.

[167] E. Siebel and W. Mühlhäuser, "Eigenspannungen beim Tiefziehen," *Mitteilungen der Forschungsgesellschaft Blechverarbeitung*, vol. 21, pp. 241–244, 1954.

[168] A. Mousavi and A. Brosius, "Improving the springback behavior of deep drawn parts by macro-structured tools," *IOP Conference Series: Materials Science and Engineering*, vol. 418, pp. 1–8, Sep. 2018.

[169] P. Tröber, R. Golle, and W. Volk, "Influence of lubrication on the measured thermoelectric voltage and temperature in the forming zone when embossing S355MC," *Dry Metal Forming Open Access Journal*, vol. 1, pp. 17–21, 2015.

[170] T. Meinders, A. W. A. Konter, S. E. Meijers, E. H. Atzema, and H. Kappert, "A sensitivity analysis on the springback behavior of the unconstrained bending problem," *International journal of forming processes*, vol. 9(3), pp. 365–402, 2006.

[171] Q. Yin, "Verfestigungs- und Schädigungsverhalten von Blechwerkstoffen im ebenen Torsionsversuch," Technische Universität Dortmund, 2014.

[172] K. Ahn, D. Yoo, M. H. Seo, S. H. Park, and K. Chung, "Springback prediction of TWIP automotive sheets," *Metals and Materials International*, vol. 15, no. 4, pp. 637–647, 2009.

[173] T. Clausmeyer, A. Güner, A. E. Tekkaya, V. Levkovitch, and B. Svendsen, "Modeling and finite element simulation of loading-path-dependent hardening in sheet metals during forming," *International Journal of Plasticity*, vol. 63, no. 1, pp. 64–93, 2014.

[174] G. Brabie, C. Schnakovszky, C. Axinte, and B. Chirita, "Analysis by simulation of the residual stresses distribution as a function of different factors in the case of hemispherical draw parts made from metal sheets," in *9th International Research/Expert Conference "Trends in the Development of Machinery and Associated Technology*, 2005, pp. 157–162.

[175] C. Yang, P. Li, and L. Fan, "Blank shape design for sheet metal forming based on geometrical resemblance," in *Procedia Engineering 81*, 2014, vol. 81, no. October, pp. 1487–1492.

[176] M. Karima, "Blank development and tooling design for drawn parts using a modified slip line field based approach," *Journal of Engineering for Industry*, vol. 111, pp. 340–344, 1989.

[177] R. Sowerby, J. L. Duncan, and E. Chu, "The modelling of sheet metal stampings," *International Journal of Mechanical Sciences*, vol. 28, no. 7, pp. 415–430, Jan. 1986.

[178] Z. Zhang and B. Liang, "Determination of blank shapes for drawing irregular cups using an electrical analogue method," *International Journal of Mechanical Sciences*, vol. 28, no. 8, pp. 499–503, Jan. 1986.

[179] K. Chung, J. Yoon, and O. Richmond, "Ideal sheet forming with frictional constraints," *International Journal of Plasticity*, vol. 16, no. 6, pp. 595–610, 2000.

[180] O. Barlat, J. . Batoz, Y. . Guo, F. Mercier, H. Naceur, and C. Knopf-Lenoir, "Optimum blank design of blank contours using the inverse approach and a mathematical programming technique," *Proceedings of the Numisheet'96*, vol. 96, pp. 178–184, 1996.

[181] T. W. Ku, H. J. Lim, H. H. Choi, S. M. Hwang, and B. S. Kang, "Implementation of backward tracing scheme of the FEM to blank design in sheet metal forming," *Journal of Materials Processing Technology*, vol. 111, no. 1–3, pp. 90–97, Apr. 2001.

[182] S. Hynbo, "Determination of optimal shape for the stamping of arbitrary shape," *Journal of Materials Processing Technology*, vol. 121, no. 1, pp. 116–122, 2002.

[183] W. F. Hosford and R. M. Cadell, *Metal forming: Mechanics and Metallurgy*, 3rd ed. Cambridge University Press, 2007.

[184] G. Oehler and K. Fritz, *Schnitt-, Stanz- und Ziehwerkzeuge*. Springer, 1973.

[185] A. Brosius, M. Schomäcker, and A. Mousavi, "Vorrichtung zum Tiefziehen eines Blechzuschnittes mit Formwerkzeugen," DE102015220231A1, 2016.

[186] A. Vanhulsel, F. Velasco, R. Jacobs, L. Eersels, D. Havermans, E. W. Roberts, I. Sherrington, M. J. Anderson, and L. Gaillard, "DLC solid lubricant coatings on ball bearings for space applications," *Tribology International*, vol. 40, no. 7, pp. 1186–1194, 2007.